COMPOSITION OF FLOATING DERELICT FISHING GEAR IN THE CENTRAL SUBTROPICAL NORTH PACIFIC OCEAN

Andrew Charles McWhirter

A Thesis submitted in partial satisfaction of the requirements
for the degree Master of Science

in

Marine Science

College of Natural and Computational Sciences

Hawai‘i Pacific University

Spring 2022

Honolulu, Hawai‘i

Advisory Committee:

Dr. Jennifer M. Lynch
Dr. K. David Hyrenbach
Dr. Sarah-Jeanne Royer

Composition of floating derelict fishing gear in the central subtropical North Pacific Ocean

by

Andrew Charles McWhirter

5/5/2022

This thesis is submitted in partial fulfillment of the requirements for the degree of Master of Science in Marine Science at Hawai'i Pacific University. We the undersigned have examined this document and have found that it is complete and satisfactory in all respects, and all revisions required by the final examining committee have been made.

Author _____
Andrew Charles McWhirter

Committee Chair _____
Dr. Jennifer M Lynch, Research Faculty

Committee Member _____
Dr. Sarah-Jeanne Royer, Research Scientist

Committee Member _____
Dr. K. David Hyrenbach, Professor of Oceanography

Dean _____
Brenda Jensen, PhD, Dean, College of Natural and Computational Sciences

ABSTRACT

Floating derelict fishing gear (DFG) has been polluting the marine environment for decades. The Hawaiian archipelago, in the center of the North Pacific Subtropical Gyre, is exposed to high levels of DFG accumulation and the associated environmental damage. The goals of this project were to develop the most effective methods for sampling and analyzing DFG composition, assess DFG composition in the subtropical North Pacific, and build evidence for sourcing DFG back to specific fisheries and manufacturers. Five methods were developed to sample and analyze DFG events with varying levels of resource requirements and data resolution. Three methods used to assess composition of DFG conglomerates were compared, named the Four Corners method, Disentanglement method, and the Hybrid method. The Hybrid method proved to be the most effective sampling option considering time, resources, and data resolution. However, the Hybrid and Disentanglement methods biased event composition, when compared to the more accurate assessment of composition by mass and count of the disentangled and sorted gear piles. The Hybrid method was used to assess DFG conglomerate composition from three central North Pacific regions, Midway (MID), O‘ahu (OAH), and the pelagic North Pacific Gyre (NPG). Composition was investigated at the DFG event level, by proportion of gear categories that make up the event, and within the nets and lines categories, by proportion of count and mass. Composition at the event level revealed that conglomerates are primarily composed of nets and lines by count and mass, with no significant variation among regions. The two dominant gear types were then compared where line composition did not show any significant difference among the regions. Net composition was significantly different among regions, and the majority of this variation was explained by Midway having more monofilament gillnets. This study produced the most detailed database on floating DFG in the subtropical

North Pacific and has archived information necessary to trace DFG found in Hawai‘i back to the source fisheries and manufacturers.

ACKNOWLEDGEMENTS

I would like to thank my advisor Jennifer Lynch, and committee members Sarah-Jeanne Royer and David Hyrenbach for their mentorship and support though this project. Thank you to Raquel Corniuk for leading our laboratory analysis effort for all of our sampling. Thank you to all of the more than 100 volunteers that invested their time and energy in the Hawai‘i humidity to disentangle and sample nets in the net shed. Thank you to Hawai‘i Pacific University for providing a warehouse to process nets in. Thank you to Hank Lynch for captaining our rapid inwater net removal response efforts. Thank you to all of the lab volunteers, federal work study students, and lab members that contributed time and energy on this project. Thank you to PMDP Hawai‘i for allowing me to participate on a marine debris mission, and all the team members that helped to collect DFG events in Papahānaumokuākea for the purpose of our research. Thank you to the HI MDAP partners that helped to coordinate rapid response and sustainable disposal of DFG, particularly DLNR, Sustainable Coastlines Hawaii, Surfrider Foundation Kauai, and Hawaii Wildlife Fund. Thank you to the Hawaii Longline Association and all the captains that brought DFG back from their fishing grounds for our research. Thank you to all the artists that used our processed material to make art with. This was a huge team effort and we would not have been able to achieve this much without our community.Funding was provided by the Norwegian Retailers’ Environment Fund. Sampling in the Papahānaumokuākea National Marine Monument was permitted by permit # PMNM-2020-015.

CHAPTER 1

Literature review of floating derelict fishing gear in the central subtropical North Pacific: Towards a regional study of its composition and origins

INTRODUCTION

Plastic in the marine environment has emerged as a global phenomenon causing negative ecological and economic impacts (Beaumont et al., 2019). Plastic was first introduced as a commercial product in the 1950's and has since been integrated into nearly every aspect of human existence due to its versatility, durability, low-cost, and convenience. In 2016, approximately 393 Mt of plastic was produced, and if our trend continues business as usual then production is expected to double within the next 20 years (Lebreton & Andrady, 2019). The rapid rise in mass production of plastic has escalated beyond the capacity of adequate waste management strategies, which has resulted in the contamination of the marine environment with plastic debris from both land and marine sources (Geyer et al., 2017; Jambeck et al., 2015). When mismanaged plastic waste is discharged into the environment, tributaries readily carry plastic to the ocean, where materials that are less dense than seawater can then be transported far from their sources and aggregate in the five subtropical gyres.

There are over 268,940 metric tons of plastic floating at the surface of the ocean, most of which is found in the five subtropical gyres (Eriksen et al., 2014). Disproportionately high concentrations of floating plastic debris observed in the North Pacific Subtropical Gyre, accounting for 35.8% of all floating plastic in the ocean, is especially concerning. Plastic waste from fishery sources, referred to as Derelict Fishing Gear (DFG), account for as much as 52% of floating plastic debris in the oceans by mass, and up to 19% of the annual emissions of mismanaged plastic waste to the oceans (Lebreton et al., 2018).

Over the past two decades global attention has focused on quantifying the magnitude and impacts of plastic marine debris. Several threats include ingestion by organisms (Gall & Thompson, 2015; Laist, 1987), bioaccumulation of persistent organic pollutants (Teuten et al.,

2009), entanglement in nets and lines (Donohue et al., 2001), ghost fishing of derelict fishing gear (Gilman et al., 2016), damage to coral reefs (Suka et al., 2020), and transport of invasive species (Therriault et al., 2018). Additionally, marine plastic pollution is a disruptive economic expense to tourism, fishing, and maritime industries (Beaumont et al., 2019).

The North Pacific Subtropical Gyre aggregates DFG and smaller floating plastics in the highest concentration observed throughout the world's oceans (Lebreton et al. 2018). High densities of DFG overlap with the Hawai‘i tuna and swordfish longline fishery fishing grounds and hinder fishing operations at a great expense (Uhrin et al., 2020). Additionally, the Hawaiian archipelago, centered within the North Pacific Subtropical Gyre, is especially vulnerable to DFG, which impacts coral reefs habitat, turtles, seabirds, and critically endangered Hawaiian Monk Seals throughout the archipelago. The DFG affecting Hawai‘i consists of large masses of fishing nets and lines that can weigh hundreds of pounds and be multiple cubic meters in size, as well as drifting fish aggregation devices (dFAD) (Figure 2.1). A dFAD typically consists of a surface raft with a drogue that can extend over 100 feet deep and is deployed to attract commercial pelagic fish species, including tuna. None of these types of fishing gear are manufactured or deployed locally in Hawai‘i by commercial fishermen, and are therefore coming from distant, to be determined origins.

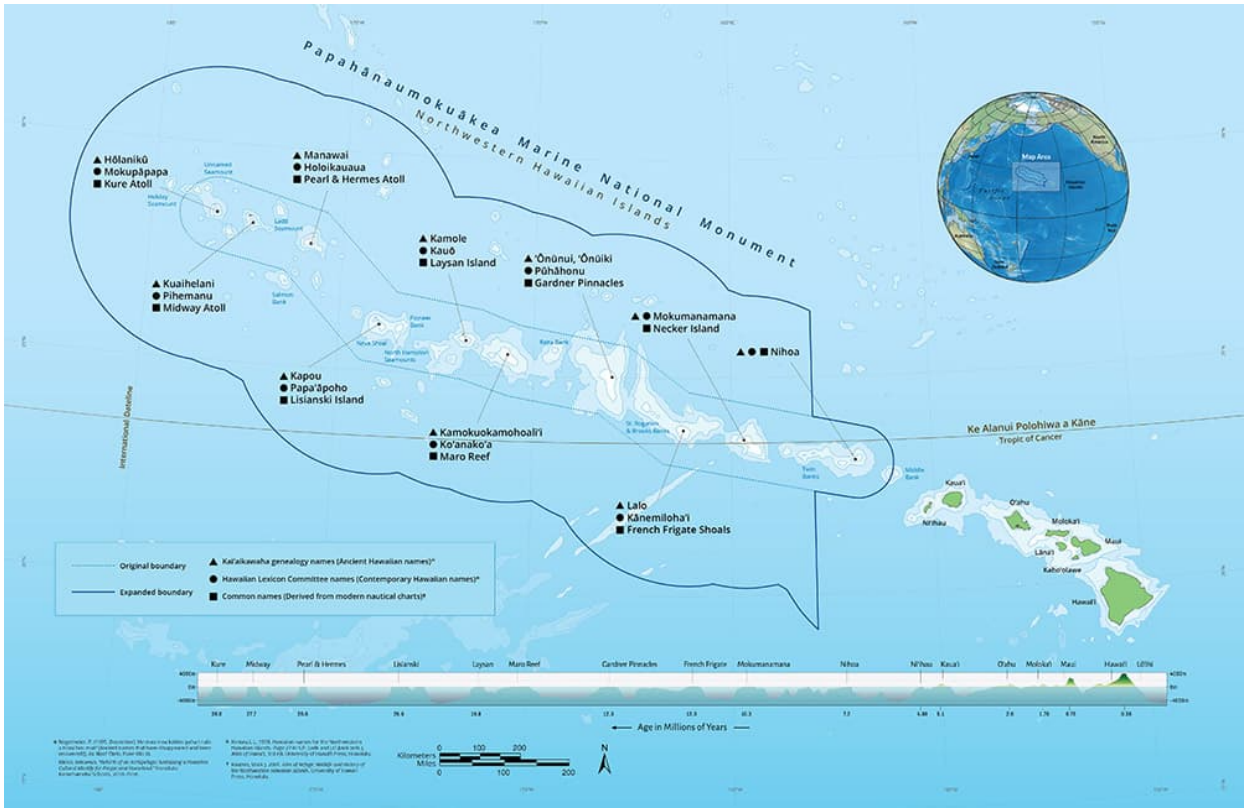

Figure 1.1. Map of the Hawaiian archipelago. The main Hawaiian islands are to the southeast, and Papahānaumokuākea Marine National Monument encompasses the reefs, seamounts, and atolls to the northwest (2020 State of Papahānaumokuākea Marine National Monument Report| Office of National Marine Sanctuaries, 2020).

The Hawaiian archipelago comprises 137 islands, islets, and atolls, and extends about 2,500 km from Hawai‘i Island in the Southeast (19.567^0 N, -155.5^0 W), to Kure Atoll in the Northwest (28.417^0 N, -178.333^0 W). Hawai‘i is the most isolated archipelago on Earth, located roughly 4,800 km from the nearest continent. This region comprises approximately 70% of the United States’ coral reef habitat, and supports many endemic species (Cesar & Beukering, 2004). Specifically, there are ~7,000 marine species that inhabit the archipelago, and roughly 25% are endemic to the region (National Marine Sanctuaries, NOAA, 2020). The Hawaiian archipelago can be divided into two distinct regions, the uninhabited atolls, reefs, shoals, islets, and islands of the Papahānaumokuākea Marine National Monument (Northwestern Hawaiian Islands), and the eight Main (Southeastern) Hawaiian Islands, with about 1.5 million residents and millions of

annual visitors. The Hawaiian archipelago is a unique region of interest on the topic of marine plastic pollution due to the magnitude of floating plastic debris that washes ashore and the inherent impacts to Hawai‘i’s marine ecosystems (Beaumont et al., 2019; Brignac et al., 2019; Donohue et al., 2001; Gove et al., 2019; Ribic, Sheavly, Rugg, et al., 2012).

SOURCES AND TYPES OF MARINE DEBRIS

To mitigate the effects of floating plastic debris in Hawai‘i, we must understand the sources of plastic pollution into the ocean and the mechanisms by which it is transported. Jambeck et al. (2015) estimated that 4.8 – 12.7 million tonnes (Mt) of plastic discharge enters our oceans every year, and as much as 90% originates from land-based sources. A recent analysis by Law et al. (2020) finds that the U.S. generates more plastic waste than any other country in the world, totaling over 42 Mt per year. Of this, as much as 2.98% is mismanaged, making the US contribution to plastic waste entering the environment as much as 1.45 Mt per year, the 3rd largest contributing country. Rivers including inland sources greater than 50 km from the coast account for up to 2.41 Mt of plastic emissions into the oceans annually, with 67% of the total emissions coming from 20 rivers in Asia (Lebreton et al., 2017). Other land-based sources of marine debris include mismanaged waste disposal and stormwater runoff. Ocean-based sources of marine debris include the fishing, shipping and maritime industries, and ocean recreation. Marine-based sources of plastic marine debris are more challenging to trace and quantify due to lack of governance on the high seas, inadequate fisheries management practices, and minimal fishing gear traceability policies. Therefore, future interdisciplinary collaboration is essential to assess marine-based debris sources more accurately.

Once plastic enters the ocean, its fate is influenced by polymer composition and density. There are thousands of different plastic polymers, but the six most common commercially

produced are polyethylene terephthalate (PET), low-density polyethylene (LDPE), polyvinyl chloride (PVC), high-density polyethylene (HDPE), polypropylene (PP), and polystyrene (PS). Of these six dominant polymers, only LDPE, HDPE, and PP are less dense than seawater (Table 1). These polymers and others that entrap air (i.e. expanded polystyrene foam) can remain afloat on the sea surface and be transported far from their sources by ocean currents (Brignac et al., 2019).

Table 1.1. Summary table of the seven most common resin codes, the polymers they represent, the density of the polymer, and typical products that are made of the polymer. In the density column, blue indicates the density is less than seawater and buoyant, and red indicates denser than seawater and sinks.

Supplementary Table 1: Resin codes, abbreviations, density and common commercial uses.				
Recycling Number	**Abbreviation**	**Polymer name**	**Density (g/ml)**	**Uses**
	PETE or PET	Polyethylene terephthalate	1.37–1.41	Fishing nets, textiles (polyester fibers), strapping, soft drink bottles, tote bags, furniture, carpet, paneling
	HDPE or PE-HD	High-density polyethylene	0.94–0.98	Trawl and seine fishing nets, bottles, grocery bags, milk jugs, recycling bins, agricultural pipe, plastic lumber
	PVC or V	Polyvinyl chloride	1.38–1.45	Pipe, foam floats, window profile, siding, fencing, flooring, shower curtains, lawn chairs, non-food bottles, children's toys
	LDPE or PE-LD	Low-density polyethylene, Linear low-density polyethylene	0.89–0.93	Plastic bags, six pack rings, various containers, dispensing bottles, wash bottles, tubing, molded laboratory equipment
	PP	Polypropylene	0.85–0.92	Ropes, auto parts, industrial fibers, food containers, dishware
	PS	Polystyrene	1.04–1.06	Plastic utensils, coffee cup lids, clamshell containers, packaging peanuts, insulation board, expanded polystyrene products
	OTHER or O	Other plastics, such as nylon, acrylic, polycarbonate, bioplastics, multilayer combinations of different plastics	1.12–1.24 *(nylon)	Bottles, plastic lumber applications, headlight lenses, and safety shields/glasses.

Most of the marine debris found in the central North Pacific and Hawaiian archipelago are buoyant plastic polymers (Blickley et al., 2016; Brignac et al., 2019; Currie et al., 2019; Ribic, Sheavly, & Klavitter, 2012; Ribic, Sheavly, Rugg, et al., 2012). Exceptions are non-buoyant polymers that are attached to or entangled with buoyant polymers, as is often the

case in large DFG conglomerates. Brignac et al. (2018) analyzed samples of plastic debris from windward and leeward beaches, the sea surface offshore, and the seafloor nearshore. A clear gradient in polymer composition was observed across sites. All sea surface plastic samples were buoyant polymers and over 90% of plastics collected on windward beaches were buoyant, where on leeward beaches less than 50% of plastics sampled were buoyant, and at seafloor sites no plastics were buoyant. Moreover, plastic quantities were approximately 1-2 orders of magnitude greater on windward beaches vs. leeward beaches. This suggests that buoyant plastics are transported by the oceanic currents and trade winds to the Hawaiian archipelago. Furthermore, they assigned a weathering code to each sample from 1 (minimal weathering), to 3 (severely weathered: obvious fractures and UV degradation). The weathering analysis provides evidence to support this hypothesis by concluding that most plastics collected from the sea surface (80.5% ± 20%) and windward beaches (52.7% ± 15.6%) were severely weathered, which provides a rough estimation of residence time in the marine environment.

Additionally, a study by Ribic et al. (2012) conducted for a period of seven years monthly debris surveys at five O‘ahu beaches, 13 sites along the Oregon-California coast, and five sites in the California Bight. Surveys were carried out on monthly intervals over 500 m stretches of beach. Debris was counted and categorized into three source categories: ocean-based, land-based, and general debris. This study determined that the majority (approximately 38% by count) of the debris observed on O‘ahu was from ocean-sources (fishing, aquaculture, maritime). Approximately 33% was defined as general-source debris, meaning the source could not be distinguished as either land or ocean-based, and only 29% was determined to be land based. Based on this study, by count, Oahu is exposed to 15% more ocean-based debris compared to the Oregon-California coast (23%), and 30% more than the California-Bight (8%).

Furthermore, the Hawaiian archipelago is heavily impacted by the accumulation of DFG (Boland & Donohue, 2003; Donohue et al., 2001; Donohue & Foley, 2007; Morishige et al., 2007; Timmers et al., 2005). DFG nets wash ashore throughout the Hawaiian archipelago year-round, and pose entanglement hazards to wildlife, such as the critically endangered endemic Hawaiian Monk Seal. DFG can also damage and scar coral reefs (Suka et al., 2020), and may transport invasive species across ocean basins (Donohue et al., 2001).

Most of the nets encountered on Hawaiian shores are trawl nets (~90%). Gillnet, seine and miscellaneous ropes and lines are also common (Boland & Donohue, 2003). There are no commercial trawl, seine, or gill net fisheries in Hawai‘i, which is a clear indication that the DFG is of foreign origins.

There is conclusive evidence that ocean-sourced marine debris is washing ashore in Hawai‘i, in relatively high concentrations compared to other coastal regions in the North Pacific. After the floating plastic debris enters the ocean, it is transported and aggregated by oceanic currents. DFG accumulations have been observed along the subtropical convergent front the north of Hawai‘i (Pichel et al., 2007), and in an anticyclonic convergent zone between Hawai‘i and California (Lebreton et al., 2018).

MARINE DEBRIS IN THE NORTH PACIFIC

Overview of North Pacific Ocean Circulation

Oceanic currents transport plastic great distances and aggregate this material in regions of surface convergence. The primary drivers of ocean surface circulation are Ekman drift, Stokes drift, and geostrophic flow (Kubota et al., 1994). Ekman transport and geostrophic flow driven by the prevailing equatorial easterly winds and subpolar westerly winds forms five anticyclonic

(convergent) subtropical gyres in each ocean basin centered about 30° latitude (Maximenko et al., 2012).

The North Pacific Subtropical Gyre (NPSG) is the largest of the five subtropical gyres, and consists of the westbound North Equatorial Current, northbound Kuroshio, eastbound Kuroshio Extension, eastbound North Pacific Current, and the southbound California Current (Figure1). Additionally, a cyclonic (divergent) North Pacific Subpolar Gyre forms at higher latitudes. At the boundary between these two gyres there is a transition zone where the subpolar and subtropical waters converge. It is important to recognize that the structure of these features vary both spatially and temporally in response to seasonal and interannual climate patterns (Howell et al., 2012). These large-scale circulation features are the primary transport and aggregation mechanism for floating plastic marine debris in the North Pacific (Howell et al., 2012; Kubota, 1994; Maximenko et al., 2012).

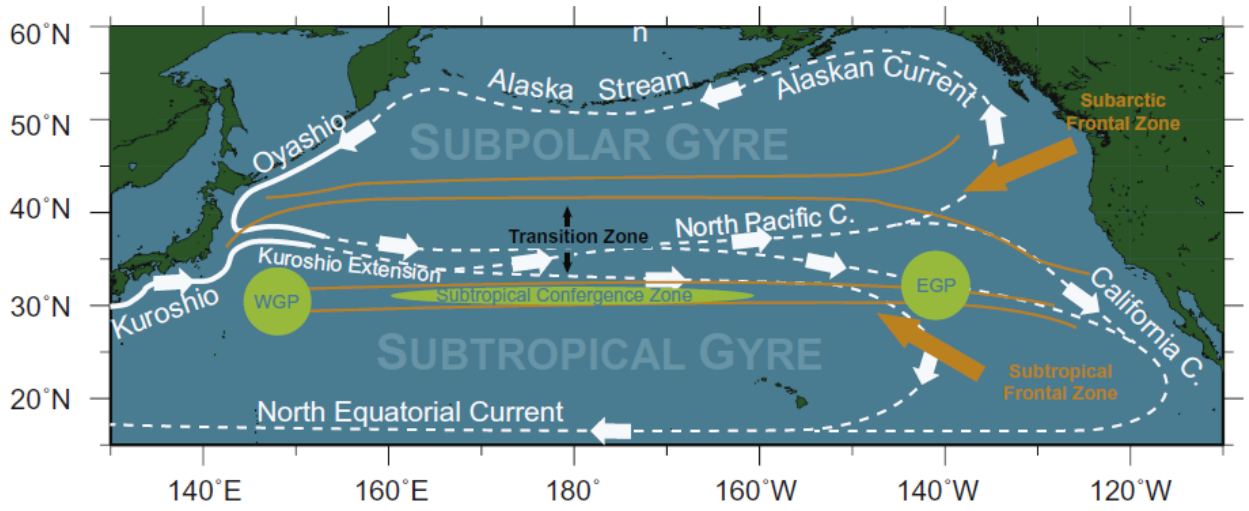

Figure 1.2: Overview of surface current circulation and accumulation zones in the North Pacific (Howell et al., 2012).

Marine Debris Convergence Zones

The NPSG contains the greatest concentration of floating plastic debris of the five subtropical gyres, with an estimated 96,400 metric tons of plastic, or 36% of the total global

floating marine plastic debris (Eriksen et al., 2014). Moreover, DFG is estimated to account for 52% of plastic debris mass in the North Pacific (Lebreton et al., 2018).

However, plastic distribution is not homogenous throughout the basin, and is determined by the convergent and divergent features mentioned above (Howell et al., 2012). Specifically, there are three major accumulation zones within the NPSG, known as the Eastern Pacific Garbage Patch (EPGP), Western Pacific Garbage Patch (WPGP), and the Subtropical Convergence Zone (STCZ). The EPGP and WPGP can be described as mesoscale semi-permanent anticyclonic eddies, or sub-gyres, though they are substantially different features. Where, the STCZ between them results from Ekman convergence of subpolar and subtropical surface waters along a front (Howell et al., 2012). We will discuss each accumulation zone in detail in the following sections.

Western Pacific Garbage Patch

The WPGP is positioned southeast of Japan and south of the Kuroshio Extension. The dynamics of this garbage patch are heavily influenced by the strength of the Kuroshio Extension and resulting eddy field. Greater northwesterly wind and equatorial easterly wind stress strengthen the Kuroshio Extension current velocity, which strengthens an anticyclonic recirculation gyre that accumulates marine debris (Howell et al., 2012). Maximenko et al. (2012) generated a 10-year numerical model simulation to resolve surface accumulation dynamics across all ocean basins, calibrated with *in situ* drifter array data from the Global Drifter Program. This simulation demonstrated that this anticyclonic feature accumulates floating marine debris. However, residence time of floating debris in the WPGP is limited by the strength of this recirculation gyre. The strength of this feature fluctuates with the phases of the Pacific decadal oscillation, which correspond to variability in wind stress and SSH. Greater wind stress along the

equator and positive SSH anomalies in the western Pacific correlate to strengthening of the recirculation gyre, creating the WPGP. Weakening of the trade winds during the El Niño phase and negative SSH anomaly in the eastern Pacific weakens the recirculation gyre and its ability to retain debris (Qiu & Chen, 2005). Essentially, the WPGP forms and dissipates on a decadal timescale, whereas the EPGP can retain floating plastic debris for decades (Qiu & Chen, 2005, Maximenko et al., 2018).

Eastern Pacific Garbage Patch

The EPGP is positioned between Hawai‘i and California and has become a high-priority region for marine debris research over the past two decades (Cózar et al., 2014; Egger et al., 2020; Law et al., 2014; Lebreton et al., 2018, 2019; Moore et al., 2001). Prevailing westerly winds across the North Pacific and southerly winds along the west coast of North America create a negative wind stress curl in this region, indicative of surface convergence. Additionally, minimal surface current velocity is observed in this region, which coincides with a persistent, yet variable, atmospheric high-pressure system known as the North Pacific Subtropical High. In general, the EPGP is concentrated further south (closer to Hawai‘i) in winter when wind forcing is maximum, and expands northeast during summer conditions (Howell et al., 2012). The model created by Maximenko et al. (2012) estimated the center of the EPGP to be near 31° N, 139° W, with the peak concentration zone (concentration > than ½ the maximum value) spanning zonal 1220 km and meridional 800 km. Accumulation in this feature favors marine debris with low windage (0% windage coefficient), which is representative of derelict fishing nets. Residence time in this feature is predicted to span years to decades (Lebreton et al., 2019; Maximenko et al., 2018). This persistent convergent zone accumulates the greatest concentration of marine

debris observed in the open ocean (Egger et al., 2020; Eriksen et al., 2014; Law et al., 2014; Lebreton et al., 2018; Maximenko et al., 2012; Moore et al., 2001).

Marine debris concentration in the EPGP has been investigated by several studies at varying size classes, spatial and temporal scales (Egger et al., 2020; Eriksen et al., 2014; Law et al., 2014; Lebreton et al., 2018; Maximenko et al., 2012, 2018; Moore et al., 2001; Titmus & Hyrenbach, 2011). The most recent and comprehensive analysis of the EPGP, by Lebreton et al. (2018), used a validated Lagrangian particle trajectory model to predict the area of the EPGP to be 1.6 million km^2, bound by surface plastic debris concentration of greater than 1 kg km^{-2}. This model integrated results from aerial photo surveys (n = 2, area = 311 km^2) and surface net tows (n = 652, area = 17.5 km^2) with significant land and ocean-based plastic debris sources and 12-years of physical parameter data for sea surface currents, wave induced Stokes drift, and surface winds (HYCOM + NCODA global 1/12° reanalysis; significant wave height, peak wave period and direction, from Wavewatch3; NCEP/NCAR global reanalysis, 10m above sea level). Results predicted that there is 79,000 MT of plastic marine debris afloat in the EPGP, which would account for approximately 82% of all the floating plastic debris in the NPSG, estimated by Erikson et al. (2014). Additionally, by integrating historical neuston tow data since 1970, this study predicts that plastic accumulation in this region is increasing at an exponential rate 1.5 times higher than concentration in North Pacific waters surrounding the patch. It is important to realize that a negative relationship exists between mass load and abundance across debris size classes. In other words, there is a greater abundance of smaller debris (e.g., plastic fragments), but large items (>5 cm) represent a greater proportion of plastic debris by mass. While derelict fishing gear represents 49.6% of the total plastic by mass in the EPGP, the mean concentration was only 3.3 nets km^{-2}.

Marine debris is not retained within the EPGP indefinitely. However, the exit mechanisms and pathways are less understood than the accumulation mechanisms (Egger et al., 2020; Howell et al., 2012; Lebreton et al., 2019; Miron et al. 2021; van Sebille et al., 2020). Some of the debris exported from this accumulation zone reaches the Hawaiian archipelago (Lebreton et al., 2018; Maximenko et al., 2018).

Subtropical Convergence Zone

Several studies have demonstrated that marine debris accumulates along the southern border of the North Pacific Transition Zone, known as the Subtropical Convergence Zone (STCZ) (Donohue & Foley, 2007; Howell et al., 2012; Kubota, 1994; Pichel et al., 2007). This convergent zone forms along the boundary of the North Pacific Subtropical Front, where southward Ekman transport from north westerly wind stress causes cool fresh water to subduct below the warmer and saltier Subtropical Front, resulting in surface convergence (Roden, 1975). The strength and position of STCZ varies temporally depending on the strength and position of the northerly and westerly winds (Howell et al., 2012; Roden, 1975). Southward shift in the STCZ during winter months is attributed to maximum wind stress forcing and decreased insolation. Conversely, decreased wind stress and increased insolation in summer months shift the STCZ to its northerly maximum (Howell et al., 2012). These seasonal fluctuations can exceed 10^0 latitude (23^0N - 37^0N) (Donohue & Foley, 2007; Kubota, 1994). Additionally, El Niño Southern Oscillation (ENSO) can exemplify these fluctuations by ± 2^0 latitude, shifting further South during El Niño conditions and further North during La Niña conditions (Bograd et al., 2004).

Aerial surveys by Pichel et al. (2007) documented marine debris concentrations along the Transition Zone Chlorophyll Front (TZCF), which serves as a bioindicator of the STCZ position.

Plastic marine debris, primarily foam fishing floats, was observed in abundance of about one item per km^2. Unfortunately, the methods used by Pichel et al. (2007) and key information unreported prevents comparisons of these results with that of other accumulation zones, such as the EPGP. For example, debris concentrations for different categories (buoys, general debris, floats, lines, nets, logs) observed were not described in items/km^2, and the total area surveyed on each flight was not presented with the total counts. Additionally, observations were not binned by size, as is for most other studies (Eriksen et al., 2014; Lebreton et al., 2018). Peak debris concentrations corresponded to Chl-*a* concentration of 0.25 mg m^{-3} and SST of 17^0C. This reflects that accumulation in this region may favor the subpolar side of the TZCF. One explanation of this pattern is that fishing activity in the subpolar gyre may be a primary source of the debris aggregated in this feature. Additionally, the eastward flow of surface currents along this boundary suggests that the STCZ provides a pathway for debris to cross the North Pacific; a vector between the WPGP and the EPGP (Maximenko et al., 2012). Future random sampling and increased sample size are needed to build a more complete estimate of the distribution, composition, and total debris concentrations along this feature.

EVIDENCE OF MARINE DEBRIS TRANSPORT TO THE HAWAIIAN ARCHIPELAGO

Few studies have documented marine debris transport to the Hawaiian archipelago (Carson et al., 2013; Donohue & Foley, 2007; Ebbesmeyer et al., 2012; Maximenko et al., 2018; Morishige et al., 2007). Two main challenges inhibit the study of the transport mechanisms and drift pathways for plastic marine debris: (i) the specific date and location of loss and recovery to constrain the physical forcing of models, and (ii) that debris rarely has unique identification tags, tracers, or other sourceable characteristics.

Overall, there is much work to be done to resolve plastic release dynamics from each convergent feature mentioned above (WPGP, EPGP, STCZ). Much of the literature has focused on the connection of the southerly shift in the STCZ, as a mechanism of debris deposition on the Hawaiian archipelago (Donohue & Foley, 2007; Morishige et al., 2007; Pichel et al., 2007). Morishige et al. (2007) observed maximum debris deposition at Tern Island, French Frigate Shoals, NWHI, during El Niño years (when the STCZ is further south), and less than half as much debris deposition during La Niña years (when the STCZ is further north). Additionally, Donohue & Foley (2007) report a trend of greater Monk Seal entanglements in Papahānaumokuākea Marine National Monument during El Niño years, which may indicate a greater amount of DFG in the Monument in years when the STCZ is further south. Nevertheless, real-time resolution of the meso and sub-mesoscale eddy field associated with the STCZ is poorly understood, even though it likely plays a critical role in debris retention and deposition.

The WPGP is the least studied of all the convergent features in the North Pacific. However, its position in relation to the source countries responsible for peak land-based marine debris emissions suggest that the WPGP could serve as a vector for Asia land-based debris to Hawai‘i. Moreover, the plastic found in the WPGP is likely different in composition and source to that of the STCZ and EPGP (Jambeck et al., 2015).

The EPGP contains the greatest concentration of floating plastic debris of anywhere in the oceans and must inevitably play a critical role in debris pathways to Hawai‘i. What is known is that the EPGP is closest to Hawai‘i in winter, especially during El Niño events, when winter winds and storms strengthen. While debris escapes the EPGP in response to these atmospheric disruptions, the exact mechanisms must be the focus of future research.

UNRESOLVED ISSUES

In summary, the literature has yet to address the sources and composition of DFG in the central North Pacific. Transport and aggregation mechanisms of floating plastic debris needs to be improved at meso and sub-mesoscales. Mechanisms of debris exiting the WPGP and EPGP and arriving in Hawai‘i is poorly understood and expected to be substantial. Whether DFG composition in the three accumulation zones and the Hawaiian Archipelago is variable or homogenous remains to be determined. A better understanding of DFG composition in these regions can reveal the potential sources, and aid in management and mitigation strategies.

OBJECTIVES AND HYPOTHESES

This study will provide the most comprehensive analysis on DFG in the North Pacific Gyre. This analysis will reveal the connection between North Pacific accumulation zones and DFG found in the Hawaiian Archipelago. Furthermore, this study will reveal variation in DFG composition between Northwestern and Southeastern regions of the Hawaiian archipelago. Additionally, this study will be the first to investigate the polymer composition of DFG in the North Pacific. The primary outcome is for this study to serve as the basis for sourcing DFG back to the fishery of origin, and gear manufacturer. We will collect DFG events from three central North Pacific regions: Oahu Island, Midway Atoll, and the pelagic North Pacific Subtropical Gyre. We use the term “DFG event”to define a single isolated DFG mass that was recovered. We will conduct a detailed analysis of the composition of DFG, determine polymer composition, compare composition across the study regions, and ultimately identify the source fisheries. Attaining this information will be the first step towards effective mitigation of the damaging effects that DFG presents to Hawai‘i’s marine ecosystem. My thesis will answer two primary

questions: What types of DFG are in the North Pacific Ocean? Is DFG composition the same across the three study regions?

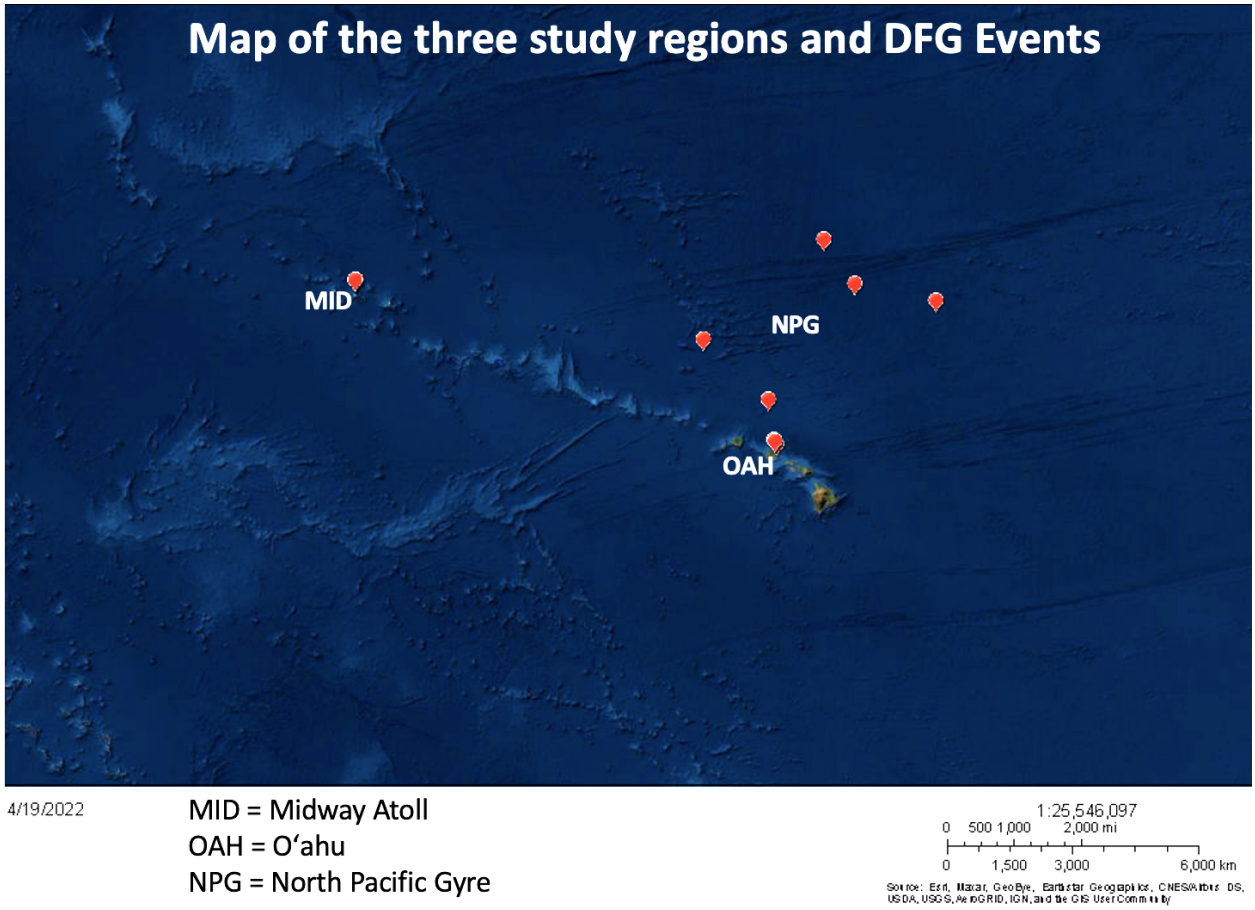

Figure 1.3: Map displaying the three study regions where DFG will be collected.

Objective I: Collect DFG events in the Central North Pacific from the three study regions.

Objective II: Develop novel robust methods for analyzing DFG composition for all types of DFG events.

Objective III: Compare DFG composition across the three region groups.

Prediction: DFG is aggregating and mixing in accumulation zones, resulting in the same DFG composition to be observed in all three study regions.

> ***Hypothesis 1:*** DFG event gear composition is different across three regions.
>
> ***Null 1:*** DFG event gear composition is the same across the three regions.
>
> ***Hypothesis 2:*** Composition within categories is different.
>
> ***Null 2:*** Composition within categories is the same.

REFERENCES

Beaumont, N. J., Aanesen, M., Austen, M. C., Burger, T., Clark, J. R., Cole, M., Hooper, T., Lindeque, P. K., Pascoe, C., & Wyles, K. J. (2019). Global ecological, social and economic impacts of marine plastic. Marine Pollution Bulletin, 142, 189–195.

Blickley, L. C., Currie, J. J., & Kaufman, G. D. (2016). Trends and drivers of debris accumulation on Maui shorelines: Implications for local mitigation strategies. Marine Pollution Bulletin, 7.

Bograd, S. J., Foley, D. G., Schwing, F. B., Wilson, C., Laurs, R. M., Polovina, J. J., Howell, E. A., & Brainard, R. E. (2004). On the seasonal and interannual migrations of the transition zone chlorophyll front. Geophysical Research Letters, 31(17).

Boland, R. C., & Donohue, M. J. (2003). Marine debris accumulation in the nearshore marine habitat of the endangered Hawaiian monk seal, *Monachus schauinslandi* 1999–2001. Marine Pollution Bulletin, 46(11), 1385–1394.

Brignac, K. C., Jung, M. R., King, C., Royer, S.-J., Blickley, L., Lamson, M. R., Potemra, J. T., & Lynch, J. M. (2019). Marine Debris Polymers on Main Hawaiian Island Beaches, Sea Surface, and Seafloor. Environmental Science & Technology, 53(21), 12218–12226.

Carson, H. S., Lamson, M. R., Nakashima, D., Toloumu, D., Hafner, J., Maximenko, N., & McDermid, K. J. (2013). Tracking the sources and sinks of local marine debris in Hawai ‘i. Marine Environmental Research, 84, 76–83.

Cesar, H. S. J. & Beukering, P. van. (2004). Economic Valuation of the Coral Reefs of Hawai’i. Pacific Science, 58(2), 231–242.

Cózar, A., Echevarría, F., González-Gordillo, J. I., Irigoien, X., Úbeda, B., Hernández-León, S., ... & Duarte, C. M. (2014). Plastic debris in the open ocean. Proceedings of the National

Academy of Sciences, 111(28), 10239-10244.

Currie, J. J., Stack, S. H., Brignac, K. C., & Lynch, J. M. (2019). Nearshore sea surface macro marine debris in Maui County, Hawaii: Distribution, drivers, and polymer composition. Marine Pollution Bulletin, 138, 70–83. https://doi.org/10.1016/j.marpolbul.2018.11.026

Donohue, M. J., & Foley, D. G. (2007). Remote sensing reveals links among the endangered Hawaiian Monk Seal, marine debris, and El Niño. Marine Mammal Science, 23(2), 468–473.

Donohue, M. J., Boland, R. C., Sramek, C. M., & Antonelis, G. A. (2001). Derelict fishing gear in the Northwestern Hawaiian Islands: Diving surveys and debris removal in 1999 confirm threat to coral reef ecosystems. Marine Pollution Bulletin, 42(12), 1301–1312.

Ebbesmeyer, C. C., Ingraham, W. J., Jones, J. A., & Donohue, M. J. (2012). Marine debris from the Oregon Dungeness crab fishery recovered in the Northwestern Hawaiian Islands: Identification and oceanic drift paths. Marine Pollution Bulletin, 65(1–3), 69–75.

Egger, M., Nijhof, R., Quiros, L., Leone, G., Royer, S.-J., McWhirter, A. C., Kantakov, G. A., Radchenko, V. I., Pakhomov, E. A., Hunt, B. P. V., & Lebreton, L. (2020). A spatially variable scarcity of floating microplastics in the eastern North Pacific Ocean. Environmental Research Letters, 15(11), 114056.

Eriksen, M., Lebreton, L. C. M., Carson, H. S., Thiel, M., Moore, C. J., Borerro, J. C., Galgani, F., Ryan, P. G., & Reisser, J. (2014). Plastic Pollution in the World's Oceans: More than 5 Trillion Plastic Pieces Weighing over 250,000 Tons Afloat at Sea. PLOS ONE, 9(12), e111913.

Gall, S. C., & Thompson, R. C. (2015). The impact of debris on marine life. Marine Pollution Bulletin, 92(1–2), 170–179.

Geyer, R., Jambeck, J. R., & Law, K. L. (2017). Production, use, and fate of all plastics ever made. Science Advances, 3(7), e1700782.

Gilman, E., Chopin, F., Suuronen, P., & Kuemlangan, B. (2016). Abandoned, lost and discarded gillnets and trammel nets: Methods to estimate ghost fishing mortality, and the status of regional monitoring and management. FAO Fisheries and Aquaculture Technical Paper, 600, I.

Gove, J. M., Whitney, J. L., McManus, M. A., Lecky, J., Carvalho, F. C., Lynch, J. M., Li, J., Neubauer, P., Smith, K. A., Phipps, J. E., Kobayashi, D. R., Balagso, K. B., Contreras, E. A., Manuel, M. E., Merrifield, M. A., Polovina, J. J., Asner, G. P., Maynard, J. A., & Williams, G. J. (2019). Prey-size plastics are invading larval fish nurseries. Proceedings of the National Academy of Sciences, 116(48), 24143–24149.

Howell, E. A., Bograd, S. J., Morishige, C., Seki, M. P., & Polovina, J. J. (2012). On North Pacific circulation and associated marine debris concentration. Marine Pollution Bulletin, 65(1–3), 16–22.

Jambeck, J. R., Geyer, R., Wilcox, C., Siegler, T. R., Perryman, M., Andrady, A., Narayan, R., & Law, K. L. (2015). Plastic waste inputs from land into the ocean. Science, 347(6223), 768–771.

Jersey Legal Information Board (2010). Sea Fisheries Regulations, 2010, (Trawling, Netting and Dredging) (Amendment No. 3) (Jersey) www.jerseylaw.je/laws/enacted/Pages/RO-098-2010.aspx

Jung, M. R., Horgen, F. D., Orski, S. V., Rodriguez, V., Beers, K. L., Balazs, G. H., ... & Lynch, J. M. (2018). Validation of ATR FT-IR to identify polymers of plastic marine debris, including those ingested by marine organisms. Marine Pollution Bulletin, 127, 704-716.

Kubota, M. (1994). A Mechanism for the Accumulation of Floating Marine Debris North of Hawaii. Journal of Physical Oceanography, 24(5), 1059–1064.

Laist, D. W. (1987). Overview of the biological effects of lost and discarded plastic debris in the marine environment. Marine Pollution Bulletin, 18(6), 319–326.

Law, K. L., Morét-Ferguson, S. E., Goodwin, D. S., Zettler, E. R., DeForce, E., Kukulka, T., & Proskurowski, G. (2014). Distribution of Surface Plastic Debris in the Eastern Pacific Ocean from an 11-Year Data Set. Environmental Science & Technology, 48(9), 4732–4738.

Law, K. L., Starr, N., Siegler, T. R., Jambeck, J. R., Mallos, N. J., & Leonard, G. H. (2020). The United States' contribution of plastic waste to land and ocean. Science Advances, 6(44), eabd0288.

Lebreton, L., & Andrady, A. (2019). Future scenarios of global plastic waste generation and disposal. Palgrave Communications, 5(1), 6.

Lebreton, L., Egger, M., & Slat, B. (2019). A global mass budget for positively buoyant macroplastic debris in the ocean. Scientific Reports, 9(1), 12922.

Lebreton, L., Slat, B., Ferrari, F., Sainte-Rose, B., Aitken, J., Marthouse, R., Hajbane, S., Cunsolo, S., Schwarz, A., & Levivier, A. (2018). Evidence that the Great Pacific Garbage Patch is rapidly accumulating plastic. Scientific Reports, 8(1), 1–15.

Lebreton, L., Van Der Zwet, J., Damsteeg, J.-W., Slat, B., Andrady, A., & Reisser, J. (2017). River plastic emissions to the world's oceans. Nature Communications, 8, 15611.

Maximenko, N., Hafner, J., & Niiler, P. (2012). Pathways of marine debris derived from trajectories of Lagrangian drifters. Marine Pollution Bulletin, 65(1), 51–62.

Maximenko, N., Hafner, J., Kamachi, M., & MacFadyen, A. (2018). Numerical simulations of

debris drift from the Great Japan Tsunami of 2011 and their verification with observational reports. Marine Pollution Bulletin, 132, 5–25.

Miron, P., Beron-Vera, F. J., Helfmann, L., & Koltai, P. (2021). Transition paths of marine debris and the stability of the garbage patches. Chaos: An Interdisciplinary Journal of Nonlinear Science, 31(3), 033101.

Moore, C. J., Moore, S. L., Leecaster, M. K., & Weisberg, S. B. (2001). A Comparison of Plastic and Plankton in the North Pacific Central Gyre. Marine Pollution Bulletin, 42(12), 1297–1300.

Morishige, C., Donohue, M. J., Flint, E., Swenson, C., & Woolaway, C. (2007). Factors affecting marine debris deposition at French Frigate Shoals, Northwestern Hawaiian Islands Marine National Monument, 1990–2006. Marine Pollution Bulletin, 54(8), 1162–1169.

National Marine Sanctuaries, NOAA. (2020). *Welcome to Papahānaumokuākea Marine National Monument – Where Nature and culture are one*. Papahānaumokuākea Marine National Monument. Retrieved February 23, 2022, from https://www.papahanaumokuakea.gov/about/

Pichel, W. G., Churnside, J. H., Veenstra, T. S., Foley, D. G., Friedman, K. S., Brainard, R. E., Nicoll, J. B., Zheng, Q., & Clemente-Colón, P. (2007). Marine debris collects within the North Pacific Subtropical Convergence Zone. Marine Pollution Bulletin, 54(8), 1207–1211.

Qiu, B., & Chen, S. (2005). Variability of the Kuroshio Extension Jet, Recirculation Gyre, and Mesoscale Eddies on Decadal Time Scales. Journal of Physical Oceanography, 35(11), 2090–2103.

Ribic, C. A., Sheavly, S. B., & Klavitter, J. (2012). Baseline for beached marine debris on Sand

Island, Midway Atoll. Marine Pollution Bulletin, 64(8), 1726–1729.

Ribic, C. A., Sheavly, S. B., Rugg, D. J., & Erdmann, E. S. (2012). Trends in marine debris along the US Pacific Coast and Hawai'i 1998–2007. *Marine Pollution Bulletin*, *64*(5), 994-1004.

Roden, G. I. (1975). On North Pacific Temperature, Salinity, Sound Velocity and Density Fronts and their Relation to the Wind and Energy Flux Fields. Journal of Physical Oceanography, 5(4), 557–571.

Suka, R., Huntington, B., Morioka, J., O'Brien, K., & Acoba, T. (2020). Successful application of a novel technique to quantify negative impacts of derelict fishing nets on Northwestern Hawaiian Island reefs. Marine Pollution Bulletin, 157, 111312.

Teuten, E. L., Saquing, J. M., Knappe, D. R. U., Barlaz, M. A., Jonsson, S., Björn, A., Rowland, S. J., Thompson, R. C., Galloway, T. S., Yamashita, R., Ochi, D., Watanuki, Y., Moore, C., Viet, P. H., Tana, T. S., Prudente, M., Boonyatumanond, R., Zakaria, M. P., Akkhavong, K., … Takada, H. (2009). Transport and release of chemicals from plastics to the environment and to wildlife. Philosophical Transactions of the Royal Society B: Biological Sciences, 364(1526), 2027–2045.

Therriault, T. W., Nelson, J. C., Carlton, J. T., Liggan, L., Otani, M., Kawai, H., Scriven, D., Ruiz, G. M., & Clarke Murray, C. (2018). The invasion risk of species associated with Japanese Tsunami Marine Debris in Pacific North America and Hawaii. Marine Pollution Bulletin, 132, 82–89.

Thevenon, F., Carroll, C., & Sousa, J. (editors), (2014). Plastic debris in the ocean: the characterization of marine plastics and their environmental impacts, situation analysis report. Gland, Switzerland: IUCN. 52 pp.

Timmers, M. A., Kistner, C. A., & Donohue, M. J. (2005). Marine Debris of the Northwestern Hawaiian Islands: Ghost Net Identification (Sea Grant Publication UNIHI-SEAGRANT-AR-05-01; p. 31). US Department of Commerce, National Oceanic and Atmospheric Administration, National Marine Fisheries Service, Pacific Islands Fisheries Science Center, University of Hawaii Sea Grant College Program, Joint Institute for Marine and Atmospheric Research, School of Ocean and Earth Science Technology.

Titmus, A. J., & David Hyrenbach, K. (2011). Habitat associations of floating debris and marine birds in the North East Pacific Ocean at coarse and meso spatial scales. Marine Pollution Bulletin, 62(11), 2496–2506.

Uhrin, A. V., Walsh, W. A., & Brodziak, J. (2020). Relative abundance of derelict fishing gear in the Hawaii-based pelagic longline fishery grounds as estimated from fishery observer data. Scientific Reports, 10(1), 7767.

United States Environmental Protection Agency, & Busterud, J. W. (2020). EPA Review of Hawaii's 2018 Section 303(d) List Supplemental Submission. Center for Biological Diversity. November 2020. https://www.biologicaldiversity.org/programs/oceans/pdfs/HI-303d-List-Suplemental-Submission-EPA-Response.pdf

Van Sebille, E., Aliani, S., Law, K. L., Maximenko, N., Alsina, J. M., Bagaev, A., Bergmann, M., Chapron, B., Chubarenko, I., & Cózar, A. (2020). The physical oceanography of the transport of floating marine debris. Environmental Research Letters, 15(2), 023003.

Young, L. C., Vanderlip, C., Duffy, D. C., Afanasyev, V., & Shaffer, S. A. (2009). Bringing home the trash: do colony-based differences in foraging distribution lead to increased

plastic ingestion in Laysan albatrosses?. *PloS one*, *4*(10), e7623.

2020 State of Papahānaumokuākea Marine National Monument Report| Office of National Marine Sanctuaries. (2020). Sanctuaries.noaa.gov. April 7, 2022. https://sanctuaries.noaa.gov/science/condition/pmnm/welcome.html

CHAPTER 2

Best practices for sampling floating derelict fishing gear

ABSTRACT

Derelict fishing gear (DFG) is affecting marine environments globally but little is known about the sources of this pollutant. Removal and systematic documentation of DFG composition is challenging due to the size, mass, and complexity of the different types of gear. The objective was to develop best practices for standardized sampling and quantification of derelict fishing gear for future studies around the world. In total, we collected and sampled 160 unique DFG events totalling over 14.5 metric tons. Six field protocols were developed to address different situations related to DFG type, availability of resources, time, space, data resolution, and research questions. The Weigh and Dispose, Four Corners, One of All, Disentanglement, Hybrid, and Reverse Engineer methods are presented in detail, specifying which protocol applies to certain situations and types of DFG. Additionally, we developed best practices for processing DFG samples in the laboratory, and provide our protocols in detail, where over 70 parameters are documented per sample. The Disentanglement method was the most detailed sampling procedure and took more than 12 months to complete a single DFG event. The Hybrid method integrated the speed and simplicity of the Four Corners method, improved sample coverage, and incorporated some disentanglement of larger samples, if time allowed. Because there was such a dramatic increase in time and resource utilization with the disentanglement method, we compared the results of one event, MID_04, that was first sampled with the Hybrid method, then sampled with the Disentanglement method. The two protocols yielded samples with different compositions. When these results were compared to the most accurate assessment of DFG composition from the mass and count of disentangled and sorted gear piles, we found that both the Hybrid and Disentanglement methods introduce substantial sampling biases. However, the

Hybrid method is recommended for most DFG composition assessments, given the efficiency and quality of data resolution.

INTRODUCTION

Derelict fishing gear (DFG) makes up 52% of floating plastic debris in the North Pacific ocean by mass (Lebreton et al., 2018). Little is known about the source polluters of DFG, such as which fisheries are losing or discarding their gear and the reasons behind these incidents, as well as which manufacturers produce the gear (Gilman et al., 2021). There are several ecological impacts of DFG on marine ecosystems including marine mammal entanglement (Bradford & Lyman, 2015), coral reef damage (Suka et al., 2020), ghost fishing (Gilman et al., 2016), and the transportation of invasive species (Therriault et al., 2018). Fishing and maritime vessels are also victims of the impacts of DFG with substantial economic costs. As a result, sourcing DFG back to the origin fisheries is needed to reduce the impacts and prevalence of this anthropogenic pollutant.

Few studies have been up to the task of DFG forensics. The World Wide Fund (WWF) for Nature Australia published *The net kit: A fishing net identification guide to North Australia* in 2004, which is a comprehensive resource of derelict fishing nets found in northern Australia and the Indo-Pacific region (White, Hamilton, Cook, 2004). This net kit was produced in response to concerns of volume of debris accumulating (~56 nets per km of coastline), the resulting ghost fishing and bycatch of whales, marine mammals and turtles, and hindrance to indiginous fishing efforts raised by Aboriginal traditional landowners in northeast Arnhem Land, Northern Territory, Australia. The North Australian guide provides photos and identification characteristics of 186 unique nets common to the region, including color, mesh size, twine diameter, and number of strands, to be matched with nets in the field. They worked with fishing gear technologists to identify the net function, fishery source, and suspected country of origin for the 186 nets in their guide. The most common net types they found were trawl nets, followed by

single monofilament gillnet, and the common suspected source countries were Taiwan, Indonesia, Korea, Thailand, Australia, India, Philippines, Japan, and China (in no particular order). This tool is very useful for field identification and documentation, but it should be mentioned that the photos of the nets are of indistinguishable resolution and the guide may need to be updated as it is now two decades old. Nonetheless, this net kit served as a milestone for marine debris research, monitoring, mitigation, and collaboration with indigenous cultures to protect natural resources. A similar effort was put forth in Hawai‘i around the same time, which we will describe in more detail later in this section.

Jumping to the Arctic Ocean, a recent relevant work that we used to develop our methods was *Svalbard Beach Litter Deep Dive*, authored by Falk-Andersson & Strietman in 2019. This report also partnered with a fishing gear technologist and other fisheries experts to source DFG by hosting deep-dive workshops with fishermen and gear technologists. Using this approach, they predicted that approximately 90% of the DFG analyzed was intentionally discarded instead of accidentally lost, and the majority of the derelict nets belonged to the bottom trawling fisheries, shrimp and whitefish, local to the Barents Sea.

Most applicable to our study, Sea Grant at the University of Hawai‘i and the National Marine Fisheries Service published *Marine debris of the Northwestern Hawaiian Islands: Ghost Net Identification* in 2005 (Timmers, Kistner, Donohue, 2005, Donohue, 2004). This study collected and analyzed 250 derelict fishing nets removed from the coral reefs of the Northwestern Hawaiian Islands from multi-year seasonal debris remediation efforts from 1998 to 2004. Net samples were analyzed by a panel of experts that included fishing vessel owners, fishermen, and net manufacturing industry representatives as well as a fishing net specialist from the NOAA Alaska Fisheries Science Center to predict the net type, fishery, and country of

manufacturer. The most common net type was trawl/seine, and a smaller number of single monofilament and multifilament gillnets. The most common suspected fisheries included shrimp, small fish, bottom fish, swordfish or shark, sardines or anchovies, baitfish, North Pacific pollock, crustaceans, and lobster (in no particular order). The most common suspected countries of gear manufacture included China, India, Singapore, South Korea, Japan, Taiwan, India, South America, Malaysia, and Europe or USA (in no particular order). This interdisciplinary and multi-agency effort is impressive and valuable, however, for most nets analyzed source fishery could not be confidently identified and were labeled "undetermined," and there were not high levels of confidence for the country of manufacturer for most nets. Their protocol included several net metrics, including net type, mesh stretch, twine diameter, twine construction, and color. We adopted these metrics for our protocol, and added major modifications to create modern best practices. We added 1) collecting metadata on each DFG event, 2) tracking which DFG event each gear sample came from, 3) including gear besides nets, 4) documenting gear configurations of multiple gears, 5) disentangling some nets and measuring full sizes, 6) documenting the fiber type of each sample, and 7) identifying plastic polymers of each gear using attenuated total reflection Fourier-transform infrared (ATR FT-IR) spectroscopy (Jung et al., 2018). We believe our novel robust approach will improve the accuracy of sourcing DFG back to the source fisheries and manufacturers.

Figure 2.1. The four primary DFG categories that were encountered, sampled and analyzed using the methods described in this document include distinct net (A), conglomerate (B), drifting fish aggregating device (C), and line (D) (See Glossary).

DFG comes in many forms, shapes, and sizes. Common DFG event types we encountered in Hawai‘i during our study period of October 2019 to December 2021 included Distinct Nets (A), Conglomerates (B), drifting Fish Aggregating Devices (dFAD) (C), and Line (D) (Figure 2.1). Here, we present a field and lab guide for sampling different types of DFG. For the sake of these protocols, we define the term *DFG event* to refer to any type of DFG that was recovered at a specific location and time, as a single mass of gear either constructed or entangled together. We designed and implemented six novel field protocols and a robust lab protocol to analyze DFG. We discuss the tradeoffs to each protocol to help others choose a protocol for their purpose. Decisions will be based on the DFG event type, gear types of interest, available labor, equipment and space, the research questions, and the data resolution needed to answer those questions. We assessed the effectiveness of each protocol based on time, space, and personnel requirements,

applicable DFG types and situations, number of samples, and data resolution. Our goal was to develop the most efficient method for sampling DFG without compromising data resolution.

METHODS

I. Data hierarchy and storage

The database for this project was created in the cloud-based data service Google Drive, and the metadata was organized in a Google Sheet with multiple tabs so that multiple team members could access, collaborate, and enter data simultaneously (See Data Dictionary at https://docs.google.com/spreadsheets/d/e/2PACX-1vTMVAQlJ1hQmIVByZtonQwGKIKdER8sGz52LJCDQLIYXBF4p67IF--37fdWJfkZs0d16Go1St-zjdf9/pubhtml to create your own database). The file was developed to capture information and data on four different levels (Figure 2.2). The first tab contains data from the highest level, the DFG events. The second tab contains data on the next three levels: samples, subsamples and components. See the Data Dictionary and the glossary for definitions of these terms and levels. In the second tab, the data related to the sample level were reported on the first row for that sample and related to the event ID through a unique identification scheme (Figure 2.3). Subsequent rows described subsamples, and component rows were inserted for each subsample. A list of data fields for the event level, and sample to component level is provided in the Data Dictionary. Photos were stored in a well organized and labeled folder structure by DFG event. Subfolders included discovery and removal, five sides, field configurations, field sample photos, and lab sample photos.

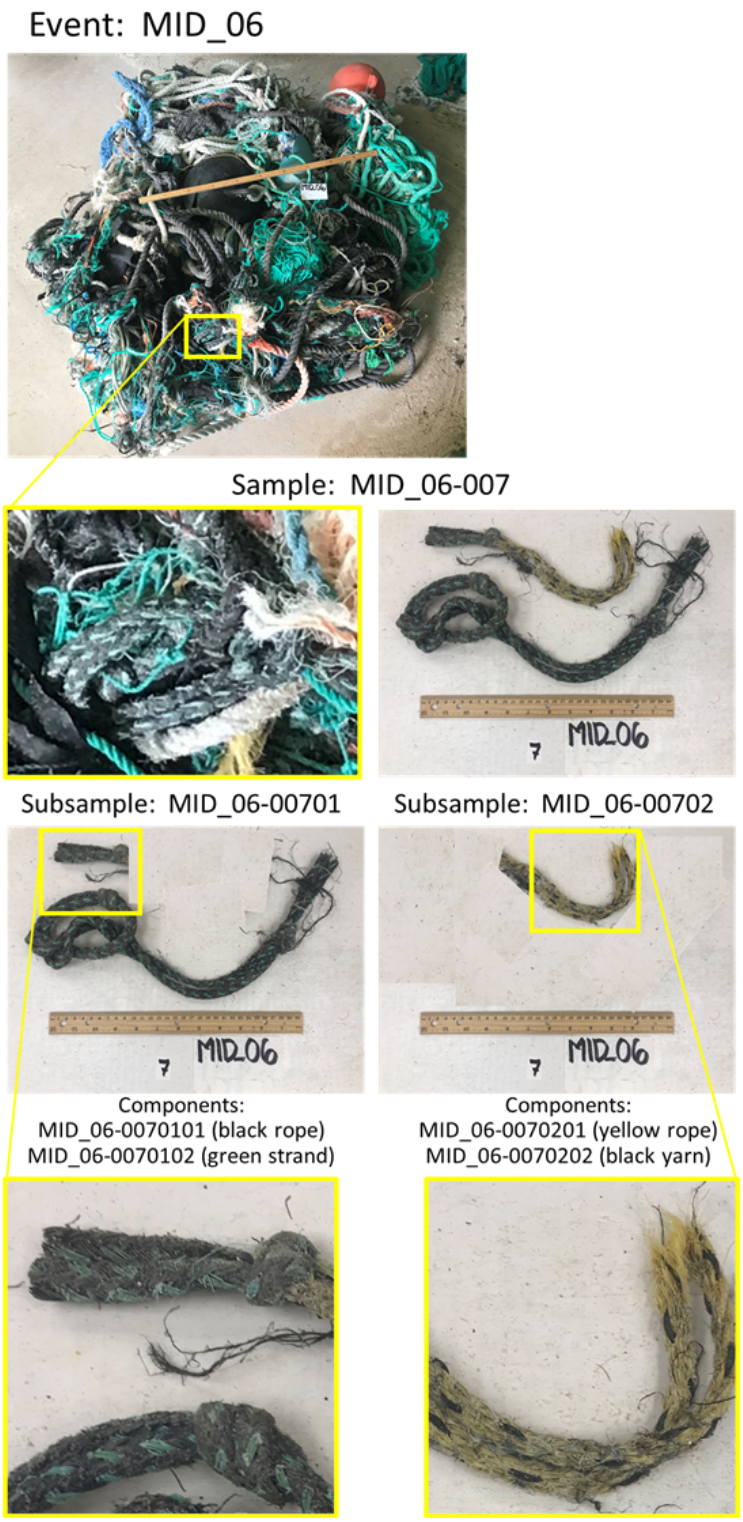

Figure 2.2. An example of DFG to explain the four levels in the data hierarchy: event, sample, subsample, components.

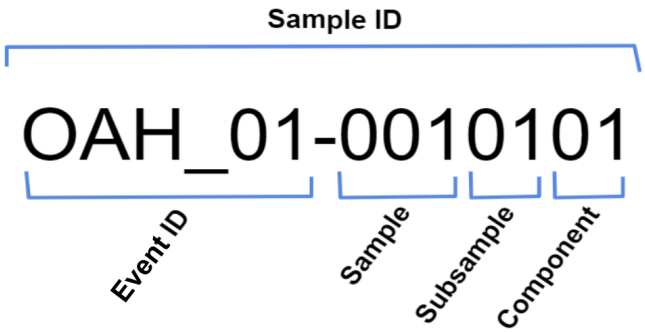

Figure 2.3. Unique sample identification scheme that indicates event ID, sample number, subsample number, and component.

II. Field Sampling Supplies

A supply list is provided here:

- ☐ Gloves (Showa Atlas Fit 300)
- ☐ Sunscreen, drinking water, insect repellent
- ☐ Closed-toed shoes
- ☐ Knives (Dexter 15403 3.25 in net/line knife)
- ☐ Bright duct tape (Green Duck Tape)
- ☐ Sharpie markers
- ☐ Scissors
- ☐ Waterproof paper (Terra Slate 8.5x11 inch 5 mil)
- ☐ Datasheets
- ☐ Pens and pencils
- ☐ Meter sticks (Westcott, made of wood)
- ☐ Measuring tape (Forestry Suppliers Inc, Jackson, MS)
- ☐ Table and chairs
- ☐ Portable flood lights
- ☐ Extension cords
- ☐ Industrial air movers
- ☐ Chain-fall
- ☐ Engine hoist (Power Torque PT34786 2-ton capacity)

- ☐ Crane Scale (CE OCS-S High Resolution Digital Crane Scale 1000 kg)
- ☐ Calibration weights (Troemner 1 pound to 10 pounds; 30 pounds total)
- ☐ Repurposed plastic bags from household goods (e.g. bread bags, zippered bags,)
- ☐ Large thick trash bags for all samples from each event (ideal if used and repurposed)
- ☐ Broom and dust pan
- ☐ Buckets for sand
- ☐ Trash can and bag

III. Field sampling protocols

This section provides an overview of the event level data collection methods, as well as each of the six sample collection protocols, in order of data resolution from least to most detailed. A summary of all six protocols, what types of DFG events they can be applied to, estimated sampling time, number of samples collected, space required, and number of personnel recommended is provided in Table 2.1. Sampling steps that are common to all protocols are outlined in section V. Field Protocol Commonalities. Then, the sampling steps that are unique to each individual protocol are described in their respective section.

Table 2.1. Summary of DFG event sampling protocols and applications.

Parameter	Description	Protocols					
		Measure & Dispose	Four Corners	One of All	Hybrid	Disentangle	Reverse Engineer
Applicable situation	Time and/or resources are extremely limited.	X					
	Event must be sampled on site before rapid disposal, and few people are available.		X				
	Time allows for sampling of small events or large events with few gear types present.			X			
	When space allows for spreading out the event, but time is too limited for the Disentanglement protocol				X		
	Research questions require a thorough analysis of gear types and proportions.					X	
	When time allows a thorough dissection and measuring of a unique event.						X
DFG event type	Conglomerates that were only partially removed, cut into many pieces during removal, or mass < 45 kg.	X					
	Conglomerates		X	X	X	X	
	Distinct Nets or Lines			X		X	X
	Drifting Fish Aggregating Devices, other unique DFG events						X
Data resolution	Documents DFG event frequency, types, and mass.	X	X	X	X	X	X
	Ensures that DFG is disposed of in the most sustainable way possible.	X	X	X	X	X	X
	Provides balanced sample coverage across the event sections and with limited labor time.		X	X	X		
	Estimates the mass of samples and proportions of gear categories.		X	X	X		
	Provides 100% sample coverage.			X			X
	Disentangles larger samples and documents mass, size, and configurations.				X		
	Provides the greatest sample coverage for large DFG conglomerates.					X	
	Disentangles, sorts, and records full size, shape, connections and configurations of all gear.					X	X
	Documents exact mass of gear categories by sorting into piles and weighing each pile.					X	X
	Documents all aspects of DFG event construction.						X
Sampling time (hours)		0.5	2 - 6	2 - 6	4 - 16	several weeks	4 - 16
Personnel		2	2	2	2	10 +	2
Space (sqft)		100	100	100	225	2500	225
Maximum number of samples		0	80	≤ 80	80	> 800	event dependent

IV. DFG event metadata and preliminary measurements:

Metadata and preliminary measurements are recorded for each DFG event before any sampling protocol is initiated. Field data sheets for DFG event measurements, Hybrid method, and Disentanglement method are provided in Appendix 1 and 2. Metadata can be recorded on site during removal, and the preliminary measurements can be taken after the DFG event has dried for at least three days.

1. Record date, time, location (latitude/longitude) discovered, as well as date, time and location of removal. Note removal partners and storage/sampling location of the event.
2. Record the DFG event type (Figure 2.1) and general observations of the event before subsampling begins: What stands out? What types of gear are included? What is the orientation and configuration of interesting features? Initial hypotheses of gear sources?
3. Measure the DFG event:
    a. Length (straight line longest dimension), width (straight line widest dimension perpendicular to the length axis), maximum height, approximate average height, and circumference.
    b. Visually estimate the total weight of dry material (optional to gauge participants ability to estimate mass).
4. Photograph all four sides and the top of the DFG with a ruler in each photo for scale, and the event ID label, as shown in Figure 2.4.
    a. For dFAD rafts, flip over and take a bottom photo as well.

Figure 2.4. Example of the standardized five photos of a conglomerate DFG event. The bottom image is a top view of the DFG event. A meterstick scale bar and DFG event ID tag are in each photo.

5. Measure the dry weight of the DFG event. Ideally, allow it to dry for three days or more. Weigh the entire dry DFG event using a crane scale on an engine hoist or chain fall. If it is too large to weigh all together, try to disentangle it into sections. Cut the event into sections only if necessary along the weakest connections and mark with bright tape all manipulations. Weigh each separated section and record the sum of weights. Before weighing, check the accuracy of the scale with calibration weights from 1 lb to 30 lbs, and record the readings in the scale's calibration log.

6. Remember to record the disposal mechanism and partners at the end of processing in the database.

V. Field Protocol Commonalities

The particular steps that are identical regardless of field protocol are described here and referenced within each detailed protocol below. Protocol commonalities include the steps necessary to collect, document and store the samples.

1. Collect samples from the DFG event using a sharp knife. Different types of gear require different sampling techniques.
    a. *Net:* sample a portion that contains at least 3 x 3 rounds, so that a 'square' of nine total rounds of netting is obtained (Figure 2.5).

Figure 2.5. One round of mesh in a net outlined in blue.

    b. *Line:* cut a sample approximately 30 cm long.
        i. If less than 30 cm is available, remove the whole sample.
        ii. If there is a unique feature about the line (*e.g.* tied in a unique knot, spliced with another type of line, configurations, or has metal attached)

make sure that feature is included in the sample (Figure 2.6). Exceed 30 cm if necessary.

Figure 2.6. Line samples that include interesting features or multiple gear associations.

c. *Other types of gear:* Remove the entire sample if necessary and record what type of gear it is and include associated connections and configurations.

2. Record the sample number and categorize the gear according to the key (Table 2.2). If a sample is composed of multiple materials or gear types, classify it as “multiple” and list the gear types as subsamples on the datasheet in order of largest to smallest volume.

Table 2.2. Categories of DFG samples.

Gear Class Key	
(M)	Multiple (when sample contains more than 1 gear item)
(N)	Net
(L)	Line / Rope
(ML)	Monofilament Line
(B)	Buoy - navigational marker, instrumentation, or mooring
(SAT)	Tracker - satellite tracker for FADs, nets or gear
(FL)	Float - used to hold fishing gear higher in water, not always foam
(FO)	Foam item / fragment
(HP)	Hard Plastic item / fragment - specify
(ST)	Plastic package strapping
(SH)	Sheet plastic bag / film / tarp
(W)	Wood - organic matter
(MT)	Metal gear / hook / lure / jig
(MS)	Plastic mesh screen, sometimes HP; not weived net
(O)	Other - specify

3. Complete all metadata for each sample and subsample (See Data Dictionary).

    a. Record the color of each sample or subsample (Table 2.3). This is the original color of the item. If an item is faded or fouled, look between the strands, or use a knife to cut into it to see the original color on the interior. If an item is multicolored, classify it as 'multiple' and record the dominant color in the notes on the datasheet, which will be entered into the "primary color" column in the database.

    b. Estimate the percent sampled from the total amount of that gear present in the DFG event. To estimate this effectively, consider the total length for lines and surface area for nets and other gear, or use simple ratios when cutting samples (1/2, 1/3, 1/4, 1/5, 1/10, 1/20, 2/100, 1/100). If the sample has subsamples, record the percent sampled for each subsample separately on the datasheet.

    c. Assign a biofouling rating of 0 to 3 for each sample and subsample (Table 2.4).

    d. Record in the notes on how each sample was connected to the rest of the event mass, and any other interesting features. This information assists identifying and categorizing samples in the lab.

        i. How is it attached / incorporated into the event mass?

        ii. What other gear types does it attach to?

        iii. Describe and sample marine organisms attached or entangled (shellfish, sponges, crabs, fishes, bones of organisms).

Table 2.3. Standardized colors assigned to DFG samples.

Acceptable Colors	
Blue	
Green	
White	
Black	
Grey	
Clear	
Red	
Pink	
Orange	
Yellow	
Brown	
Purple	
Silver	

Table 2.4. Biofouling key.

Biofouling Key		
code	Description and image	% cover
0	No biofouling. 	0%
1	Light biofouling. 	1 - 40%
2	Moderate biofouling. 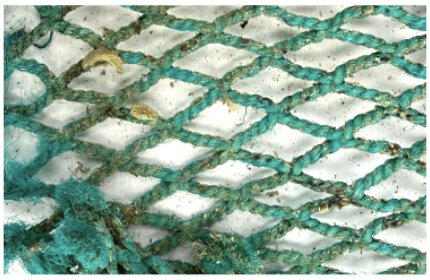	41 - 75%
3	Heavy biofouling. 	> 75%

4. If possible, lay out the samples in ascending order with their sample labels on a clean floor space. This helps to keep track of what has and has not been sampled.
5. Consider taking preliminary sample photos for future reference in the laboratory. Upload photos to the appropriate labeled folder on Google Drive.
6. Bag each sample into a reused plastic bag with its sample number label included in the bag. Label the outside of the bag with its sample number. Seal each sample bag and place it into a larger bag that is labeled with the event ID in bright tape. Seal the large bag. Transport samples to the lab for further analysis.
7. The rest of the DFG event is free to dispose of in the most sustainable means available.
8. Photograph field datasheets (even if these are not the final version) and upload them along with the sampling photos to the appropriate Google Drive folder at the end of each day.
9. Enter data from field data sheets into the Google Sheet database (as defined in the Data Dictionary).
10. Photograph the final datasheet after all samples are collected and upload it to Google Drive. Then, scan all datasheets and upload the scanned files to Google Drive. File the physical datasheets in a filing cabinet.

1. Measure and Dispose Protocol

This protocol records only the DFG event metadata and preliminary measurements described in the methods section IV, and does not include the collection of samples. Once the preliminary DFG event data is collected, the event is disposed of by the most sustainable means available.

2. Four Corners Protocol

This protocol allows the sampling of up to 80 gear items per DFG event by dividing the event into four equal sides (Figure 2.7) and collecting 20 samples from each side. The event is not moved, flipped, or manipulated during the sample collection.

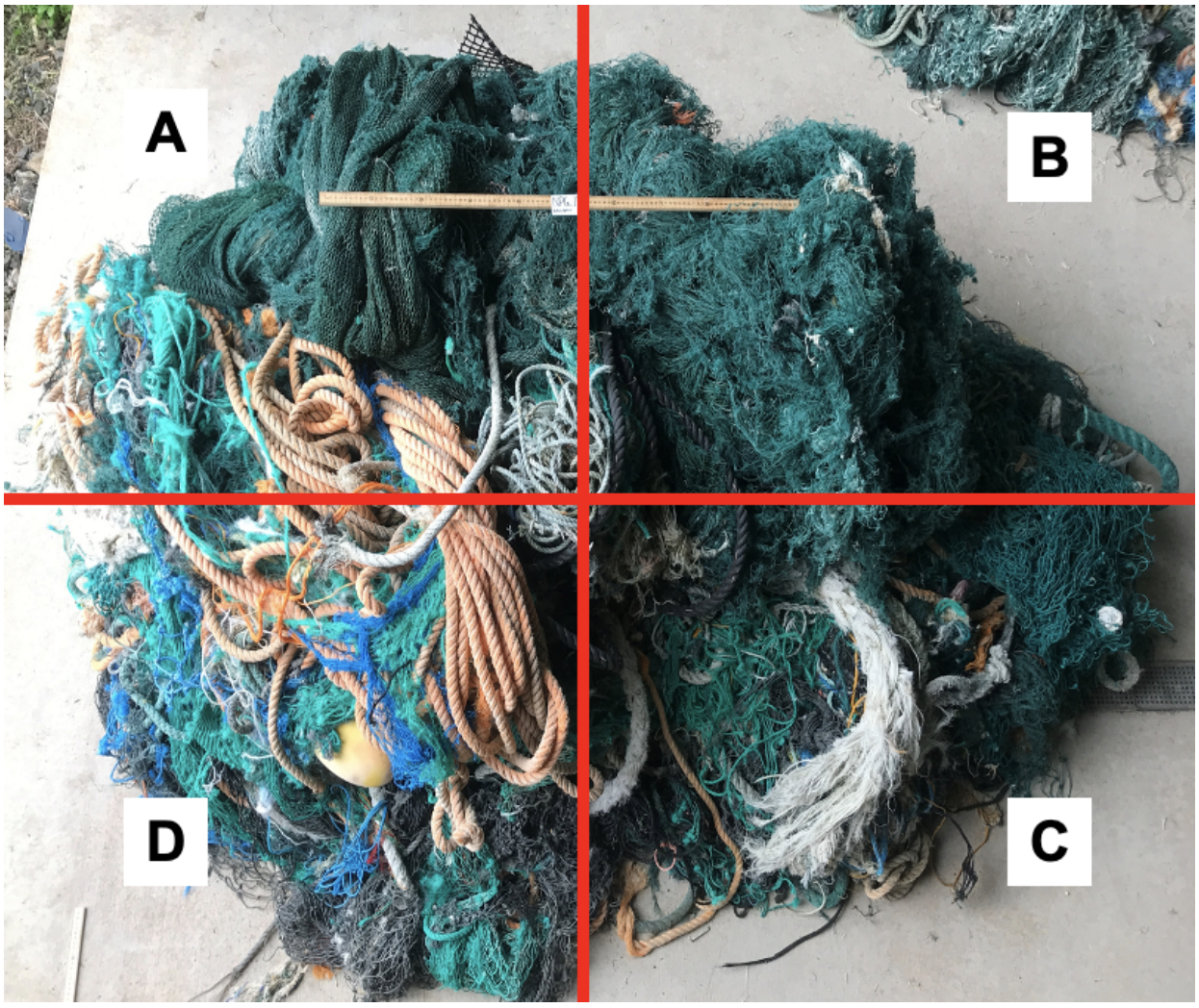

Figure 2.7. Diagram describing the Four Corners DFG sampling protocol.

Protocol specific steps:

1. Visually divide the DFG event into four equal sections with imaginary borders.

2. Collect samples. Use a sharp knife to remove one piece of every different type of material, up to 20 samples from each section. Bias collection of samples to the largest gear by volume in the whole event and section, unique items, and gear with configurations or markings. Each gear item should only be sampled once, even if it is present in multiple sections.
3. Record the section that the sample was removed from (A, B, C, or D).
4. Visually estimate and record the percent by volume of gear that was not sampled in each section (this step was not used in our current study, but is recommended for future use).

For all other sampling steps, refer to the methods section *V. Field Protocol Commonalities.*

3. One of All Protocol

This protocol collects a sample of every piece of gear in a DFG event, providing 100% sample coverage, and is ideal for smaller events that have less than 80 unique pieces of gear. More than 80 samples can be collected if necessary.

Figure 2.8. This figure shows a smaller DFG event on the left that was sampled with the One of All method. On the right is one sample of each type of gear from the DFG event.

Protocol specific steps:

1. Collect one sample of each piece of gear.
2. For all other sampling steps, refer to the methods section *V. Field Protocol Commonalities.*

4. Hybrid Protocol

This protocol is a synthesis of the Four Corners method and the Disentanglement method. The DFG event is spread out before dividing it into sections that contain different types of gear, which offers greater visibility of the different gear types and configurations. Up to 80 samples are collected from each DFG event. This protocol encourages the disentanglement of large samples to record the measurements and weights of an entire gear piece.

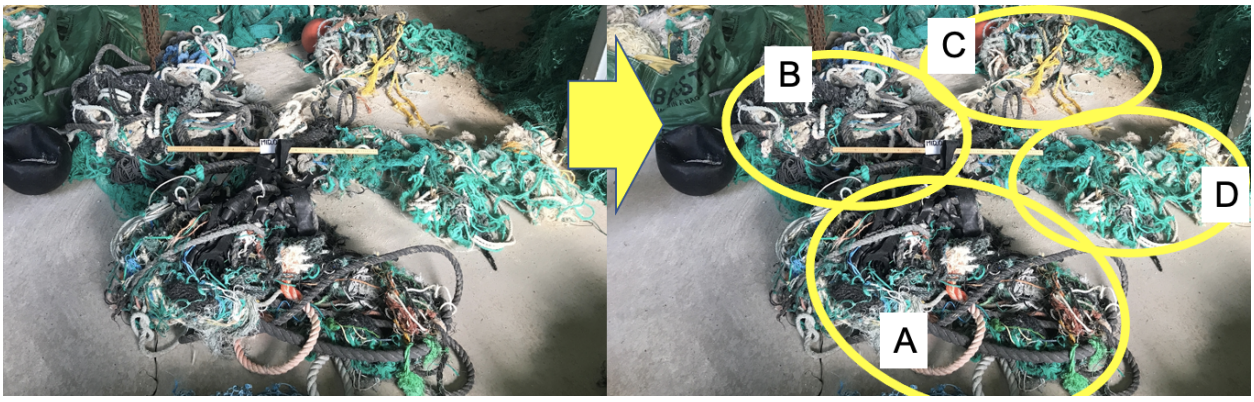

Figure 2.9. This figure shows a DFG event that was sampled using the Hybrid method. The event was spread apart into sections, as shown on the right.

Protocol specific steps:

1. Spread the DFG event out and loosen up the bundle. Ideally, separate the bundle into sections that have different, distinct gear types that are not intentionally tied together. Designate sections to balance out sample coverage. It is recommended to designate four relatively equal sections; however, this depends on the size and composition. Some events might only be divided into two sections, or one very large gear type may be designated as its own fifth section.
2. Take a photo of the spread-out event and the designated sections before sampling and sketch the event on the datasheet marking each section (A, B, C, or D).

3. Ideally, collect 20 samples from each of the four sections. If a section has less than 20 unique gear items, collect more samples from other sections that have more than 20 unique gear items. If there are less than four designated sections, still collect 80 samples total, allocated in a way to optimize sample coverage.
4. Start by sampling the largest gear items in the event. If time allows and it is feasible, disentangle these larger items to measure length, width, mass, and take photos of the whole gear before cutting a sample.
5. For all other sampling steps, refer to the methods section *V. Field Protocol Commonalities.*
6. Visually estimate and record the percent by volume of each section that was not sampled, and the total percent by volume not sampled of the whole DFG event.

5. Disentanglement Protocol

This protocol dissects DFG events and sorts the contents into distinct piles by gear category (Figure 2.10 & 2.11). Each pile is measured, weighed, photographed, and sampled. Up to 100 samples are collected from each pile. Each sampled gear item is laid out, measured, photographed, and weighed individually.

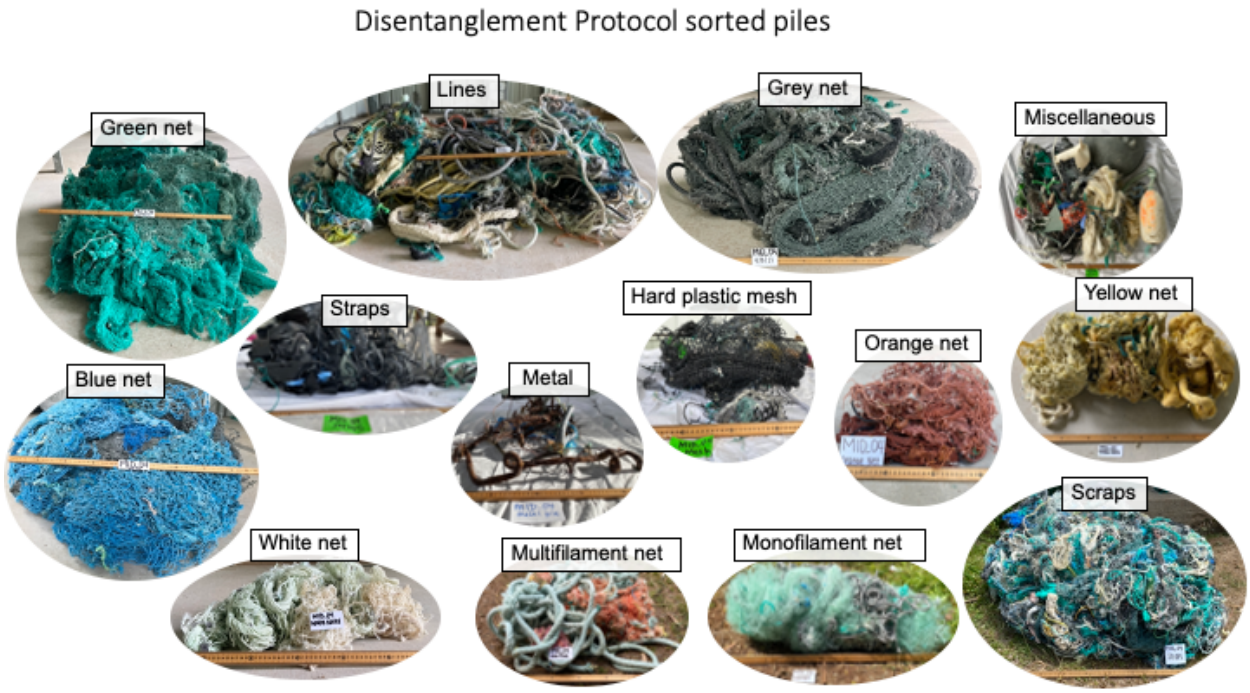

Figure 2.10. Diagram of the individual piles of gear types expected from a disentangled conglomerate.

Protocol specific steps:

1. Work in a team to disentangle the net mass without cutting anything. If items are intentionally tied together, keep them together to understand the gear function or the intention.
2. Sort the gear into piles by category: Green net, grey net, blue net, white net, yellow net, orange/red net, multifilament net, monofilament net, line (rope), hard plastic mesh, straps, metal, miscellaneous, and scraps (see Glossary).

3. Collect the preliminary measurements of the sorted piles: length, width, maximum height, approximate average height, circumference, and mass.

4. Take photos of the five sides of the sorted pile, including a meter stick for scale and the event ID_pile ID label.

Figure 2.11. A grey net pile being sorted into largest to smallest gear and matching like items to each other.

5. Starting with one pile, sort the gear items individually and organize them across the floor from the largest to the smallest (Figure 2.11). While doing so, match identical gear together that may have been cut, ripped, or separated at sea or during the disentanglement.

    a. The following considerations were used to determine net matches:

        i. Twine diameter and construction match (twist direction or braid).

ii. At least three meshes stretched in the Normal (N) direction are equal (Figure 2.22; Vincent et al., 2020).

iii. Mesh stretch is oriented the same way.

iv. Color is very similar, if not identical.

b. Consider the following nuances/assumptions when determining a match:

i. Different parts of a net experience different load stresses which can stretch mesh and slip knots differently, which changes mesh size and stretch orientation.

ii. Weathering and sun exposure can change the color of the material.

iii. Fresh cut seams that match up perfectly indicate a true match.

iv. If a net was cut during removal, there should be a perfect match to the cut seam if 100% of the net was removed.

v. Nets that match but do not share a common fresh cut seam or orientation are assumed to have been part of the same net. When a net has been cut into too many pieces, it is very difficult to piece it back together perfectly. Therefore, we assume that the pieces are from the same net and piece them together in a way to capture length and width measurements to understand surface area.

vi. Depending on the size of the pile, if it is over 200 kg it may be necessary to create sub-piles to match like with like more easily. In this case, we recommend the following sub-piles for nets and lines:

1. Large mesh, thick twine
2. Large mesh, thin twine

3. Small mesh, thick twine
4. Small mesh, thin twine
5. Knotless nets
6. Lines: by color and diameter

6. Count the total number of items within a pile with a clicker counter and record.
7. Collect up to 100 samples from each pile. Choose samples by:
    a. 50 largest samples by volume
    b. 25 unique samples
        i. Marked gear
        ii. Multiple gear types intentionally connected
        iii. Multiple different types of nets that are connected
        iv. Gear that has never been seen before or has a different quality to that which is more frequently observed.
    c. 25 randomly selected samples
        i. Count the remaining number of gear items and divide by 25; sample at that interval (i.e. if 500 items remain, 500 / 25 = 20. Select every 20th gear laid out on the floor to sample)
8. Measure and record the mass, length and width of the full gear item before cutting a sample.
    a. If the sample mass is less than the scale can read (< 0.2 kg in our case), then write "<0.2" for the weight on the datasheet and weigh on a more sensitive balance in the lab. Extrapolate the total mass based on percent removed.

b. If there are multiple pieces of the same item, match up the pieces where they were cut and measure the length and width of the whole sample.

c. If pieces cannot be matched perfectly along their cut or ripped sides, then piece them together as best as possible to measure length and width as an approximate surface area for the sample. Make sure that the mesh is oriented in the same direction.

9. While the gear item is laid out fully, take field sample photos. Include a meter stick and label with event_pile_sample number.

    a. For larger gear items, take the photos outside or where there is enough space to spread out the item fully. Use large font on the label to make sure they are visible in the photo. Take a photo from above and several photos from multiple directions, if necessary.

    b. Check the photo quality and make sure the label is visible. Retake if necessary.

    c. Make sure photos get uploaded to the appropriate Google Drive folder the same day.

10. Make sure that at least one piece of every distinct gear is collected as part of the sample (i.e. a patch of net connected to a topline with different twine).

11. When labeling the sample bag, be sure to include the Pile ID.

12. Record the count of items and the total mass of items not sampled from each pile.

13. When entering the field data, add a new row in the event tab for each pile.

14. For all other sampling steps, refer to the methods section *V. Field Protocol Commonalities.*

Protocol 6. Reverse Engineer

This protocol dissects DFG events and documents construction in a way that it can be reconstructed. The goal is to understand the construction of unique DFG events and use this information to source the gear back to fishery. This protocol is presented as applied to dFADs (Figure 2.12) because this was the most common type of DFG sampled with this method. When sampling a complete unique gear item, including dFADs, the whole event is a single sample, since all components are intentionally connected. Therefore, consider each unique piece of gear collected as a subsample.

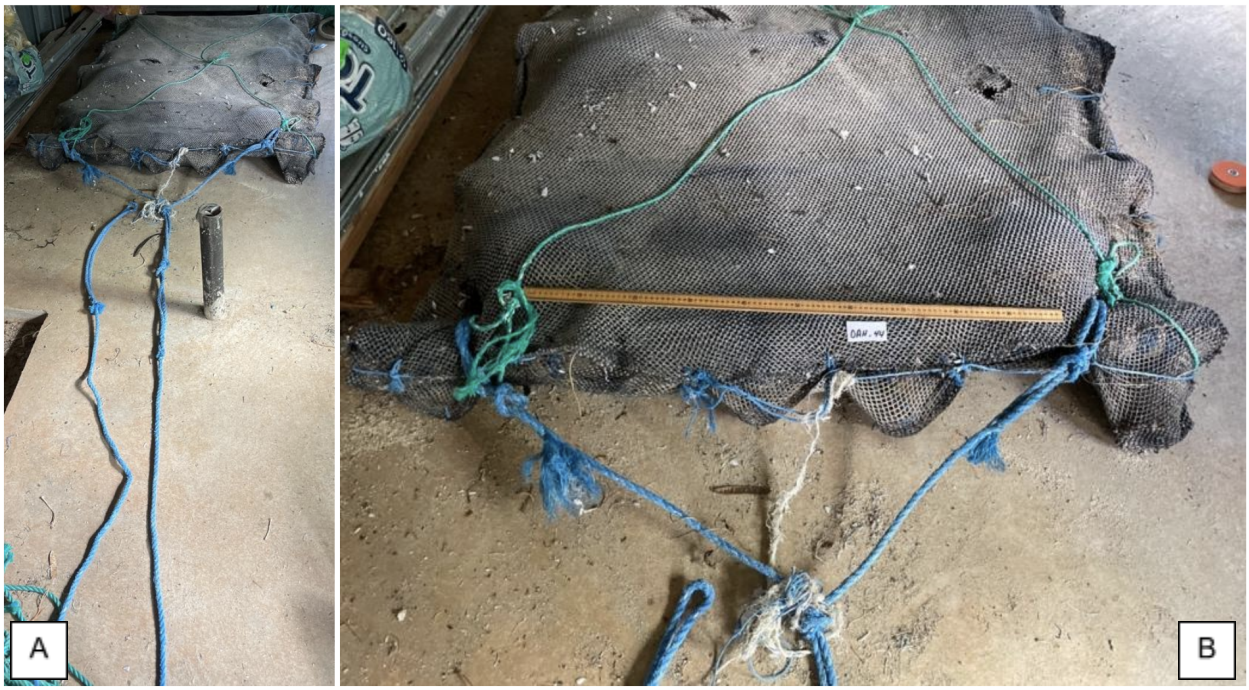

Figure 2.12. Drifting fish aggregating device (dFAD) from the tropical tuna purse seine fishery. A) The blue line makes a bridal and attaches to the SAT buoy that is stretched out to measure the length. B) Close-up of the blue bridal line and green lines created as a pick point to lift the dFAD.

Protocol specific steps (for a dFAD):

1. Carry out the preliminary DFG event measurements and measure additional features of the dFAD, including the drogue (tail) length, the length of the line attaching to the satellite buoy, and other apparent features.
2. Take additional photos of all aspects of the dFAD, including how the drogue and satellite buoy line are attached to the raft, how the web is lashed to the bamboo or pipe, and any other distinguishable features.

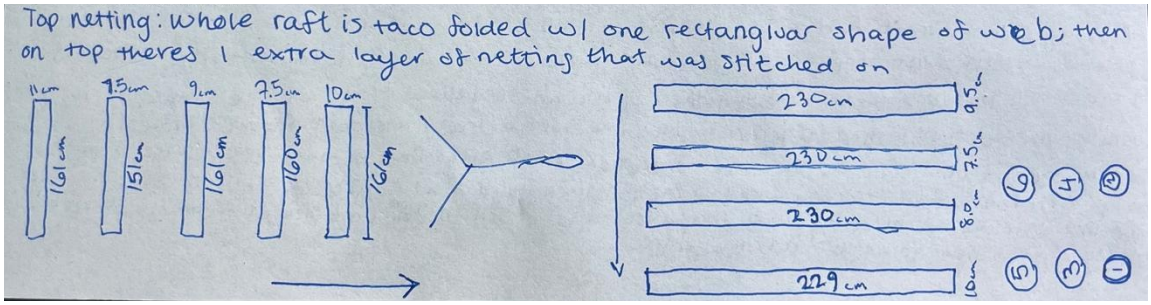

Figure 2.13. An example of a hand drawn diagram of pieces from the dFAD with individual measurements and lay out of construction.

3. Draw a diagram of the dFAD before and throughout the deconstruction process to keep track of everything as it is deconstructed and sampled (Figure 2.13). A dFAD should be deconstructed and sampled in the following order:
    a. SAT buoy
    b. Bridal and line that connects the satellite buoy to the raft
    c. Tail (similar to a drogue or sea anchor) that is attached to the bottom side of the raft (usually two lines of twisted up and lashed net that can extend up to 30+ m with a weight at the bottom).
    d. Net that is wrapping the raft frame.
    e. Bamboo or pipe frame.

f. Floats.

g. Lashing twine.

4. The standard sampling metrics are to be collected for each subsample in the following order:

    a. Color and primary color

    b. Biofouling code

    c. Length and width

    d. Mass

    e. Photos

    f. Percent removed

5. Details on how to sample each gear that makes up a dFAD are provided here:

    a. Sample the SAT buoy. Measure the height and diameter, and mass. Find the serial number, take a photo of it and record it. Record any other writing or markings on the buoy.

    b. Sample the line that attaches to the SAT buoy. Measure the whole length of the line and distance between the knots. Cut the line from the raft and weigh the entire line. If there are multiple lines, cut samples that include the connection points of the various lines.

    c. Sample the tail (if there is one still present). Measure the full length, width, and distance between the knots or sections of netting. If the tail is fully intact, there should be a weighted sea anchor at the bottom and several sections of netting between the raft on the surface to the sea anchor at depth. Measure the length and width of each panel and sea anchor. Cut the whole tail off and weigh each gear

subsample separately, including different types of netting used, and the actual weighted sea anchor.

d. Begin to deconstruct the dFAD raft by cutting all the twine lashing the net to the bamboo or pipe structure of the raft.
    i. Create a pile of all the lashing twine to measure and weigh once deconstruction is complete (Figure 2.14).
    ii. Leave the twine that is lashing the bamboo (pipes) and float to the raft together until step j.

Figure 2.14. Pile of all the lashing twine to be weighed and measured as a bundle.

e. Unwrap the netting off the raft frame.
    i. Weigh the netting.
    ii. Spread the netting out and take a photo with a meter stick for scale, sample number, and the net ID label (Figure 2.15).
    iii. Measure length and width.
    iv. If there are gored seams or sections of netting, measure the length and width of each one.

v. If there are multiple pieces of netting (there are often several layers), check to see if the netting is the same or different. Measure the length and width of each complete layer. If they are different nets (mesh and twine sizes do not match), cut one sample from each of them.

Figure 2.15. The black netting that wraps a dFAD raft laid out to measure.

f. Take photos of the raft frame with the netting removed. Capture images of the twine lashing the raft together, and the floats that are lashed to the frame (Figure 2.16).

Figure 2.16. A photo of a dFAD raft structure after the netting has been removed.

g. Cut all the twine lashing the bamboo / pipes together and the floats. Leave everything in place.

h. Remove each bamboo (pipe) piece one at a time. Assign it a number and record the number on the diagram (Figure 2.13). Measure the length and diameter of each piece. Record the number of bamboo pieces in each direction in the diagram. Weigh the bamboo or pipes, either one by one or all together. Discard or reuse the bamboo, but keep subsamples of any plastic pipes.

i. For floats, measure length, width, and inner diameter of the hole. Check to see if each float is the exact same, or if there are variations, both visually and based on the metrics measured. Take a photo of each float and any logos that are visible. Keep track of what part of the raft each float came from with the diagram and a numbering system. Make sure to collect one of each unique float as subsamples.

j. Last, sample all the lashing twine. If there are multiple types, sample separately. Measure length, width, and mass of each pile.

6. For all other sampling steps, refer to the methods section *V. Field Protocol Commonalities.*

Laboratory Protocols

Once the samples are collected, they can be inspected, categorized, and polymer composition tested in the laboratory. Take standardized photos of each sample, then perform the lab categorization protocol. Metrics recorded in the laboratory on the samples, subsamples and components can be found in the Data Dictionary and will not be described in great detail here in the text.

Laboratory Supplies

- ☐ Camera
- ☐ White board
- ☐ Paper for labels
- ☐ Ruler or meter stick
- ☐ Markers, pens, pencils
- ☐ Three balances (readability to 0.1 g, 0.2 g, and 0.0001 g or better)
- ☐ Calibration weight set (Troemner)
- ☐ Laptops connected to internet
- ☐ Tape measure with mm resolution
- ☐ Digital calipers with 0.01 mm resolution
- ☐ Scissors
- ☐ Extra reused bags
- ☐ Attenuated total reflectance Fourier-transform infrared spectroscopy instrument (Thermo Fisher Scientific iS5 or Agilent Cary 630)
- ☐ Isopropanol
- ☐ Kim wipes
- ☐ Razor blades
- ☐ Quartz cutting surface

- ☐ Differential scanning calorimeter (TA Instruments DSC 25 with Refrigerated Cooling System 40)
- ☐ DSC pans (Tzero)
- ☐ Microanalytical balance (readability 0.0001 mg)

Sample Photos

1. Take photos of each sample or subsample in the lab under controlled lighting to improve quality and standardization of the photo format (Figure 2.17).
2. From a single event or pile, place the samples on top of their individual bags and sort them in ascending order on a large lab bench.
3. Set up the photo station. At the minimum, use a plain white or neutral background, a meter stick for scale, and a high-resolution phone camera in landscape orientation.
4. Place the event ID (optionally with the date of removal) in the bottom middle of the camera frame.
5. Transfer the sample ID label to the right of the event ID label.
6. Photograph one sample at a time in ascending order by placing the sample in the center of the photo board and camera frame. Make sure the net/pile ID and sample ID are in the frame, along with the meter stick for scale.
7. Check the quality of each photo. Delete and retake if necessary.
8. Once each sample has been photographed, rebag each sample with the sample label and store it nearby for lab categorization.

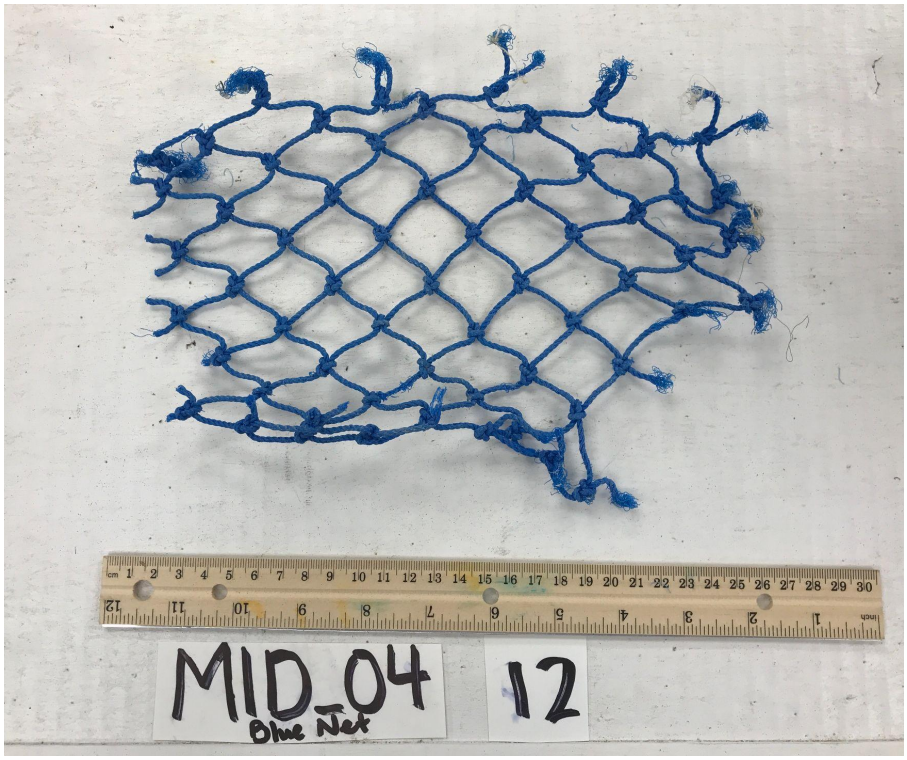

Figure 2.17. Example of a sample photo taken in the lab of a blue net, with the event ID and sample number labels and a centimeter ruler for scale.

Lab Categorization Protocol

1. Remove and unbag one sample at a time and open the Google Drive database on a laptop connected to the internet. No handwritten datasheets are used at this stage. Data are recorded directly into the database (as defined and listed in the Data Dictionary).
2. Quality check the transcribed field data in the database.
    a. Check that the gear is categorized correctly based on the gear type class key (Table 2.2).
    b. Check that color is correctly assigned as the original color not the weathered color (Table 2.3).
    c. Check that biofouling level was correctly assigned (Table 2.4).
3. Weigh each sample and record the mass (g).

a. Calibrate each balance with calibration weights before its use each day.

b. Record which balance was used. We primarily used the *Scout Pro* balance calibrated from 1.0 g to 100.0 g. For larger samples we used a Pelouze balance calibrated from 0.5 kg to 13.6 kg.

4. Decide if data will be collected for all samples, subsamples and components. Time limitations may call for a reduced categorization protocol.

    a. We reduced the number of samples categorized by:

        i. Including samples that were <10% removed (the gear sampled was likely large), all nets, all samples with writing, or a sample that was unique or identifiable.

        ii. Excluding all samples that were >75% removed (the gear sampled was likely small), samples that were >10% removed and was a net <0.4154 kg or a line <1.1 kg, or in cases where the sample was composed of >3 subsamples, the sample was either excluded or only the dominant subsample was included.

    b. We reduced the number of columns recorded by excluding:

        i. Weathering code, sample and subsample length (unless the item was 100% removed), % of sample by weight estimate for samples and subsamples, component specific questions, number of yarns per strand, and whether knots or splices were present.

        ii. All columns referring to the use of the FT-IR were replaced with the person guessing the polymer ID, best guesstimate on polymer ID, and polymer ID guess reasoning for samples that could be hypothesized with a

high percentage of confidence. This was implemented after thousands of samples were analyzed on the FT-IR and correlations could be made based on the construction and gear type. For consistency only one person was designated to do this and as a quality assurance, polymer ID guesstimates were performed on 103 materials and then FT-IR. Our percent accuracy was 98.05%.

5. If using the full protocol, insert rows into the Sample tab of the database to represent the number of subsamples and components present. Each subsample and component gets its own row in the database.
6. Record all metrics in the Data Dictionary for each sample, subsample and component.
7. Estimate and record the percentage of the total sample (by mass) for each subsample and/or component.
8. Look for any identifiable writing, symbols, logos or features. If identifiable features are present, transcribe them in the database and take a photo and upload it to the photo folder.
9. Assign weathering code according to the Table 2.5.

Table 2.5. Weathering codes for derelict fishing gear, modified from Brignac et al., 2019.

Weathering Code	
1	Minimal to none; looks nearly new 
2	Light to moderate weathering; slight color fading; some fraying and fragmentation of fibers (or hard plastics) 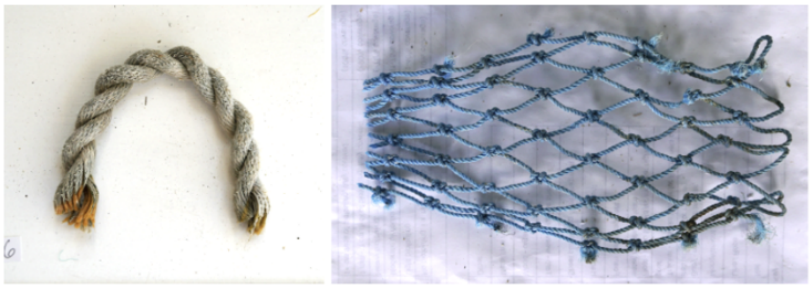
3	Heavily weathered; significant color fading; fibers (or hard plastics) are brittle, frayed and heavily fragmented 

10. Enter the complexity of lines or nets (Figure 2.18). (i.e., If it is a monofilament line of a single fiber = 1, If there are multiple fibers making a single yarn = 2, If there are multiple fibers making yarns of a strand = 3, If there are multiple fibers making yarns that are making strands that are making line = 4).

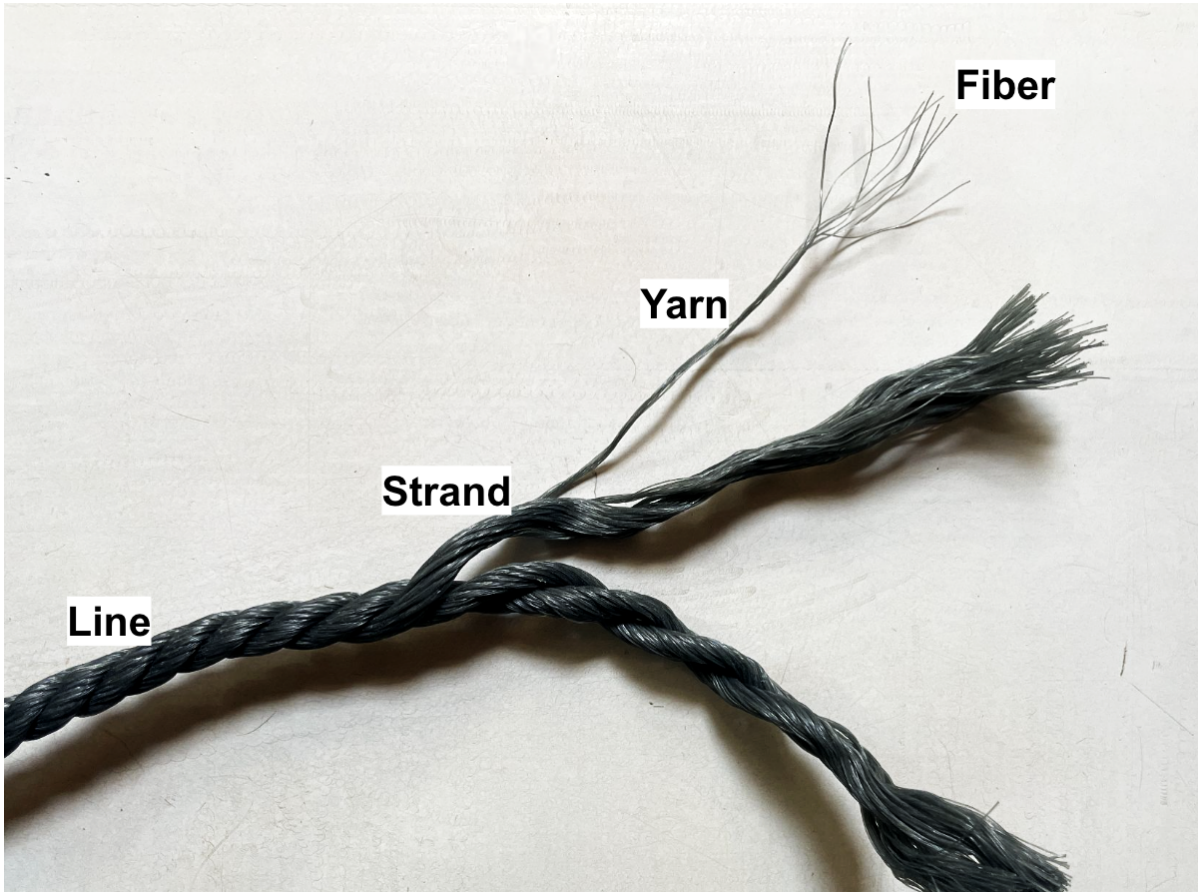

Figure 2.18. Diagram showing the four complexity levels of a line, and how a line is constructed.

11. Enter the line / twine construction (Figure 2.19).

    a. S = twisted clockwise

    b. Z = twisted counterclockwise

    c. B = braided

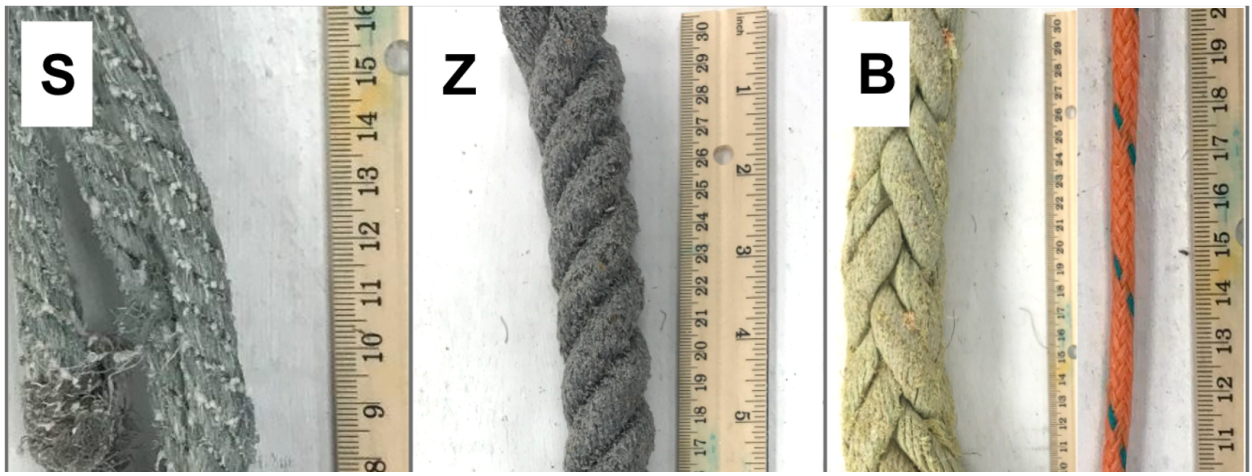

Figure 2.19. Different line or twine constructions. Z = Z-twisted, S = S-twisted, and B = braided.

12. Record the fiber type (Figure 2.20):

    a. monofilament (mono)

    b. multifilament (multi)

    c. film/tape (film)

    d. staple fiber (staple)

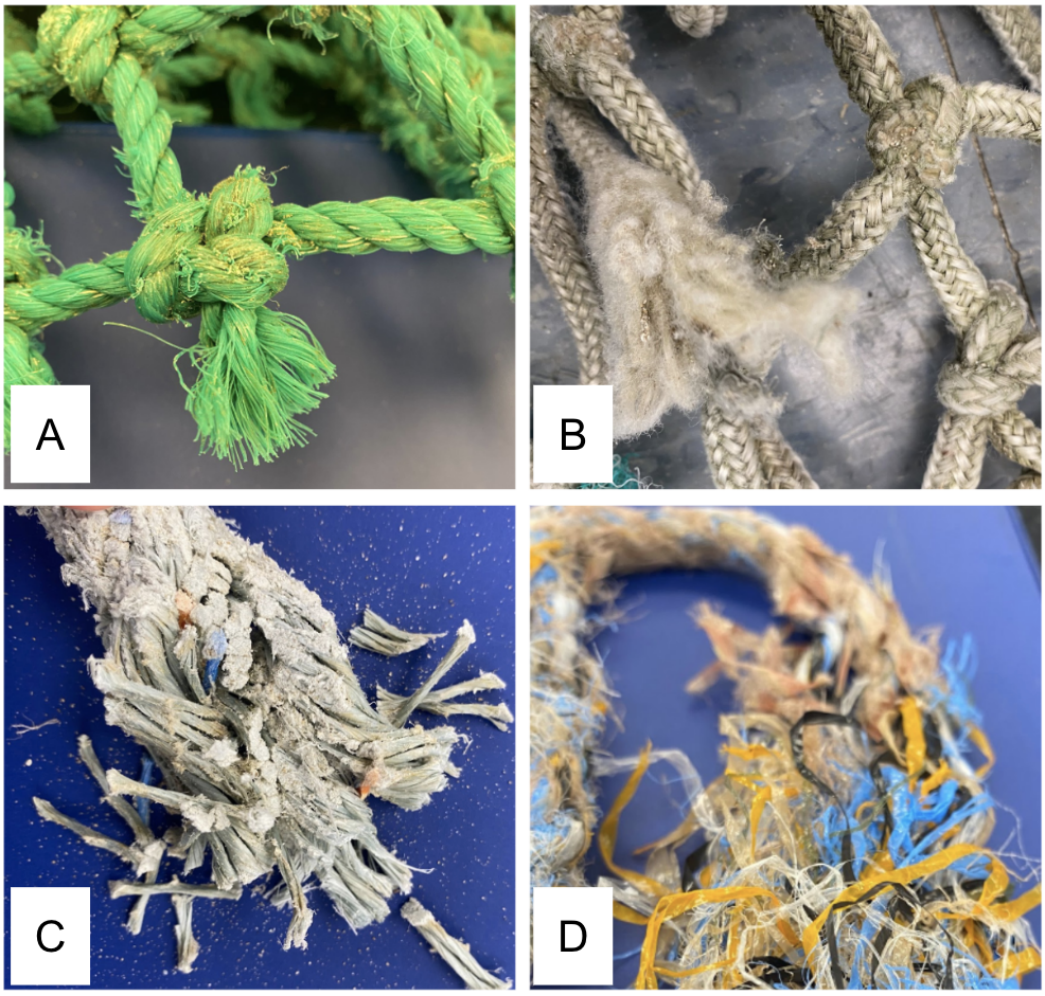

Figure 2.20. Fiber types of line and net twine. A) monofilament, B) multifilament, C) staple fiber, D) film.

13. Record the net construction according to Figure 2.21.

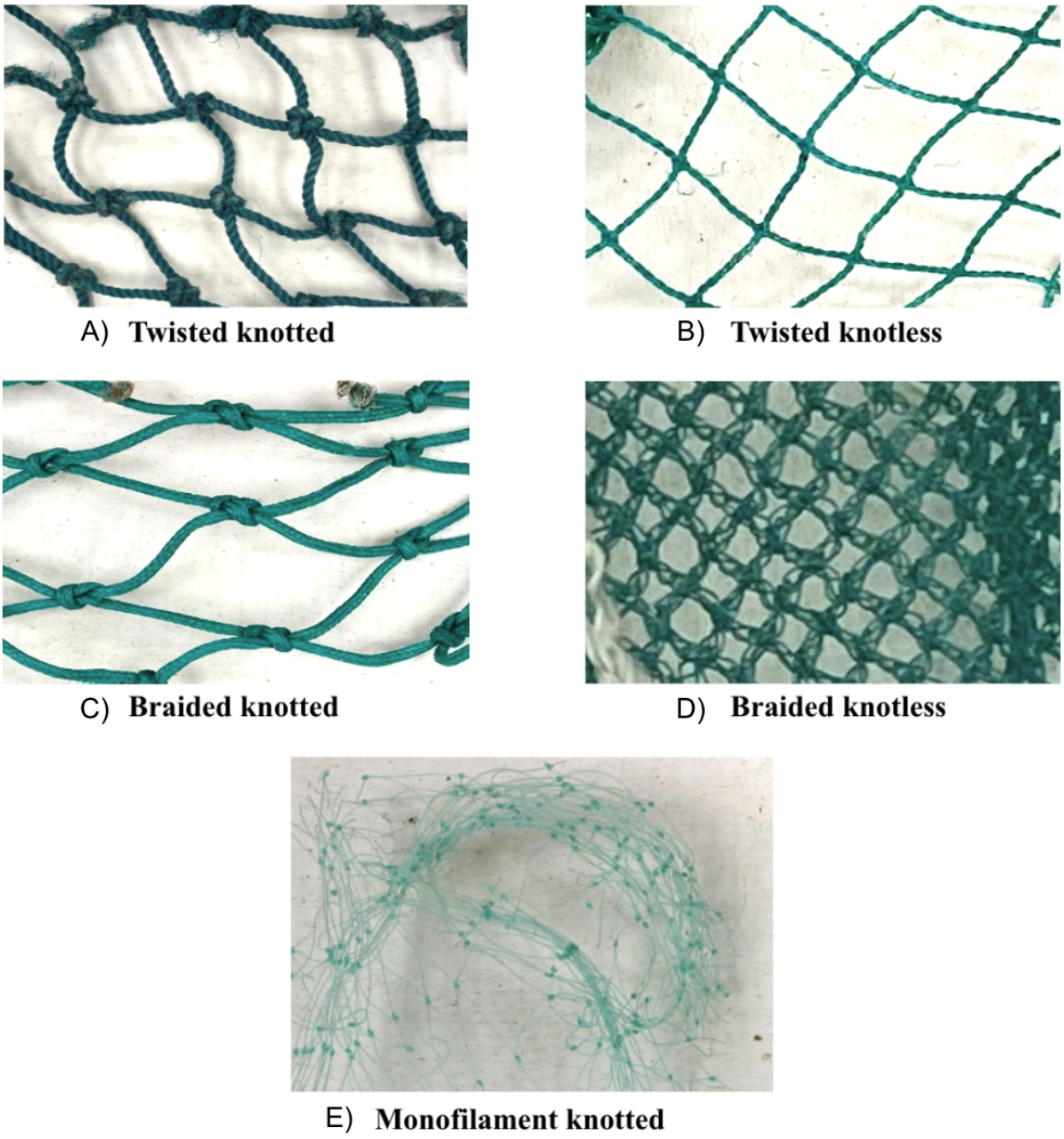

Figure 2.21. Five most common net construction types: A) Twisted-knotted, B) Twisted-knotless, C) Braided-knotted, D) Braided-knotless, E) Monofilament-knotted.

14. Measure the net stretched mesh size for three fully intact random mesh rounds (cm) in the Normal (N) direction (Figure 2.22).

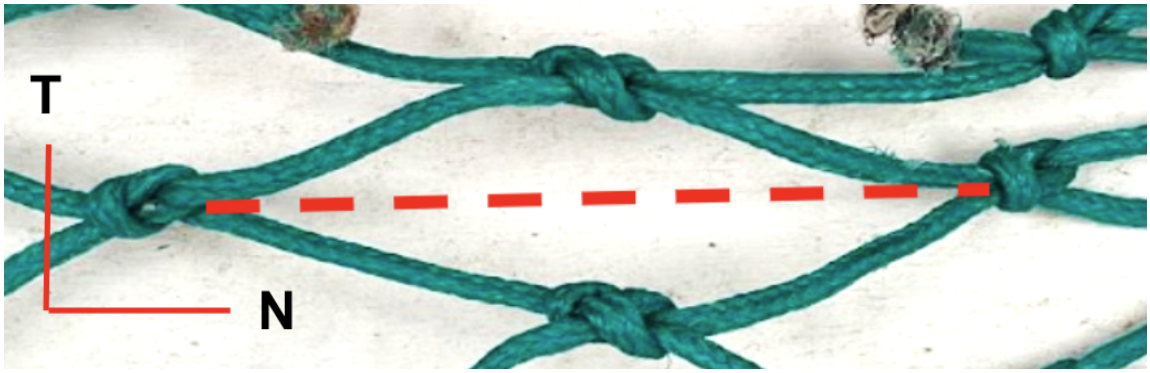

Figure 2.22. Net mesh stretched in the Normal (N) direction to measure net mesh size.

15. Refer to the Data Dictionary for more metrics specific to line, nets, floats, hard plastic mesh, strapping, oyster spacers and hagfish trap entrances.

16. Record notes along the way, if necessary.

Categorizing Subsamples and Components

Fill in the additional rows in the database to describe subsamples and components. Some data fields may not need to be entered.

Polymer Identification:

Polymer identification of gear samples, subsamples, and/or components was performed using a multiple step workflow. Step one captured a spectrum of one clean surface of the material using attenuated total reflectance Fourier-transform infrared (ATR FT-IR) spectroscopy according to methods described in Jung et al., 2018 using either a Thermo Scientific ATR FT-IR iS5 or an Agilent Cary 360. Polymer identification was determined by visually comparing the spectrum to reference spectra in Jung et al., 2018 with matches using the four largest or distinct absorbance bands. We could process up to 80 samples per day. ATR FT-IR is not ideal for

distinguishing different types of polyethene (PE), such as high-density PE (HDPE), low-density PE (LDPE), and linear low-density PE (LLDPE). Therefore, step two analyzed selected PE samples using differential scanning calorimetry (DSC) methods (Corniuk et al., in preparation). Polymer identification was based on peak melting temperature.

ANALYSIS

When assessing which protocol to implement, many of the tradeoffs are obvious without further analysis, including time, space, personnel, resources, number of samples, and resolution of data (Table 2.1). With time investment and data resolution being such a substantial trade off between the disentanglement protocol and the other protocols, it is important to compare the sampling coverage and comprehensiveness across the protocols. To compare sampling coverage, sample mass extrapolation was required for all protocols besides Disentanglement, since all disentangled gear piles were weighed, as well as every sample counted. Percent removed estimates and lab sample masses were used to extrapolate the total mass of each gear item that was sampled. Sampling coverage was calculated as the total mass of sampled items divided by total event mass for the Disentanglement protocol; and total extrapolated mass of sampled items divided by total event mass for all other protocols. The percent sampled by mass of each DFG event was calculated, and results were averaged for each protocol. Additional tests were performed to assess the results of the disentangled events, including percent of total items in the event that were sampled, and percent of total event mass sampled excluding scrap mass. MID_04 was a unique case study where the Hybrid protocol was conducted first, followed by the Disentanglement protocol. This allowed a direct comparison of composition and sampling coverage of the two protocols from the same event. Additionally, composition resulting from the

Hybrid samples and Disentanglement samples were compared to that of the Disentanglement piles, since this protocol weighed each sorted gear pile before sampling. A total count of all gear items that made up MID_04 were totalled up at the end of sampling, including those that were not sampled, and a total composition by gear count was obtained. The miscellaneous gear pile mass and count was attributed to the hard plastics gear category. Scrap mass was excluded in this analysis of composition of MID_04.

RESULTS

Results obtained from the six sampling protocols are summarized in Table 2.6, including number of DFG events processed, average number of samples, average mass of lab samples, and sampling coverage (proportion of total DFG event mass accounted for by sample mass). When comparing sample coverage by mass for the Four Corners, Hybrid, and Disentanglement protocols there is no significant difference in sampling coverage among the three methods (p-value = 0.5775, F = Ratio = 0.596, df = 2, Chi-squared = 0.071; Figure 2.23).

Table 2.6. Summary table of the six DFG sampling protocols reporting the number of DFG events processed, average number of samples, average mass of lab samples, and sampling coverage (proportion of total DFG event mass accounted for by sample mass).

Protocol	Number of DFG Events Processed	Avg. Number of Samples Collected	σ samples collected	Avg. total mass of samples (kg)	σ lab samples mass (kg)	Avg. Proportion of Sampling Coverage	σ sampling coverage
Measure Dispose	16	0	X	X	X	X	X
Reverse Engineer	17	3	4	1.7	0.9	1.00	0.0
One of All	74	10	17	6.6	7.2	1.00	0.0
Four Corners	8	72	31	8.8	5.7	0.53	0.22
Hybrid	36	66	45	11.1	6.5	0.64	0.21
Disentanglement	3 (36 piles)	472	128	42.2	25.4	0.64	0.15

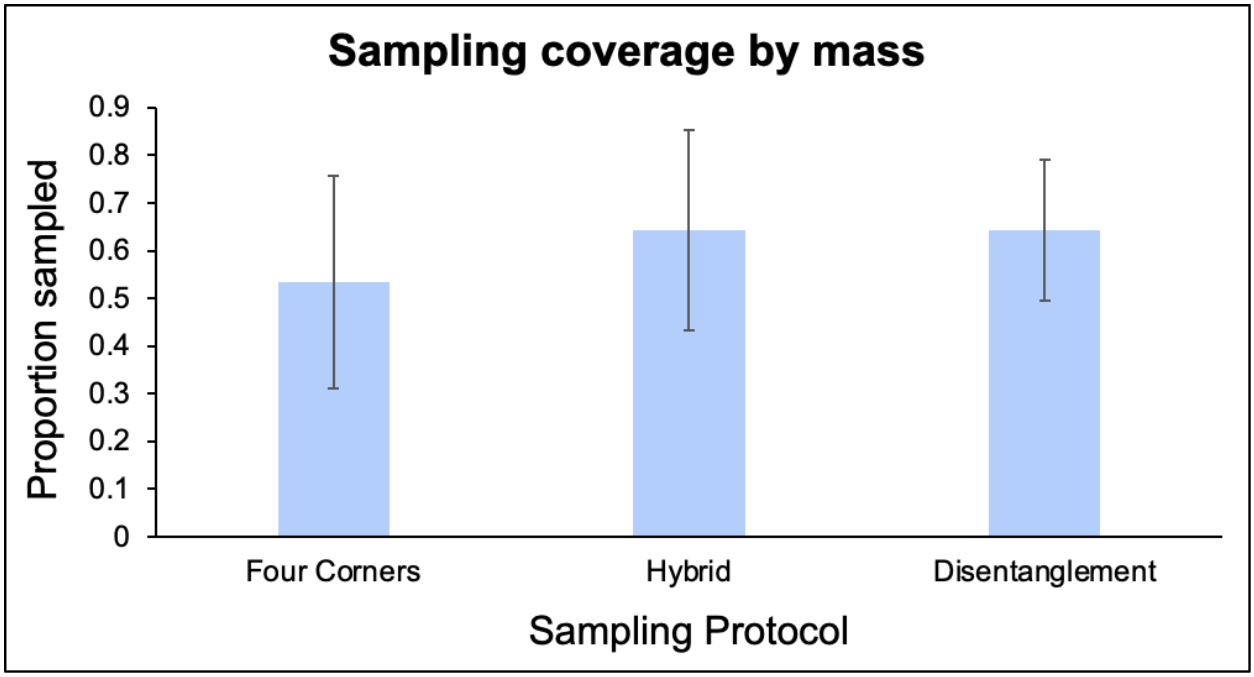

Figure 2.23. The average proportion of DFG events by mass sampled by the Four Corners, Hybrid, and Disentanglement protocol. Error bars represent one standard deviation from the mean value. Sample sizes were 5, 10 and 3 for the Four Corners, Hybrid, and Disentanglement, respectively (including all DFG events that had sample mass measured in the lab at the time of analysis).

For event MID_04, composition by sorted gear piles revealed that there were close to double the number of lines compared to nets (61.4% and 27.8%, respectively), but by mass nets and line proportions were nearly equivalent (46.7% and 50.4%, respectively). All other categories totalled around 10% of the event composition by count and less than 5% by mass. Composition by item, mass, and pile were vastly different between the two methods (Figure 2.24 & 2.25). The Disentanglement method collected six times the number of samples, four times the mass of lab samples, and had a sample coverage of 64% by mass, compared to 41% for the Hybrid method (Table 2.7). Composition by item was nearly equal for nets, but the Hybrid method favored approximately twice as many lines as the Disentanglement method. When comparing composition by mass, the Hybrid method collected less nets by about 66%, and collected nearly twice as many lines as the Disentanglement method. For both protocols, other gear categories besides nets and lines are relatively negligible by mass. However, the

Disentanglement method shows greater variety and approximately double the mass of other gear categories than the Hybrid method. Comparing compositions derived from the sorted gear pile masses to that of the Hybrid and Disentanglement method samples showed that both protocols produced biased results. By count, nets were underrepresented by about 50% for both protocols. By mass, the Hybrid method underrepresented nets mass by 24%, where the Disentanglement method overrepresented nets mass by 15%. Furthermore, lines were greatly underrepresented by count, and the Hybrid method accounted for 66% of the line proportion, and the Disentanglement method only accounted for 33% of the line proportion determined by the disentanglement piles. By mass the Hybrid method overestimates line proportion by 50%, and the Disentanglement method underestimates line proportion by 30%.

Table 2.7. MID_04 protocol comparison for the Hybrid protocol and Disentanglement protocol.

MID_04 protocol comparison			
Protocol	Number of Samples	Mass of Lab Samples (kg)	% sampled by mass
Disentangle	496	32.1	64%
Hybrid	81	8.8	36%

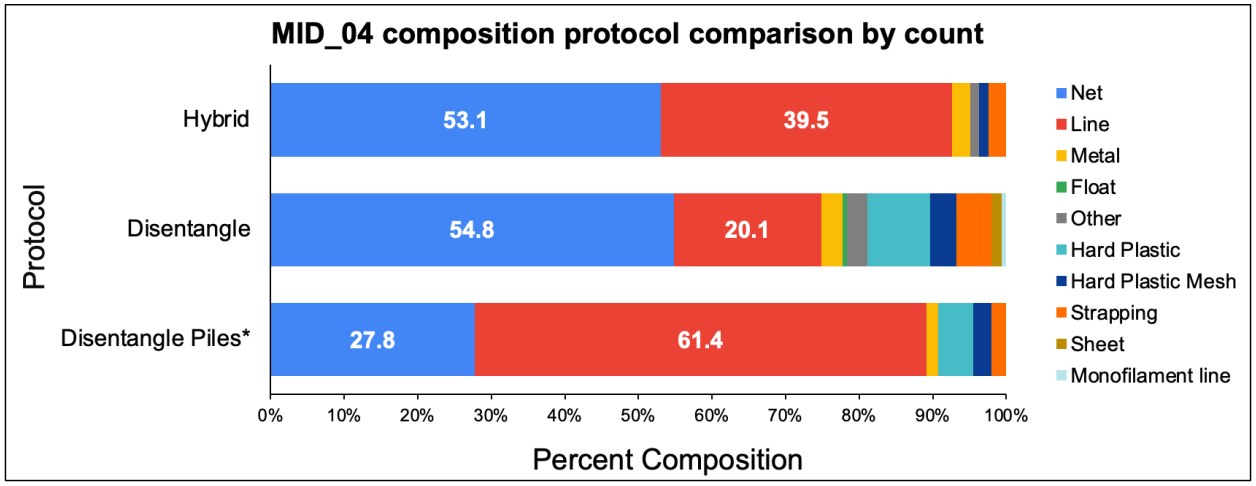

Figure 2.24. Gear composition by count of gear items in event MID_04 sampled using two field sampling protocols compared to the total count of gear items in the disentangled piles.

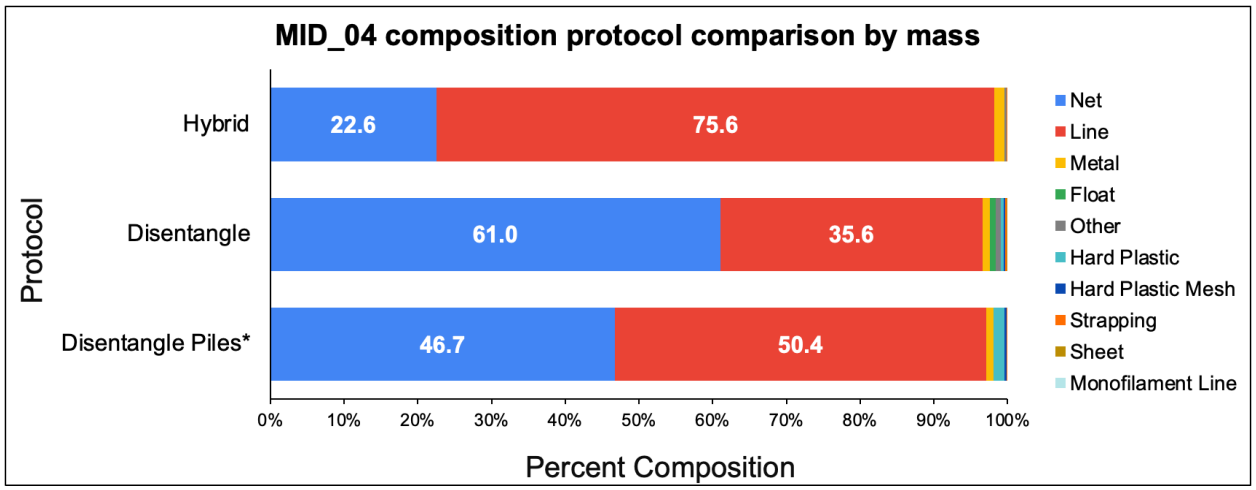

Figure 2.25. Gear composition by mass of gear in event MID_04 composition sampled using two field sampling protocols compared to the total mass of gear in the disentangled piles.

The three events that we implemented in the Disentanglement protocol were the largest events that we analyzed. By disentangling all the gear, we were able to assess how much of the DFG mass was composed of scrap fragments of nets, lines and miscellaneous items that were too small to sample. The results indicate that scraps accounted for an average of 12% of disentangled event volume by mass. By removing scrap mass from the sampling coverage calculation, sample coverage increased by an average of 8% (Table 2.8). OAH_17, which weighed approximately

four times the mass of the other two events, contained over five times the scrap mass (Table 2.8, Figure 2.26).

Table 2.8. The mass and influence of scraps in sampling coverage of disentangled events**.**

Events	OAH_17	NPG_11	MID_04	AVG	σ
Total gear items	3285	630	1343	1752.7	1374.1
Total number of samples	1051	333	496	626.7	376.4
% sampled by item	32.0%	52.9%	36.9%	41%	11%
Event Mass (kg)	1613.6	440.8	503.4	852.6	659.8
SUM Mass of Samples (kg)	798.7	348.8	323.4	490.3	267.4
Mass of Scraps (kg)	247.8	34.2	51.6	111.2	118.6
% sampled by mass	49.5%	79.1%	64.2%	64.3%	14.8%
% scrap by mass	15.4%	7.8%	10.3%	11.1%	3.9%
% sampled by mass excluding scraps	58.5%	85.8%	71.6%	71.9%	13.7%
Δ % sampled by mass	9.0%	6.7%	7.3%	7.7%	1.2%

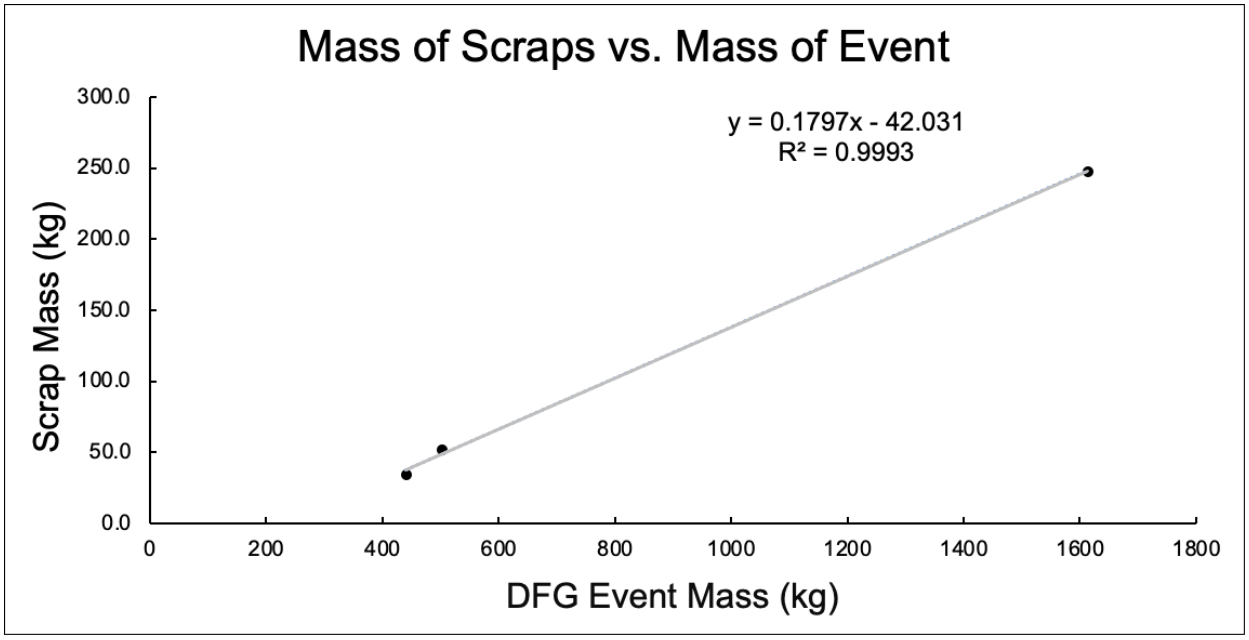

Figure 2.26. Scrap versus event mass (kg) from the three disentangled DFG events OAH_17, NPG_11, and MID_04.

The Disentanglement protocol is the only protocol that allows us to measure and weigh the whole gear items before sampling. Therefore, we heavily relied on mass extrapolation from the estimated percent removed of the whole gear during sampling with the Hybrid, Four Corners, and One of All methods. We assessed the accuracy of our estimations by comparing all samples from the three disentangled events that had both mass measured of the whole gear and an estimated percent removed (n = 861). A significant linear relationship ($p = <2.2$ e-16) with a goodness of fit Chi-squared = 0.69 shows that using estimated percent removed to extrapolate to sampled mass is worthwhile (Figure 2.27).

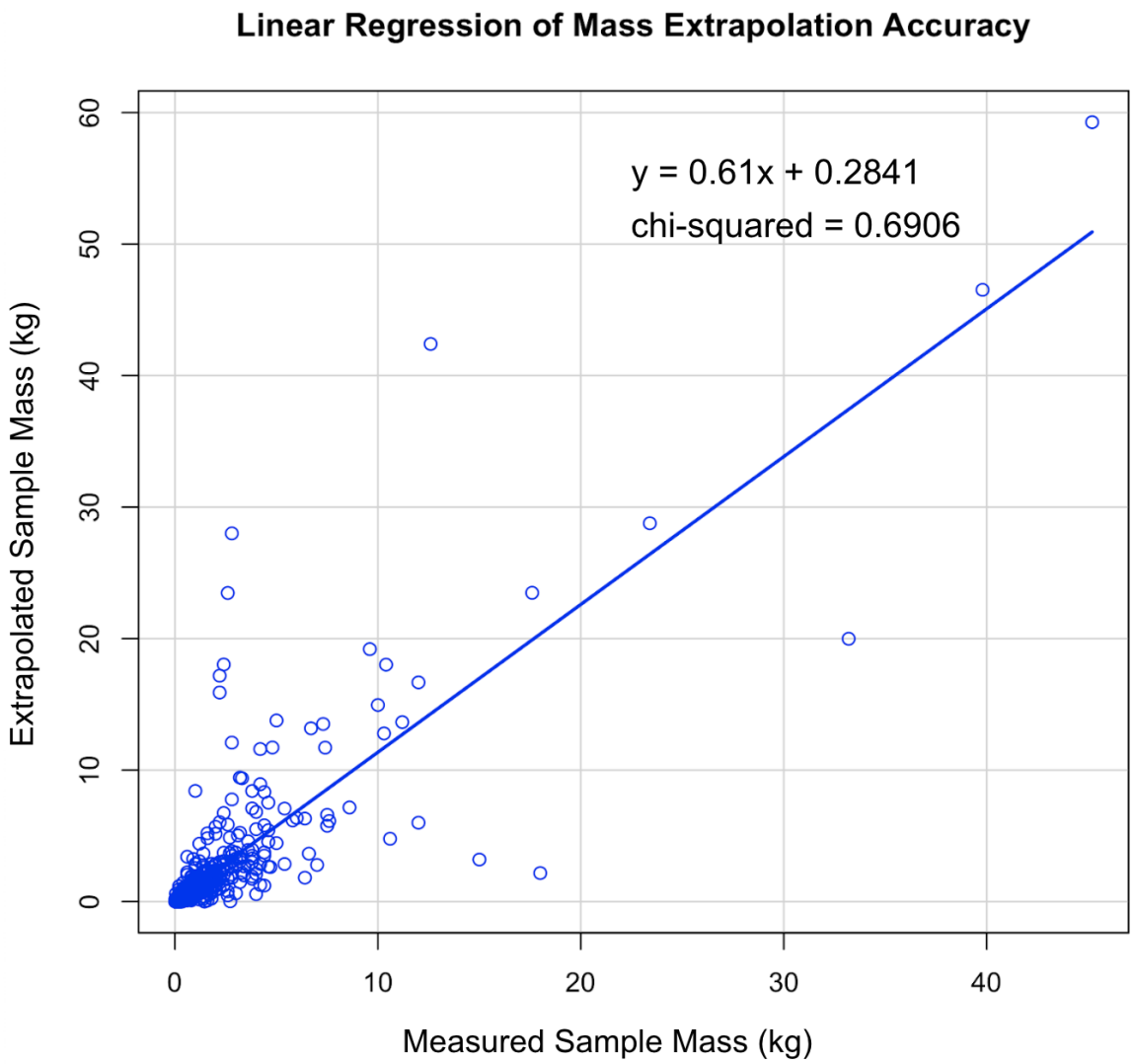

Figure 2.27. Linear regression of mass extrapolation accuracy including all DFG conglomerates and distinct nets and lines. F = 1920, df = 1 and 859, p = <2.2 e-16.

It is also not always feasible to weigh DFG with time and resource constraints. We created linear models to predict mass based on various dimensional measurements of event bundles (not events laid out). Only conglomerates or distinct nets were included in this analysis; thus the models can only be used for estimating the mass of these types of events. Circumference or the multiplication of event length, width and maximum height were both related to measured mass with Chi-squared values of 0.789 and 0.894 (Figures 2.28 and 2.29), respectively. A larger Chi-squared (0.936) was obtained from a model using an equation for the volume of a

half-sphere (4/3 x 3.14159 x radius^3 /2) (Figure 2.30). Radius was determined as the average of half the length, half the width, and the average height of the bundle. The masses calculated from the three models were averaged to obtain estimated event masses (kg) for DFG events that could not be weighed.

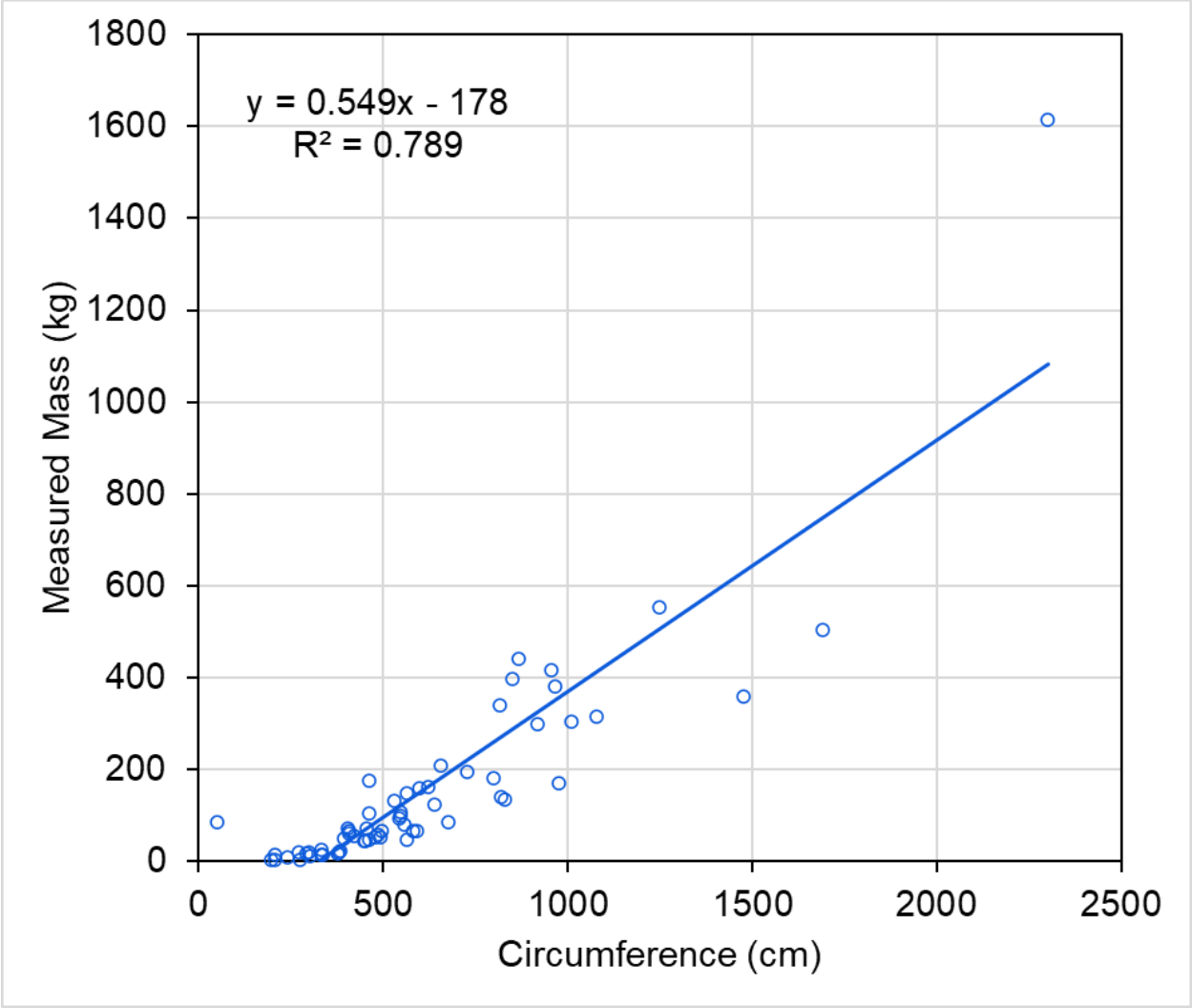

Figure 2.28. Linear model of mass to circumference of only conglomerates and distinct nets that were measured as a bundle.

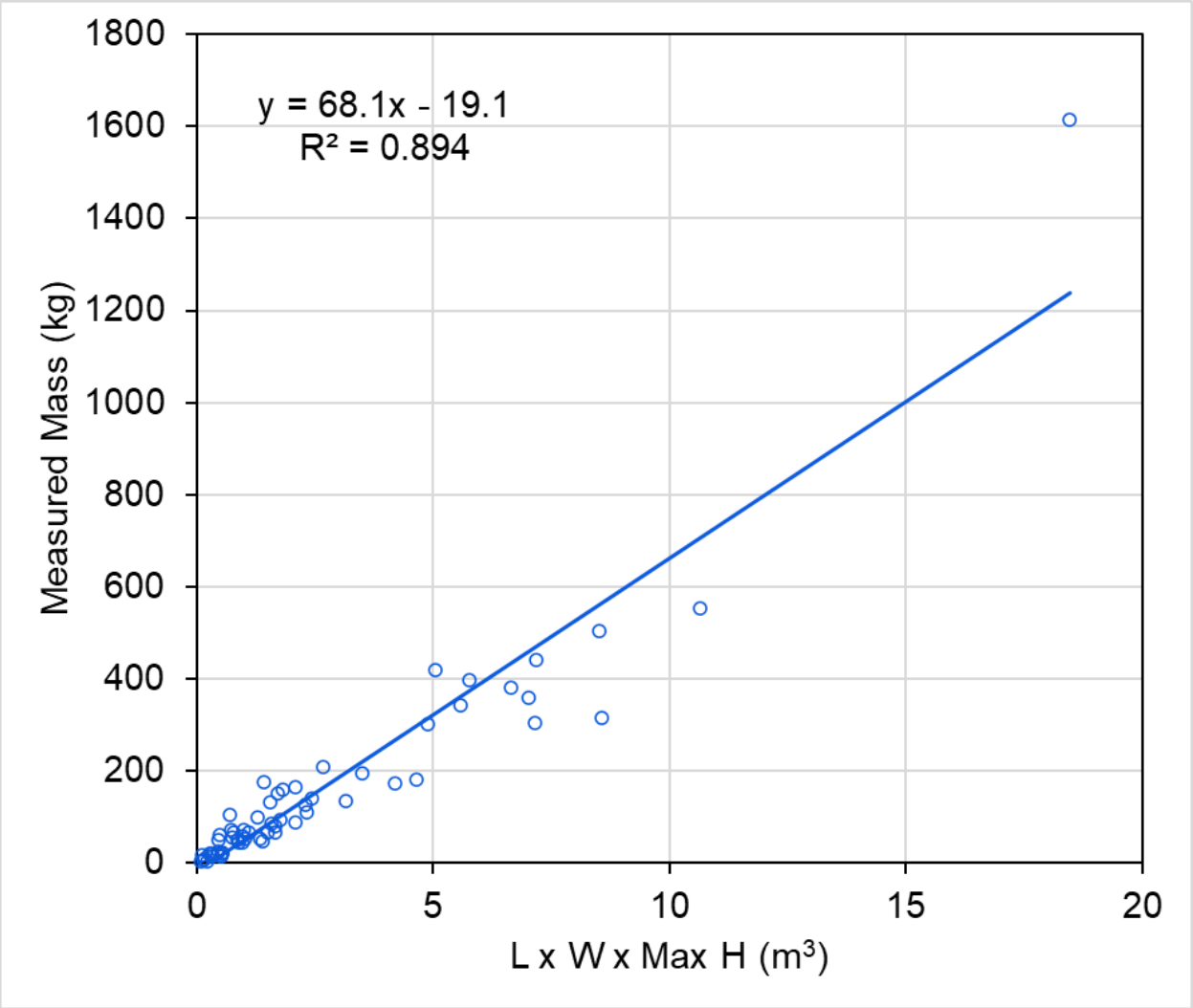

Figure 2.29. Linear model of mass to the multiplication of length (L), width (W), and maximum height (Max H) of only conglomerates and distinct nets that were measured as a bundle.

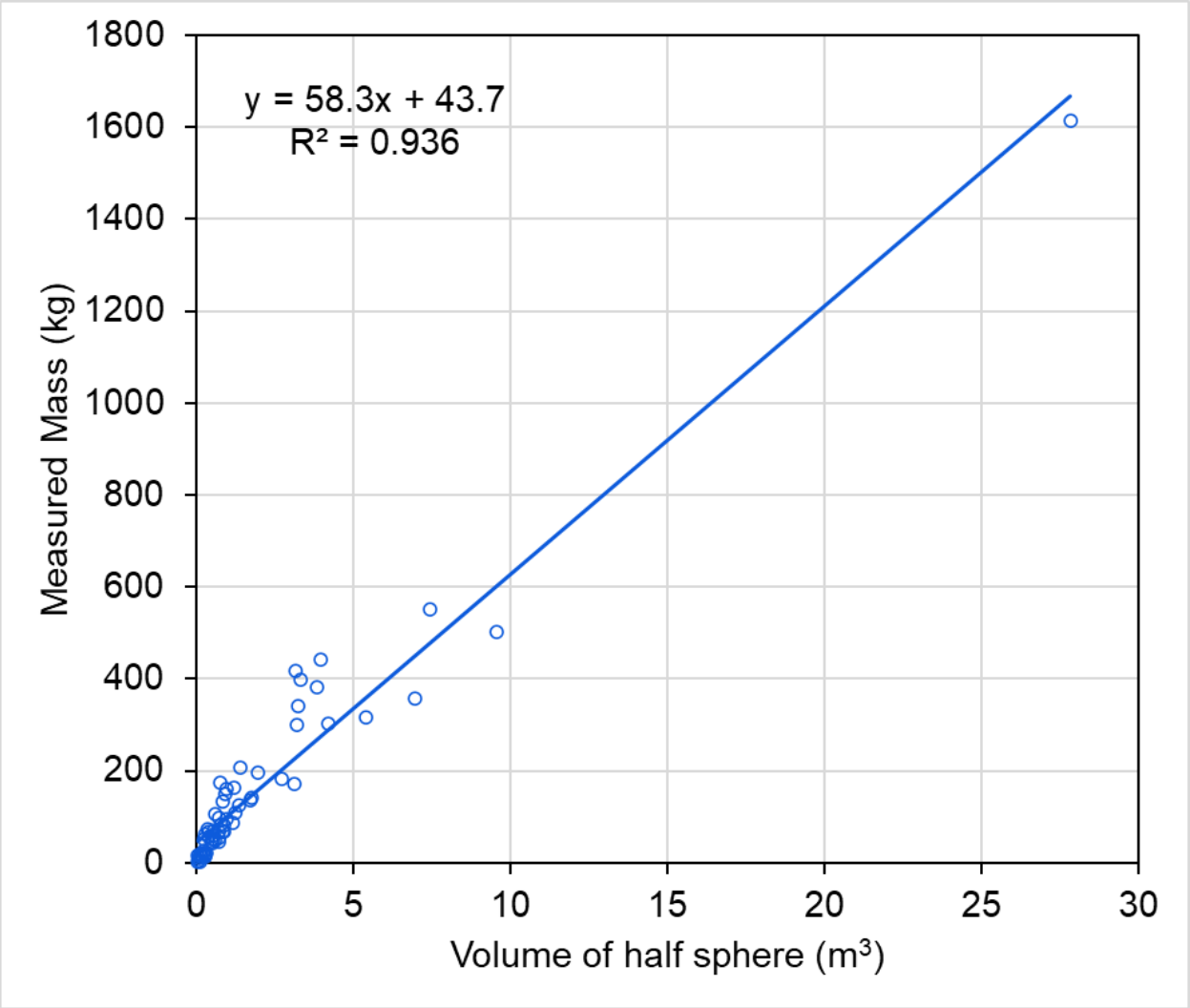

Figure 2.30. Linear model of mass to the estimated half-sphere volume of only conglomerates and distinct nets that were measured as a bundle.

DISCUSSION

These protocols developed and evolved over two years of collecting and sampling DFG. We were constantly seeking to improve our methods, streamline data collection, reduce sampling and processing time in the field and lab, and continually gaining new resources. Our original protocol was the Four Corners method, which was developed to be implemented on a ship with very limited time constraints to obtain samples before other partners disposed of the DFG. This method is efficient in that it can be applied in just about any field condition and saves time and space, but it is limited in sample coverage.

Initially we did not have a crane scale to weigh DFG events. This is a critical piece of equipment for a DFG study because it provides accurate accumulation data and enables assessment of DFG event composition by mass. Our linear regression models serve as a viable alternative when a scale is not available.

The Disentanglement protocol was developed once we gained access to a warehouse to process DFG. Access to a sheltered work space allowed us to stockpile DFG, set up a crane scale, and dry DFG to accurately assess mass. This method provided incredible resolution of DFG construction and configuration, and revealed that most DFG conglomerates did not seem to be intentionally assembled, but rather a tangled mass of discrete gear pieces could be easily, but time-consumingly, disentangled. This method provided the most accurate assessment of DFG composition and also the most valuable for sourcing DFG back to the origin fisheries and manufacturers since each gear item was viewed and measured in full size and shape. However, this method came at a steep cost of processing time and personnel resources.

The Hybrid method evolved as the solution to still retain some of the detail that the Disentanglement method offers, but only for selected high priority samples that make up a large

portion of the DFG event by mass. It streamlines sampling efficiency by capping collection at 80 samples, the same as the Four Corners method, but it reveals more of the gear composition by spreading out the DFG event more before sampling. Samples were prioritized by volume from largest to smallest. The Hybrid method is the recommended method for future studies for these reasons. However, based on the MID_04 comparison, both the Hybrid and Disentanglement sampling protocols will result in samples that will deviate from the accurate gear composition of an event. The only solution to those inherent biases is to sample every item in the event using the One of All or Reverse Engineering methods. The Disentanglement method provides a means of understanding the accurate gear composition by recording the non-sampled gear counts and mass, but one must keep in mind that the lab samples do not reflect this composition. . The selection of protocol will largely depend on the research questions of future work.

The One of All method is essentially the Four Corners method for events that are too small to be divided into four sections or have less than 80 total pieces of gear. The Reverse Engineering method was created primarily for dFADs but also applies well to other unique gear, such as local set nets. It retains the greatest amount of information and is great for smaller DFG that is a high priority to source back to the original fishery and function. The Measure and Dispose method was created when we were overloaded with DFG and could not process the events anymore. However, we wanted to make sure we were at least documenting type, size, mass, and discovery location for understanding quantities and frequencies.

These methods provide deep-dive DFG forensic techniques to collect the necessary data and evidence to assess DFG composition and link source to impact for effective resolution. DFG continues to be a pervasive threat to Hawaiian waters, and globally. Sourcing it back to the fisheries and manufacturers is essential in solving this issue.

ACKNOWLEDGEMENTS

Funding was provided by the Norwegian Retailers' Environment Fund. Sampling in the Papahanaumokuakea National Marine Monument was permitted by permit # PMNM-2020-015. These protocols were included in my thesis for rapid dissemination to the public, but our entire team was instrumental in protocol development, implementation, and writing. The citation of this chapter should read McWhirter, A., Corniuk, R., Royer, S-J., Lynch, J.M. 2022. Best practices for sampling floating derelict fishing gear in the subtropical North Pacific. Chapter 2 of McWhirter, A.C. 2022. "Composition of floating derelict fishing gear in the central subtropical North Pacific Ocean." Thesis: Hawai‘i Pacific University Masters of Marine Science, Honolulu.

GLOSSARY

Our team wrestled with finding stable, tight definitions of terms. As our awareness of materials grew, so did our terminology. Recognizing there are standardized lists of marine debris item categories published, we were frequently debating the accurate name of gear types and other terms. The ultimate goal of this project was sourcing the DFG, so gear type names were selected primarily on the use of the gear (e.g. net, float, tarp), rather than shape or texture of the plastic (e.g. hard plastic fragment, foam, film). A regret is that we lumped hooks and lures under the category of metal.

Buoy - a buoyant float intended for navigation, visual aid, mooring, or instrumentation.

Component - one part of a single gear item (subsample or sample) that is distinct in construction, composition or color, but part of the same whole gear item.

Conglomerate - tangled mass of nets, lines, other gear, and miscellaneous material making up a DFG event.

DFG event - any type of DFG that was recovered at a specific location and time, as a single mass of gear either constructed or entangled together.

Distinct Line - a single line or multiple lines tangled together and discovered as an isolated DFG event, with minimal other gear entangled.

Distinct Net - a single net or many parts of the same gear tangled together and discovered as an isolated DFG event, with minimal other gear entangled.

Drifting Fish Aggregating Device (dFAD) - often consists of a bamboo raft wrapped in black netting, with a tail that sinks down up to over 30 meters, and often has a satellite tracking buoy attached to the raft, commercially produced by the tuna purse seine fishery.

Fiber - fine or coarse, continuous or not continuous, bundled, twisted, or pressed together to make yarn or strands.

Film fiber - thin film (sometimes called tape or sheet) is sometimes twisted so it appears to be a circular fiber. This tape may be fibrillated or split so it appears to be a collection of small flat fibers which cling to each other.

Float - gear that is buoyant foam or hard plastic.

Hard Plastic - items that did not fit in other gear types that were made of plastic things like eel trap entrances, oyster spacers, hard floats, planters, toothbrushes, and hangers.

Hard Plastic Mesh - range of flexibility from nearly inflexible to very flexible. The very flexible should not be called HP, that was a misnomer from the beginning. Mesh is probably also a misnomer. In construction this is called “barrier fence netting”. The nodes are always molded together, no knots.

Line - a rope with a determined function.

Mesh Stretch - the size of the opening of a stretched round of mesh measured as the distance between adjacent knots. Mesh can be stretched in the Normal (N) or Transverse (T) directions (see definitions).

Monofilament fiber - coarse continuous fibers used to construct yarn, twine and rope.

Monofilament Line - thick single-fiber fishing line, or webbed to make a monofilament net, usually used as a gillnet.

Multifilament fiber - continuous fibers that are very fine and hair-like, typically about 0.023 mm diameter, spun, twisted or braided to construct yarn, twine, and rope.

Net - a flexible web that may be composed of twisted or braided, knotted or knotless constructions, and forms mesh rounds, or squares. Mesh stretch is most typically >0.5 cm. Nets are distinguished from fabric by having secured nodes at the intersection of each weave. The nodes are secured by knots, whether they are a single knot or a complicated braid, like Racheal or Ultracross. The nodes are not molded together, like hard plastic mesh.

Normal (N) Mesh Stretch Direction - Mesh stretched in the direction of the sheet bend knots. This is typically the longest stretched direction and the two middle knots should touch and the round of mesh should completely stretch and flatten, opposed to transversely (T) stretched mesh (Vincent et al., 2020).

Plastic Mesh Screen - Hard plastic mesh that is commonly entangled in DFG conglomerates.

Rope - two or more strands twisted or braided together, typically in the opposite direction as the twine twisted to maximize strength.

Round - one square or diamond section of net mesh.

Sample - can be a single gear item or a group of gear items that are associated or configured together in a particular way, intentional or unintentional, and removed from the net as a unit.

Scrap - insignificant pieces of material that do not meet the size requirements to be considered a potential sample. They are usually small, frayed pieces of net or line.

Sheet - defined loosely as any material that was thin with a large surface area and without holes like a net. These could be thin film plastic sheeting like plastic bags, tarps of any kind (e.g. woven tarpaulins), fabric, rugs, or canvas.

Staple fiber - fibers of limited lengths processed like natural fibers to form staple yarn.

Strand - yarn twisted together to form a strand. Two or more strands are twisted together to form a rope.

Strapping - thin film plastic straps that were between 5 mm and 2 cm in width with long lengths, occasionally also included woven textile straps.

Subsample - a single gear item that is representative of a sample and is one part of a multiple gear sample.

Tracker - A buoy with a GPS satellite tracking instrument embedded. Common on dFADs.

Transverse (T) Mesh Stretch Direction - net mesh stretched in a direction that is perpendicular to the sheetbend knot direction. This stretch direction does not allow the stretched sides to touch, has rounded ends, and is typically shorter than the distance measured from N-stretched mesh (Vincent et al., 2020).

Yarn - spun bundles of fiber.

REFERENCES

Bradford AL, Lyman EG. 2020. Injury Determinations for Humpback Whales and Other Cetaceans Reported to NOAA Response Networks in the Hawaiian Islands During 2018. U.S. Dept. of Commerce, NOAA Technical Memorandum NOAA-TM-NMFS-PIFSC-103, 18 p.

Brignac, K. C., Jung, M. R., King, C., Royer, S.-J., Blickley, L., Lamson, M. R., Potemra, J. T., & Lynch, J. M. (2019). Marine Debris Polymers on Main Hawaiian Island Beaches, Sea Surface, and Seafloor. Environmental Science & Technology, 53(21), 12218–12226.

Boland, R. C., & Donohue, M. J. (2003). Marine debris accumulation in the nearshore marine habitat of the endangered Hawaiian monk seal, *Monachus schauinslandi* 1999–2001. Marine Pollution Bulletin, 46(11), 1385–1394.

Corniuk, R., Royer, S. J., McWhirter, A. C., Lynch, H., Shaw, K., Lynch, J. M. in preparation. Polymer Identification of Floating Derelict Fishing Gear from O‘ahu, Hawai‘i.

Falk-Andersson, J., & Strietman, W. J. (2019). *Svalbard Beach Litter Deep Dive* (Technical Report No. 1033; p. 44). SALT. https://www.sysselmannen.no/Svalbardsmiljovernfond/Resultat---Rapporter/

Gilman, E., Chopin, F., Suuronen, P., & Kuemlangan, B. (2016). Abandoned, lost and discarded gillnets and trammel nets: Methods to estimate ghost fishing mortality, and the status of regional monitoring and management. FAO Fisheries and Aquaculture Technical Paper, 600, I.

Gilman, E., Musyl, M., Suuronen, P., Chaloupka, M., Gorgin, S., Wilson, J., & Kuczenski, B. (2021). Highest risk abandoned, lost and discarded fishing gear. Scientific Reports, 11(1), 7195.

Jung, M. R., Horgen, F. D., Orski, S. V., Rodriguez C., V., Beers, K. L., Balazs, G. H., Jones, T. T., Work, T. M., Brignac, K. C., Royer, S.-J., Hyrenbach, K. D., Jensen, B. A., & Lynch, J. M. (2018). Validation of ATR FT-IR to identify polymers of plastic marine debris, including those ingested by marine organisms. Marine Pollution Bulletin, 127, 704–716.

Lebreton, L., Slat, B., Ferrari, F., Sainte-Rose, B., Aitken, J., Marthouse, R., Hajbane, S., Cunsolo, S., Schwarz, A., & Levivier, A. (2018). Evidence that the Great Pacific Garbage Patch is rapidly accumulating plastic. Scientific Reports, 8(1), 1–15.

Royer, S. J., Lynch, J. M., Corniuk, R., McWhirter, A. C., Lynch, H. in preparation. Distribution and frequency of floating discarded (derelict) fishing gear and drifting fish aggregating devices in the Northern Pacific Ocean.

Suka, R., Huntington, B., Morioka, J., O'Brien, K., & Acoba, T. (2020). Successful application of a novel technique to quantify negative impacts of derelict fishing nets on Northwestern Hawaiian Island reefs. Marine Pollution Bulletin, 157, 111312.

Timmers, M. A., Kistner, C. A., & Donohue, M. J. (2005). Marine Debris of the Northwestern Hawaiian Islands: Ghost Net Identification. Sea Grant Publication UNIHI-SEAGRANT-AR-05-01; p. 31.

Therriault, T. W., Nelson, J. C., Carlton, J. T., Liggan, L., Otani, M., Kawai, H., Scriven, D., Ruiz, G. M., & Clarke Murray, C. (2018). The invasion risk of species associated with Japanese Tsunami Marine Debris in Pacific North America and Hawaii. Marine Pollution Bulletin, 132, 82–89.

Vincent, B., Simon, J., & Di Cesare, N. (2020). Development of a model for flexural rigidity of fishing net with a spring mass approach and its inverse identification by metaheuristic parametric optimization. Ocean Engineering, 203, 107166.

White, D., Hamilton, C., & Cook, K. (2004). *The net kit: A fishing net identification guide for Northern Australia*. World Wide Fund for Nature Australia.

CHAPTER 3

Composition of floating derelict fishing gear from three subtropical North Pacific regions

ABSTRACT

Derelict fishing gear (DFG) represents the greatest mass of floating plastic debris in the ocean. Large quantities of DFG aggregate in the convergent features of the North Pacific Subtropical Gyre (NPSG), and wash ashore along the Hawaiian archipelago, which extends diagonally through the center of the NPSG. Hawai‘i is impacted by DFG year-round, including damage to coral reefs and endangerment of endemic marine species. Understanding the sources of the DFG that is affecting the Hawaiian Archipelago and surrounding waters is a critical step in the effective mitigation of this issue. Five DFG conglomerates were collected and sampled from three geographically distinct regions (Midway, O‘ahu, and the pelagic North Pacific Gyre), and their composition was compared. DFG event composition was assessed by the proportion of gear categories by mass and by count. Nets and lines made up the greatest proportion of DFG conglomerates by mass and by count, and no significant variation was observed in event level composition among regions. When line and net composition was compared across regions, no significant variation in line composition was observed. However, both the lines and nets from Midway were significantly less biofouled than those washed ashore on O‘ahu or sampled collected at sea. Significant variation in net composition was observed among regions, which was related to by greater abundance of monofilament gillnet at Midway relative to the other two regions. This study establishes the quantitative framework for characterizing the composition of DFG in the central North Pacific, and facilitates the sourcing of this material back to the fisheries of origin.

INTRODUCTION

Plastic in the marine environment has emerged as a global phenomenon causing negative ecological and economic impacts (Beaumont et al., 2019). Synthetic polymers were first commercialized in the 1960s and have since been integrated into nearly every aspect of human existence due to the material's versatility, durability, low-cost, and convenience. In 2016, annual global plastic production was estimated to be 422 million metric tons (Jambeck et al., 2015), and production is expected to double by 2040 (Carney Almroth & Eggert, 2019). The rapid rise in mass production of plastic has escalated beyond the capacity of adequate waste management strategies, resulting in leaching of plastics into the environment from both land and marine sources (Geyer et al., 2017; Jambeck et al., 2015).

Over the past two decades, global evidence of the magnitude and impacts of plastic marine pollution has increased. Plastic debris is causing a myriad of detrimental impacts: discarded plastic is ingested by organisms (Gall & Thompson, 2015; Laist, 1987), aids bioaccumulation of persistent organic pollutants (Teuten et al., 2009), entangles and kills marine organisms (Donohue et al., 2001, Gilman et al., 2016), damages coral reefs (Suka et al., 2020), and transports invasive species (Therriault et al., 2018) and pathogens (Bowley et al., 2021). Additionally, marine plastic pollution impacts tourism, fishing, and maritime industries (Beaumont et al., 2019; Carney Almroth & Eggert, 2019). In particular, marine debris sourced from fishing activity, referred to as Derelict Fishing Gear (DFG), has emerged as one of the most destructive forms of plastic pollution in marine ecosystems around the world (Gilman et al., 2021; Macfadyen, Huntington, Cappell, 2009). DFG accumulates in high concentrations in the North Pacific Ocean, which is especially concerning for the state of Hawai‘i, USA, located in the center of the North Pacific Subtropical Gyre (NPSG).

Floating plastic marine debris from nano-plastics to DFG weighing several metric tons, accumulates in the NPSG, reaching some of the highest observed concentrations globally (Lebreton et al. 2018). Additionally, DFG accumulation zones in the NPSG overlap with the Hawai‘i longline fishery fishing grounds and interactions hinder fishing operations at a great economic expense (Uhrin et al., 2020). Several categories of floating DFG are common in the North Pacific, including drifting Fish Aggregation Devices (dFADs), distinct nets, lines, floats, buoys, and conglomerates composed of a vast diversity of fishing gear including nets and lines of many sizes tangled together. Distinct nets, lines, and conglomerates pose the greatest risk for animal entanglement, substrate damage, and navigational hazards of any debris type (Gilman et al., 2021). This study focuses on DFG composition of conglomerates because of the impacts listed above, and the diversity of gear types contained.

For decades, large DFG conglomerates have washed into the reefs and beaches of the remote islands and atolls of the Hawaiian archipelago, causing ecological damage, killing coral reefs, turtles, and critically endangered Hawaiian Monk Seals (Shomura and Yoshida, 1985). Yet, several knowledge gaps exist, including a detailed compositional analysis of DFG that includes polymer identification, and a comparison across major accumulation regions in the North Pacific. Ultimately, by allowing the attribution of DFG to specific fishery sources, this information will facilitate the management and prevention of this threat and the reduction of the damaging effects of DFG on Hawai‘i’s coral reef ecosystem.

We present the first deep dive analysis of DFG composition from three central subtropical North Pacific regions: Main Hawaiian Islands (removed from O‘ahu), Northwestern Hawaiian Islands (removed from Midway Atoll), and the pelagic central North Pacific (removed by the Hawai‘i-based pelagic longline fishery) (Figure 3.1). DFG composition within each region is

quantified by gear type, construction, and plastic polymer types, and compared across the three regions. Based on the seasonal variability of the convergent oceanographic features that aggregate this material in the North Pacific Ocean, we hypothesize DFG composition, based on the proportion of gear categories making up DFG conglomerates and the variation within the nets and lines categories, will be the same across the study regions.

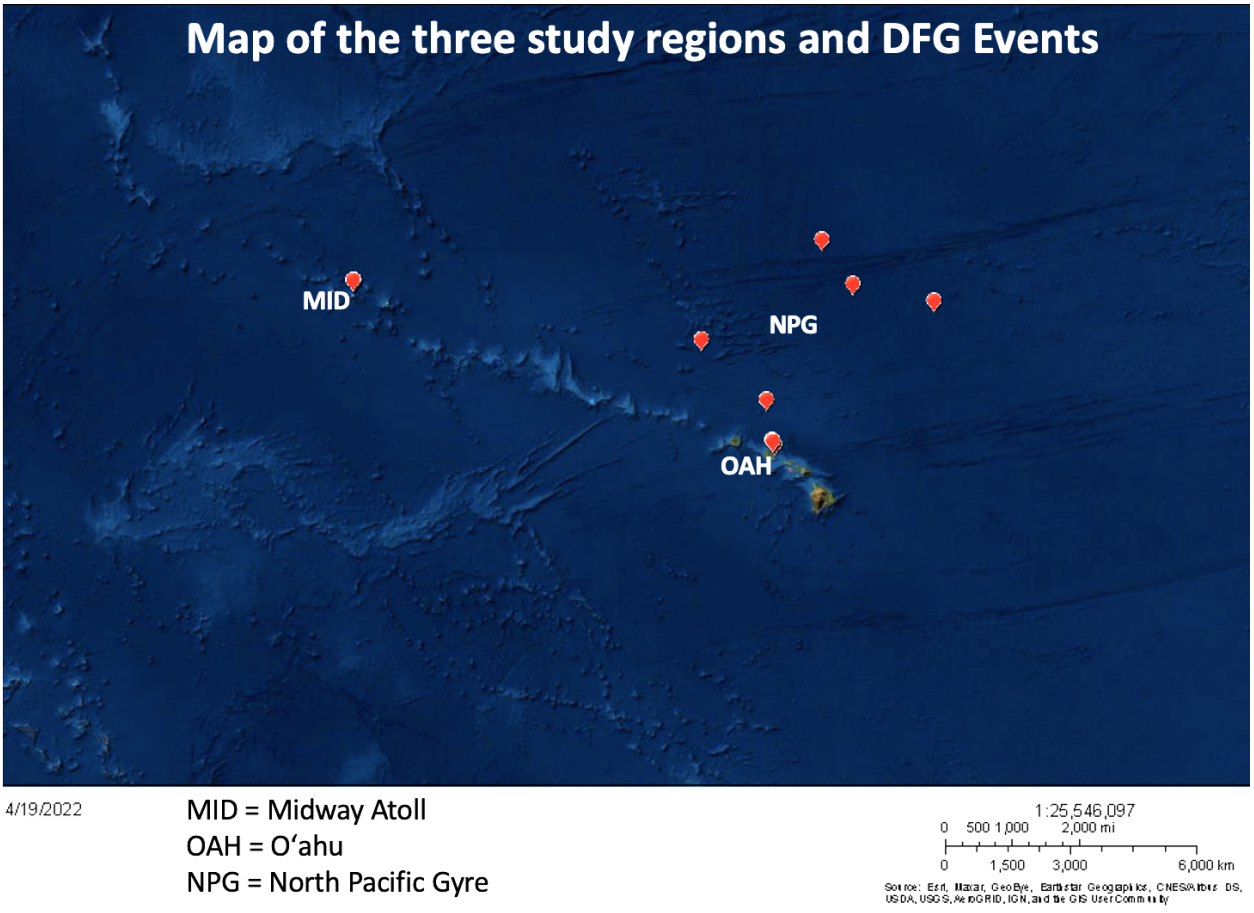

Figure 3.1a. Map of the Hawaiian archipelago indicating the three study regions, labeled with their respective three letter identifier. A scale is given in the bottom right corner. The islands of O'ahu (Figure 3.1b) and Midway (Figure 3.1c) where shore-based samples were collected and the locations where DFG conglomerates were collected from the North Pacific Gyre are shown.

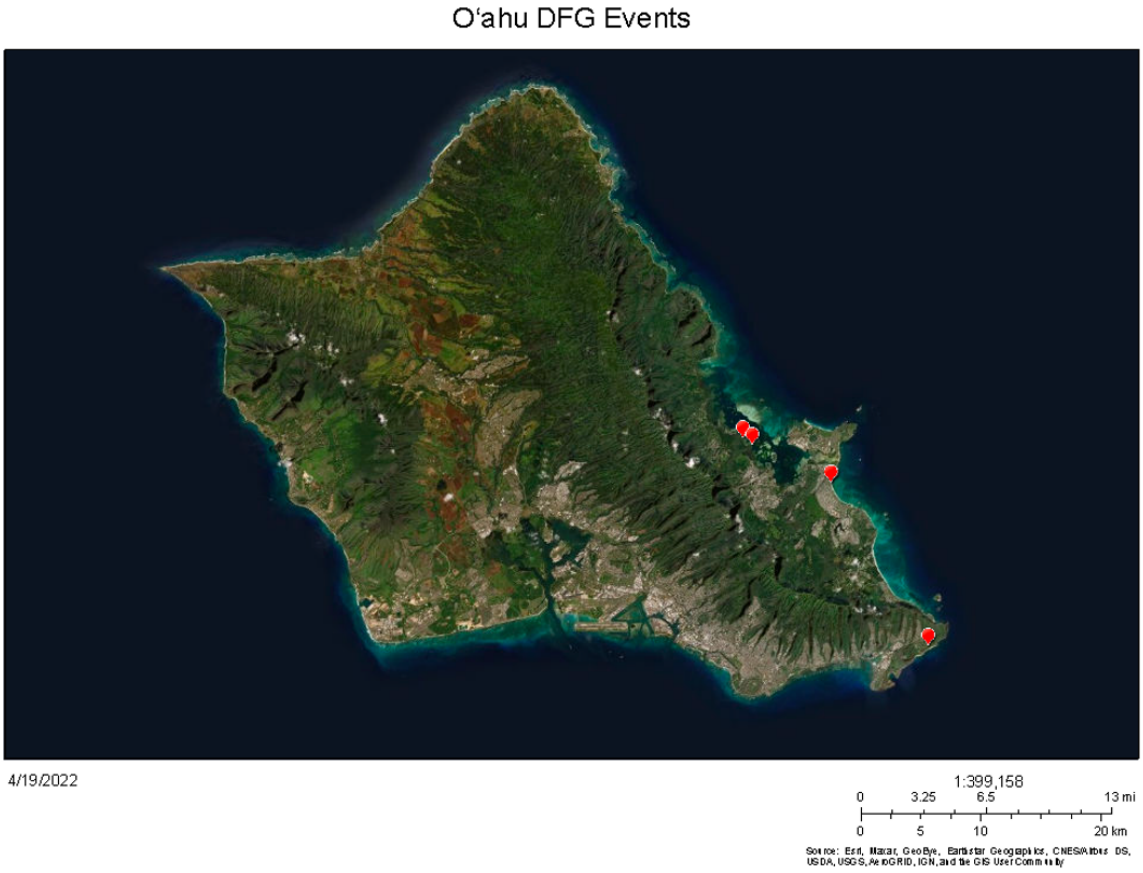

Figure 3.1b. Map of O‘ahu showing the locations where each DFG conglomerate was collected. Two DFG conglomerates were collected from the same location at different times and their respective pins are overlapping.

Figure 3.1c. Map of Midway Atoll showing the locations where each DFG conglomerate was collected.

METHODS

1. DFG Event Collection

In total, this project collected 160 unique DFG events between October 2019 and April 2022. Of this total, five DFG conglomerates were selected from each of the three locations: O‘ahu (OAH), Midway Atoll (MID), and pelagic central North Pacific northeast of Hawai‘i (NPG) (Table 3.1). The selection criteria for the 15 events analyzed in this study included that they needed to be conglomerates, mass of events had to have been measured, the event had to be

greater than 45 kg, and the first five conglomerates that were sampled and processed through the lab protocol that met these criteria were selected. Collection was dependent on detection, surveillance, and removal logistics for each region. For OAH, conglomerates were collected from shorelines and reefs on the east side of the island, and in-water removals were limited to Kāneʻohe Bay. In Papahānaumokuākea Marine National Monument, conglomerates were collected from the shorelines of East Island, Midway Atoll, during the marine debris removal mission with Papahānaumokuākea Marine Debris Project in April 2021. We partnered with the Hawaiʻi Longline Association commercial tuna fleet to obtain DFG that interrupted their fishing operations northeast of the Hawaiian Islands. Once the DFG was removed and in our possession, we transported the debris to our processing facility for sampling.

Table 3.1. Summary of 15 DFG conglomerates analyzed in this study.

15 DFG Conglomerates										
Study Region	Event	Latitude	Longitude	Date Collected (yyyy/mm/dd)	Mass (kg)	Length (cm)	Width (cm)	Height (cm)	Estimated Avg. Height (cm)	Circumference (cm)
MID	MID_03	28.214	-177.331	2021.04.09	66.4	120	118	56	42	408
	MID_04	28.214	-177.331	2021.04.09	503.4	677	170	74	61	1690
	MID_05	28.213	-177.332	2021.04.09	132.8	183	140	61	44	529
	MID_06	28.209	-177.340	2021.04.09	163.2	205	185	55	37	621
	MID_07	28.208	-177.343	2021.04.09	417.6	319	233	68	38	956
NPG	NPG_01	28.070	-154.020	2020.06.17	113.8	177	155	40	29	505
	NPG_05	27.387	-150.267	2020.10.02	381.2	320	250	83	63	965
	NPG_16	25.756	-161.097	2021.02.15	160.0	188	143	68	57	598
	NPG_17	23.195	-158.066	2021.02.15	58.4	174	113	50	40	487
	NPG_18	29.883	-155.467	2021.03.03	341.4	290	250	77	52	815
OAH	OAH_05	21.446	-157.814	2019.12.14	105.0	107	124	53	26	462
	OAH_06	21.291	-157.665	2020.06.04	127.2	173	144	54	43	572
	OAH_08	21.441	-157.806	2020.07.31	45.2	149	141	42	28	451
	OAH_13	21.413	-157.743	2020.08.23	66.8	231	98	49	44	591
	OAH_21	21.413	-157.743	2020.11.19	397.4	320	200	90	70	850

2. Field Sampling Protocol

Field sampling consisted of assessing the conglomerates by preliminary measurements and conducting our sample collection protocol (Chapter 2). Preliminary measurements included general observations of the whole event, distinguishing features, configuration, dominant gear types, and observations regarding gear sources or function. We measured the net bundles, including length (longest axis), width (widest axis perpendicular to length axis), maximum height, average height, and the perimeter of the event. After measurements, we took photos of each event from all four sides and top, including a meter stick and DFG event ID label in each photo. We weighed the events using a crane scale, rated to 4000 kg, mounted on an engine hoist rated to 1000 kg. After these preliminary DFG event metrics were complete, we began the sample collection process of distinct gear items from each DFG event. Sampling was conducted by trained team members, and volunteers provided additional support. We collected gear samples by disentangling or cutting them out following the Hybrid method protocol as outlined in detail in Chapter 2 (Figure 2.9) and described briefly below.

The goal of this sampling method was to divide DFG events into four nearly equal sections by volume and to collect a total of 80 samples, 20 from each section, to ensure even distribution of sample collection. We divided larger and more complex DFG events into sections by quickly spreading out the tangled bundle. This process often revealed sections of the DFG event that were greatly tangled, connected to one another by fewer, less tangled gear, such as lines (Figure 2.9). Spreading out the event is also important to reveal more material for potential samples and how different gear items are connected. Smaller DFG events, typically less than 100 kg, were not always divided into four sections, and some larger events, greater than 300 kg, were

divided into more than four sections, however no more than 80 samples total were collected. Sections were defined by imaginary borders and assigned a letter (A, B, C, or D) to document which samples were collected from each section. We used sharp serrated fishing knives to cut and remove samples of distinct pieces of gear. Some sections were very complex and contained greater than 20 unique gear items, and some were less complex with under 20 unique gear items. If there were less than 20 unique gear items available to sample from one section, then more samples were collected from more complex sections to reach a total of 80 samples. Sample selection was prioritized by largest to smallest gear items after estimating the volume of entire gear items before collecting samples. Unique items, gear configurations, and identifiable gear with markings were also prioritized. Each gear item was only sampled once, even if it was present in multiple sections. For each sample, we estimated the percent of the whole gear that was removed as a sample. Each gear item collected was assigned a unique sample number. The gear was classified into one of 14 possible categories (Table 2.2). Once a section was completed, the total percent by volume and by item sampled for each side was estimated.

Different gear types required different sampling considerations. Lines were considered for sampling if they were greater than 100 cm. However, shorter lines were considered if they had unique configurations or features as specified below. Approximately 30 cm length was cut out for line samples. If a sampled line had unique features (e.g., tied in a unique or identifiable knot, spliced, contained an eye loop, knotted or spliced with another type of line or gear, identifiable configurations, had metal attached, or was otherwise an uncommon construction) that feature was included in the sample, and the 30 cm size was exceeded if necessary. For nets to be included for sampling they needed to have at least nine rounds of webbing intact (Figure 2.5). For other types of gear, depending on the size, we collected the whole item, and the gear

type was recorded, as well as any associated connections to other gear. We also recorded the color of each sample. If an item was faded or bio-fouled, the original color, which was often distinguishable between twine strands or along a fresh cut, was used. If an item was multicolored, it was categorized as such, and the dominant color was recorded for the purposes of the current study. Each sample was assigned a biofouling rating from 0 to 3 (Table 2.4). If a sample was composed of multiple materials or gear types, this was noted, and the subsamples were documented in the lab. As samples were collected, we recorded notes on how each sample was connected to other gear within the DFG event, as well as any interesting features about the sample. We also documented if there were any marine organisms attached or entangled in the sample. Samples were separately bagged and sent to the lab for further analysis.

3. Lab Protocol

The lab protocol included sample categorization and polymer identification methods, described in detail in Chapter 2. We photographed the samples with standardized photo quality and documentation for future reference. Each sample and subsample were assigned a weathering code, evolved from Brignac et al. (2019) (Table 2.5). Each sample was weighed to 0.1 g or 0.00001 g analytical balances. Float measurements consisted of length, width, circumference, and inner diameter of the hole, if applicable. Lines were given a complexity rating of 1 - 4 based on how many complexity levels were present (Figure 2.18). Additionally, the line construction type was recorded as S = twisted clockwise, Z = twisted counterclockwise, or B = braided (Figure 2.19). The diameter of lines, and net twine, was measured in three intact and visually similar random parts of the sample or subsample, and averaged. The number of strands in the construction of a net or line was recorded. Furthermore, the type of fiber, the net twine or line it was composed of was recorded as monofilament, multifilament, film, or staple fiber (Figure

2.20). We categorized net construction by single or double stranded, twisted-knotted, twisted-knotless, braided-knotted, braided-knotless, monofilament-knotted, or other (Figure 2.21). Net mesh size was measured for three random mesh rounds by stretching the mesh in the depth direction (Figure 2.22). (See Chapter 2 for more detail).

For polymer identification of samples and subsamples we followed methods outlined in Jung et al., 2018. The polymer analysis was carried out using an attenuated total reflectance Fourier-transform infrared (ATR-FTIR) spectroscopy (Thermo Fisher Scientific iS5 or Agilent Technologies Cary 360). Polymer identity was determined by visually matching at least the top four absorbance bands in each spectrum to known polymer spectra as shown in Jung et al. (2018).

4. Data Analysis

Approach

Spatial differences in DFG composition among the three regions was assessed using a hierarchical two-level approach: (1) event composition by gear categories and (2) composition within gear categories. In the first level assessment, DFG event composition was calculated in two different ways, using the relative proportion of ten gear categories found in the events analyzed by number of items (count) and by mass. In the second level assessment, the composition of the two dominant gear categories, nets and lines, were also calculated by count and by mass.

It was common for samples to be composed of multiple subsamples of the same or different types of gear, such as multiple connected nets, or a net connected to a line and float. In these instances, for the current study, we classified multiple samples based on the primary subsample, identified by gear function. For example, if a multiple sample was composed of a net

and line and a float, we classified it as a net. If a float had a line attached, it was classified as a float. Samples with multiple nets were classified as net and the metadata of the larger net by mass was used to represent the whole sample.

Statistical Tests

4.1. Composition of DFG Events

To assess DFG event composition by gear category, two complementary multivariate approaches ideally suited to identify patterns in cross-correlated categorical and numerical variables with non-normal distributions were performed (McCune Grace 2002). Multi Response Permutation Procedure (MRPP) was used to determine if the three regions were significantly different from one another ($\alpha = 0.05$), followed with an Indicator Species Analysis (ISA) to identify the variables responsible for the observed group differences (Dufrene & Legendre 1997). Finally, the patterns in the data were explored using a non-metric multidimensional scaling (NMDS) ordination, which does not assemble discrete groupings of samples, but plots them along a multi-dimensional continuum representing combinations of the explanatory variables (Kenkel and Orloci, 1986).

4.2. Composition of Lines and Nets

To assess variation in line and net composition across the three regions, univariate statistics were performed in JMP, version 16.2.0, to test regional differences for each variable. A subset of nets and lines samples were selected for this comparison based on the following criteria: 1) all data metrics were measured for the sample, 2) the sample was estimated to be <10% removed from the whole gear, or 3) the sample was estimated to be <50% removed but was a net >0.4154 kg or a line >1.1 kg. Some samples did not have complete data due to lab

sample processing restraints, which resulted in prioritization of samples that represented large gear items, and samples that did not meet our selection criteria were deemed negligible in the scope of the whole DFG event mass and were not considered for this level two comparison. For lines, there were 211 included samples. For nets, there were 271 included samples (Table 3.1). Contingency tables (chi-squared or Fisher's Exact tests) compared the categorical data, and Kruskal-Wallis tests, followed by Wilxocon post-hoc tests, compared the numerical variables. A total of 11 categorical variables and three numeric variables were analyzed, eight categorical and two numeric variables pertained to lines and nets, and an additional three categorical and one numeric variable pertained to just nets (Table 3.2). All variables were tested as relative proportion by count. Additionally, nominal categorical variables were also weighted by extrapolated sample mass to test the relative proportion by mass (color, twine/line type, fiber types, polymer ID, construction, net monofilament, single or double net twine, and net knotted or knotless). Overall, we performed 54 tests, and assessed significance at the alpha = 0.05 level. These non-parametric approaches were selected due to the non-normal distribution of the data, with outliers, large skewness and kurtosis, and unequal group variances.

Following the univariate tests, the same composition data were analyzed considering all variables at once, separately for lines and nets, using the two same multivariate approaches applied to the composition of DFG events by gear categories, as described above. MRPP and NMDS tests were only applied to the line and net proportion by count data; we did not test the variables weighted by mass.

PC-ORD 6.22 software (McCune, B., Mefford, M.J., 1999) was used to run the MRPP and NMDS analyses, and the relative Sorensen measure was used to assess the distances between pairs of samples in ordination space, and to quantify the proportion of the variance in the

n-dimensional space that was captured by the k-dimensional ordination. NMDS followed a step-down approach with $k \leq 6$, and each axis was tested using randomization tests with 999 runs at the alpha = 0.05 level. Once the significance axes were identified, Clarke's approach was used to select the optimal dimensions of the ordination (McCune B, Grace JB, (2002) Analysis of ecological communities. MjM Software Design, Gleneden Beach, OR). Kendall Tau non-parametric correlations were used to identify significant correlations between the variables and the ordination axes (Walker, 2003).

4.3. Multivariate Data Matrices

For the Level 1 multivariate analysis of DFG event composition by gear proportion, matrix 1 included 15 rows representing individual DFG conglomerate events and 20 columns, representing the proportion by item and the proportion by mass of each of the ten gear categories: net, line, hard plastic mesh, hard plastic, float, metal, monofilament line, sheet, strapping, and other. Matrix 2 consisted of the 15 DFG events and a single category, region. Additionally, we ran MRPP of composition by item and by mass independently. In these analyses, each Matrix 1 included the ten gear categories; one matrix contained proportion by count and the other was proportion by mass. Matrix 2 remained consistent with the NMDS analysis.

For Level 2 analysis, multivariate analysis of composition within the nets and lines gear categories was carried out by NMDS and MRPP. Only categorical and continuous variables that describe line and net construction types were included in the multivariate analysis. Continuous variables that describe line or net construction including line/twine diameter and net mesh size, were binned to be included in the matrices as categorical data. All possible outcomes for each variable were separated into columns and set up as a binary matrix. Different matrices were

created for nets and lines to test variability in composition among the three regions. For lines, Matrix 1 involved 35 parameters that classified line color, binned line diameter, number of strands, construction, fiber type, and polymer composition. Matrix 2 included the DFG event, region, and all continuous variables for lines (extrapolated mass, line diameter, biofouling, and weathering). One DFG event had no line samples (OAH_13) that met the inclusion criteria, so only 14 events were included in the matrices (Table 3.1). For nets, matrix 1 involved 42 parameters that classified net color, binned twine diameter, number of yarn strands in the twine, twine construction, fiber type, binned mesh size, single or double twine strands, knotted or knotless, and polymer composition. Matrix 2 included DFG event, region, percent removed, extrapolated mass, twine diameter, mesh size, biofouling, and weathering (Appendix 4 - multivariate data workbook).

Table 3.1. The number of samples analyzed to assess the composition of the line and net categories from five events in each region.

Selected line and net samples by event and region									
				Lines			Nets		
Study Region	Event	Total # samples	Total Selected	Total	Selected	Excluded	Total	Selected	Excluded
MID	MID_03	61	18	34	10	24	14	8	6
	MID_04	81	61	32	21	11	43	40	3
	MID_05	80	26	34	15	19	30	11	19
	MID_06	80	31	60	25	35	10	6	4
	MID_07	82	57	40	37	3	31	20	11
	MID Total	**384**	**193**	**200**	**108**	**92**	**128**	**85**	**43**
NPG	NPG_01	77	15	29	3	26	37	12	25
	NPG_05	93	47	26	6	20	56	41	15
	NPG_16	79	17	43	11	32	18	6	12
	NPG_17	84	14	44	6	38	25	8	17
	NPG_18	89	48	31	15	16	42	33	9
	NPG Total	**422**	**141**	**173**	**41**	**132**	**178**	**100**	**78**
OAH	OAH_05	79	19	54	11	43	19	8	11
	OAH_06	126	33	70	9	61	40	24	16
	OAH_08	72	8	43	7	36	12	1	11
	OAH_13	115	20	19	0	19	80	20	60
	OAH_21	81	68	43	35	8	35	33	2
	OAH Total	**473**	**148**	**229**	**62**	**167**	**186**	**86**	**100**
	Grand Total	**1279**	**482**	**602**	**211**	**391**	**492**	**271**	**221**

RESULTS

Level 1: DFG Event Composition by Gear Type

On average, DFG conglomerates were primarily composed of nets (37.1% by count, 46.0% by mass) and lines (48.1% by count, 52.0% by mass) (Figures 3.3 and 3.4). All other gear categories accounted for 14.7% of DFG events by count, and only 2.0% by mass. The three regions did not significantly differ in composition of DFG events by count or by mass (Level 1 MRPP p-values = 0.4397 and 0.5231, respectively).

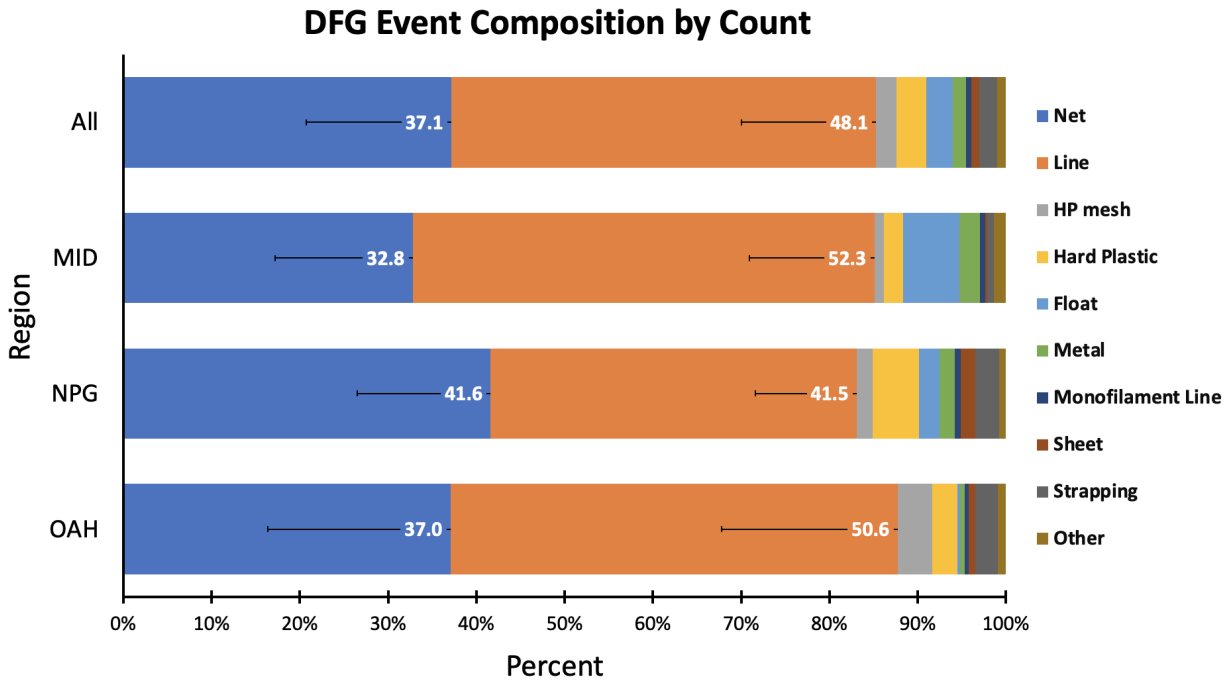

Figure 3.3. Derelict fishing gear (DFG) event composition by percentage of gear counts. The top bar represents the average DFG event composition of all 15 events. Each of the other bars represents the average DFG event composition of the respective study region. Error bars of one standard deviation are shown for the categories of nets and lines (MRPP p = 0.4397). HP mesh = hard plastic mesh.

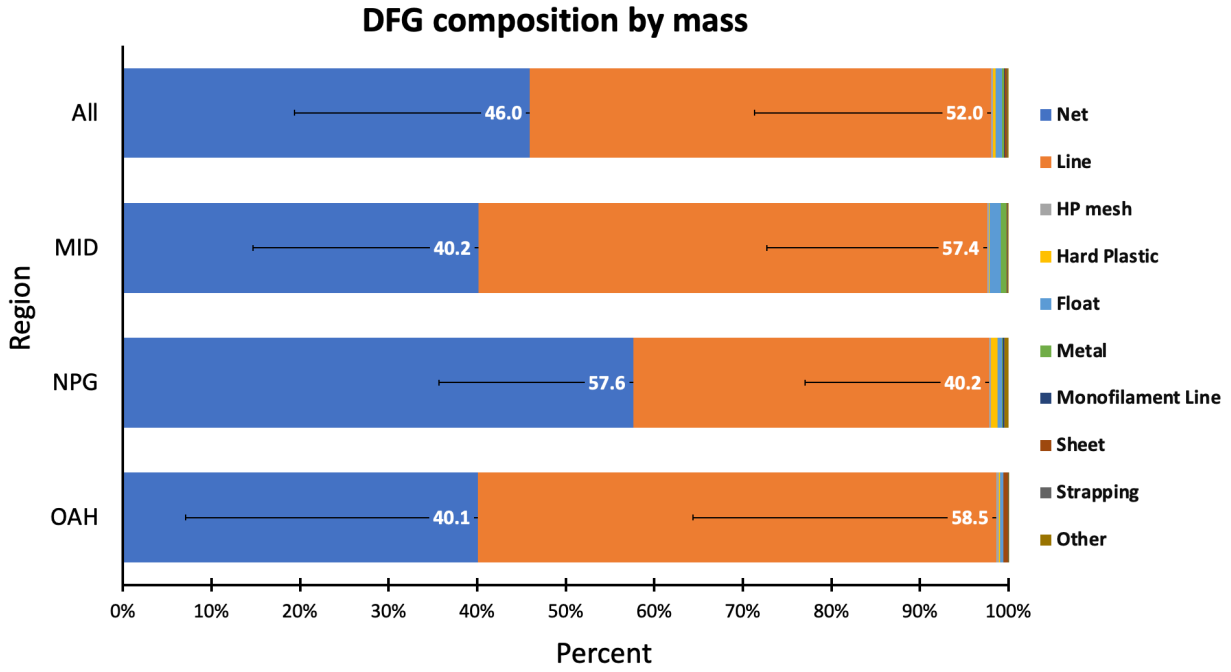

Figure 3.4. Derelict fishing gear (DFG) event composition by percentage of gear mass. The top bar represents the average DFG event composition of all 15 events. Each of the other bars represents the average DFG event composition of the respective study region. Error bars of one standard deviation are shown for the categories nets and lines (MRPP p = 0.5231). HP mesh = hard plastic mesh.

The DFG events showed no patterns in the output of the NMDS ordination of proportional gear by item and by mass (Figure 3.5). A 2-dimensional analysis based on the stress reduction with additional axes resulted in a minimum stress of 4.388 (p-value = 0.001), and explained 98.3% of the pattern in the data (orthogonality = 47.5%). Axis 1 explained 57.8% of the overall variance, and was negatively correlated with hard plastic mesh by mass and count, positively correlated with line mass, and negatively correlated with net mass. Axis 2 explained an additional 41.1% of the variance, and was negatively correlated with line mass and count, and positively correlated with net mass and count. Results of the MRPP of all proportional gear categories by count and by mass together confirmed no significant difference in DFG composition across regions (p-value = 0.5136).

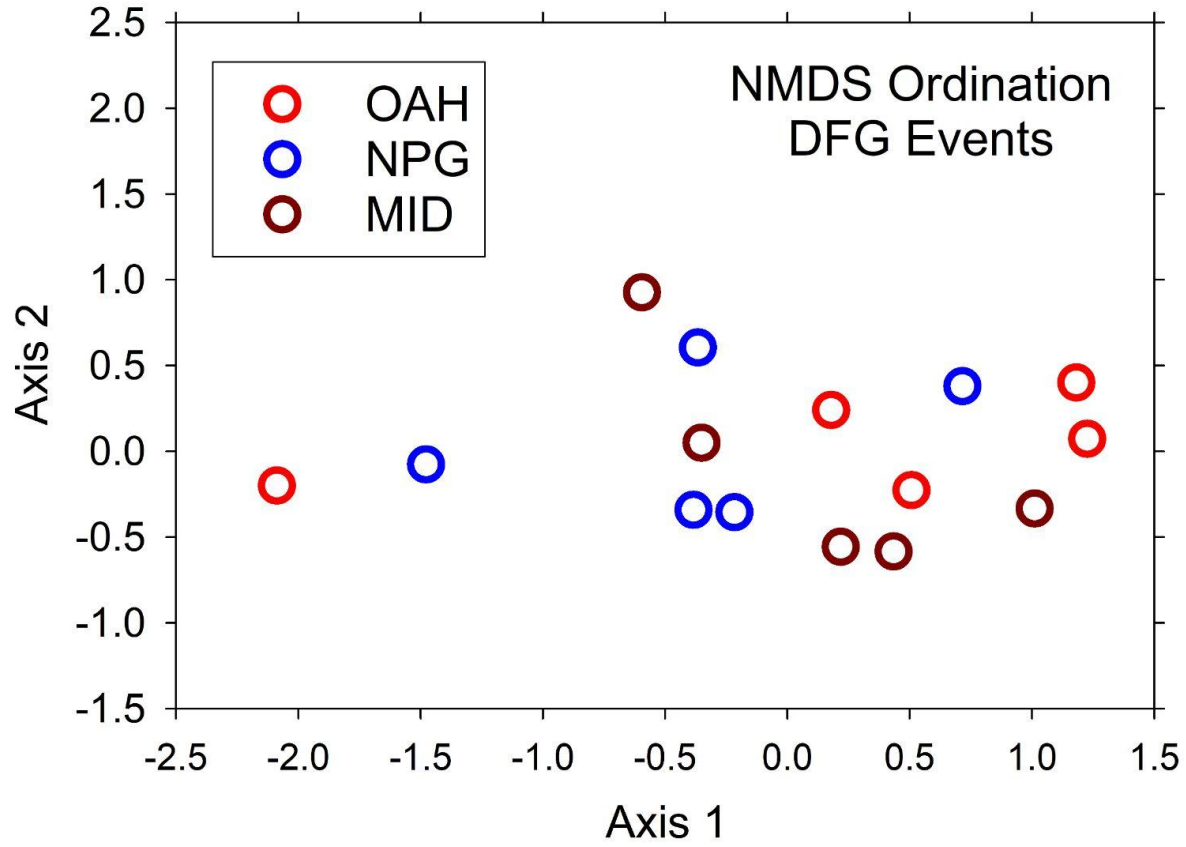

Figure 3.5. Two-dimensional ordination plot showing the results from the NMDS of DFG event composition by proportion of gear types. The 15 events are indicated by the blue triangles, and the vectors represent the different gear categories by count and by mass. The size and orientation of the vectors indicate their correlation to the axes.

Level 2: Composition of Lines and Nets

Exploring variation within the line and net categories revealed differences in gear composition across the regions. Table 3.2 summarizes the univariate results for both gear types and all parameters tested.

Table 3.2. Results of Level 2 univariate statistical tests of line and net variables assessed by count and by mass. Categorical (blue) or numeric continuous (yellow) variables with significant p-values (red) are shown.

Summary Table of Gear Variables and Significance									
Variable	Categorical or Numeric	By Count				Weighted by Mass			
		Test	Line p-value	Test	Net p-value	Test	Line p-value	Test	Net p-value
Mass	Numeric	χ2	0.9277	χ2	0.0630	-	-	-	-
Color	Categorical	Fisher's	0.2620	Fisher's	0.0288	Fisher's	0.0005	Fisher's	0.0005
Biofouling	Categorical	χ2	<0.0001	χ2	<0.0001	-	-	-	-
Weathering	Categorical	χ2	0.2341	χ2	0.5126	-	-	-	-
Line / Twine diameter	Numeric	χ2	0.1727	χ2	0.0007	-	-	-	-
Number of strands	Categorical	χ2	0.9616	χ2	0.0006	-	-	-	-
Line / Twine type	Categorical	Fisher's	0.6004	Fisher's	0.0005	χ2	<0.0001	Fisher's	<0.0001
Fiber type	Categorical	Fisher's	0.1340	Fisher's	0.0007	Fisher's	<0.0001	Fisher's	<0.0001
Polymer ID	Categorical	Fisher's	0.0903	Fisher's	0.0044	χ2	<0.0001	χ2	<0.0001
Line / Net construction	Categorical	Fisher's	0.0495	Fisher's	0.0010	Fisher's	0.0005	Fisher's	0.0005
Net mesh size	Numeric	-	-	χ2	0.1470	-	-	-	-
Net monofilament or not	Categorical	-	-	χ2	0.0006	-	-	χ2	<0.0001
Single or double net twine	Categorical	-	-	Fisher's	0.3058	-	-	Fisher's	0.0459
Net knotted or knotless	Categorical	-	-	χ2	0.1328	-	-	χ2	0.8924
Multivariate MRPP	Categorical	MRPP	0.075	MRPP	<0.0001	-	-	-	-

Lines: spatial differences by count

The results of the univariate tests for lines indicate only biofouling and line construction variables were significantly different among regions (Table 3.2). MID lines were less biofouled than OAH and NPG (Figure 3.6; MID = 0.64 ± 0.57, OAH = 1.17 ± 0.38, NPG = 1.19 ± 0.81, chi-square = 38.0834, p = <0.0001). There was no difference in line mass across regions (Figure 3.7; p = 0.9277), the average extrapolated line mass was 4.54 kg. Line color in all regions was dominated by white, grey, green, and black (Figure 3.8; p = 0.2620). Most lines were moderate to severely weathered with no regional difference (Figure 3.9; p = 0.2341). The average line diameter was 17 mm and there was no significant difference among regions (Figure 3.10; p = 0.1727). Most lines were three stranded, and there was no difference between regions (Figure 3.11; p = 0.9616). Line type was the same across regions, most commonly Z-twisted (84.8%), followed by S-twisted (10.1%) and Braided (5.2%) (Figure 3.12; p = 0.6004). Line fiber type

was not significantly different across regions and primarily made of monofilament fibers (57.3%) and staple fibers (40.8%) (Figure 3.13; p = 0.1340). Polymer composition for lines was not significantly different across the regions, and composition consisted of PE (56.0%), PE/PP blend (41.2%), and PP (2.8%) (Figure 3.14; p = 0.0903). The two most common line construction types by count were three stranded Z-twisted staple fiber PE/PP blend, and three stranded Z-twisted monofilament fiber PE. Yet, the Fisher's Exact test revealed significant differences among regions (Figure 3.15; p = 0.0495). However, the multivariate results showed no significant differences in line composition among the three regions (MRPP p = 0.0750).

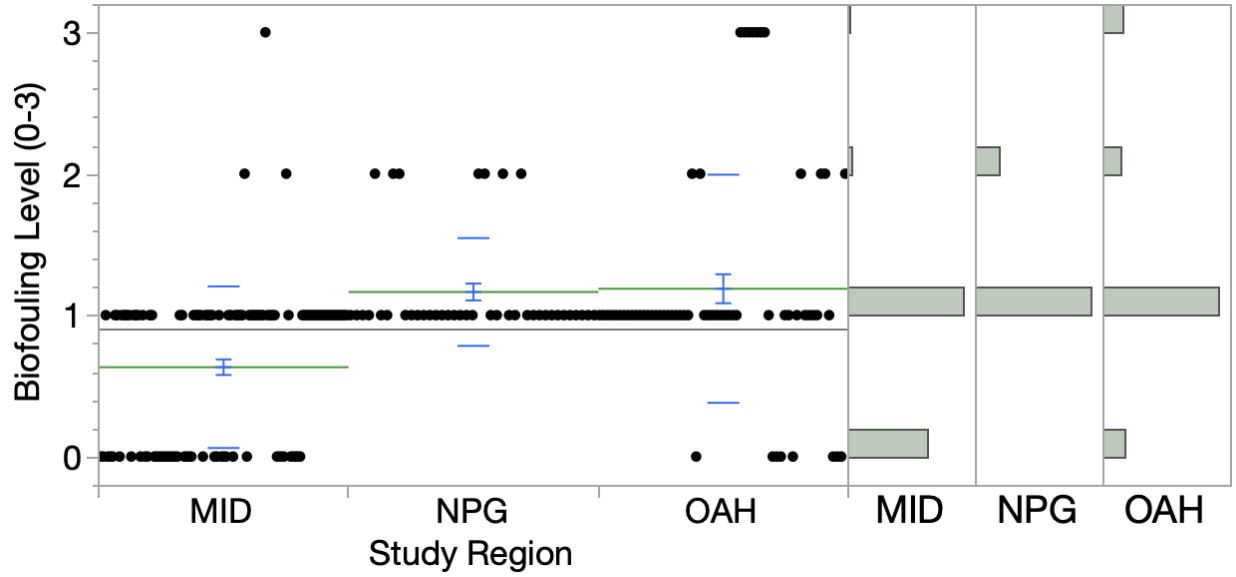

Figure 3.6. Biofouling level (y-axis) for each line sample (black dot) from each region, listed along the x-axis. The regional means are indicated by the green horizontal lines. The narrower blue bars overlapping the mean line are standard errors. The wider blue lines above and below the mean represent the standard deviation. The grey line across all three regions indicates the grand mean. Histograms summarizing each region are provided on the right. (Chi-squared test = 38.08, p = <0.0001)

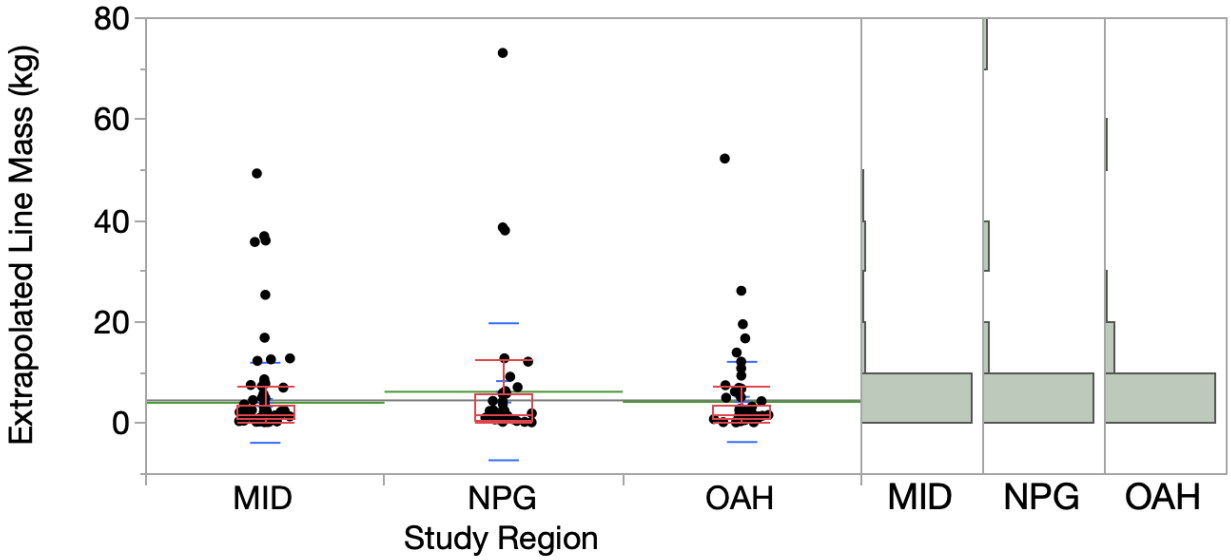

Figure 3.7. Extrapolated sample mass in kg (y axis) for each line sample (black dot) from each region, listed along the x-axis. Regional means are indicated by the green horizontal line. The narrower blue bars overlapping the mean line are standard errors. The wider blue lines above and below the mean represent the standard deviation. The grey line across all three regions indicates the grand mean. Red box plots show the interquartile range, and the whiskers indicate the maximum and minimum values excluding outliers. Histograms summarizing each region are provided on the right. (Chi-squared test p = 0.9277)

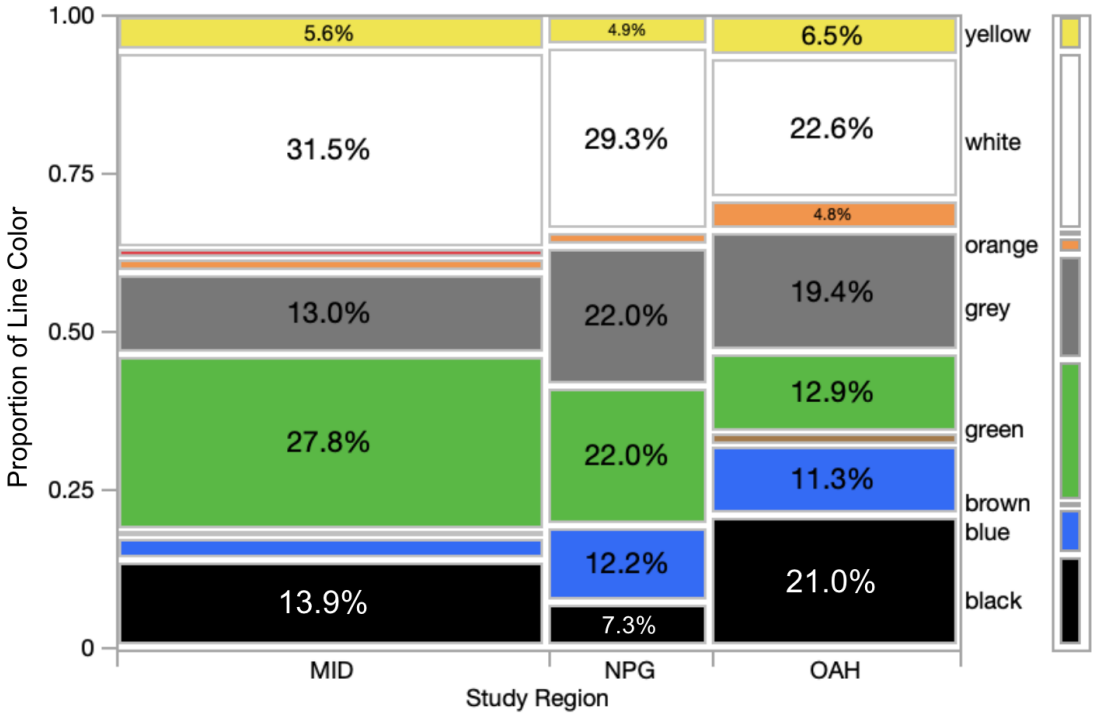

Figure 3.8. Mosaic plot of line color proportion by count. The width of the region column indicates the proportion of the total sample size. The legend on the right shows the color of each group and the average proportions across all regions. (Fisher's Exact test p = 0.2620)

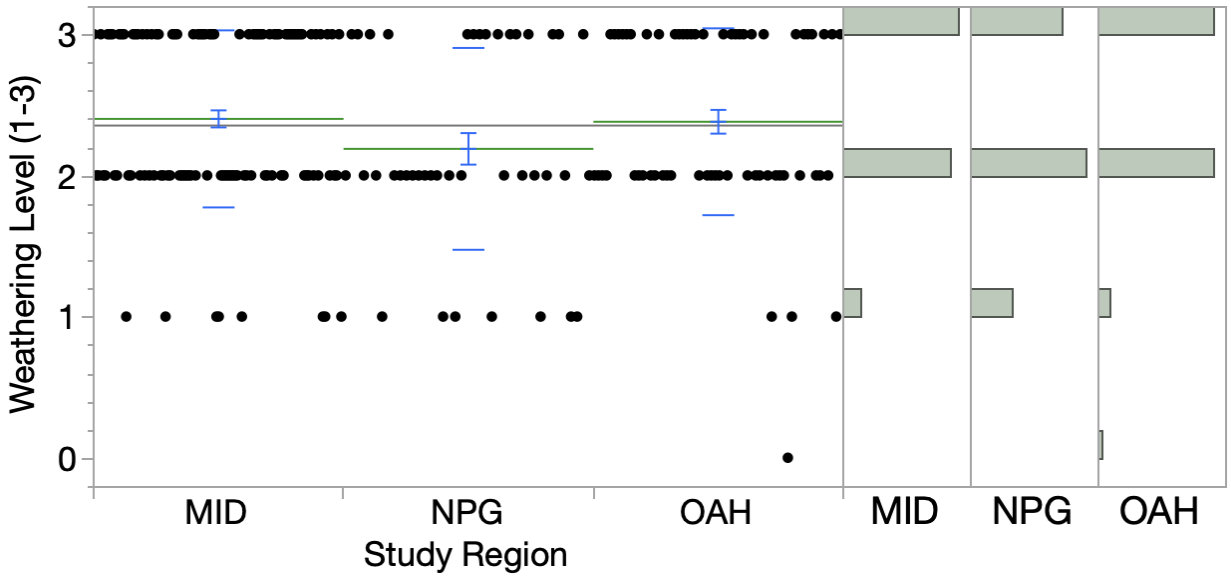

Figure 3.9. Weathering (y-axis) for each line sample (black dot) from each region, listed along the x-axis. The regional means are indicated by the green horizontal lines. The narrower blue bars overlapping the mean line are standard errors. The wider blue lines above and below the mean represent the standard deviation. The grey line across all three regions indicates the grand mean. Histograms summarizing each region are provided on the right. (Chi-squared test = 2.90, p = 0.2341)

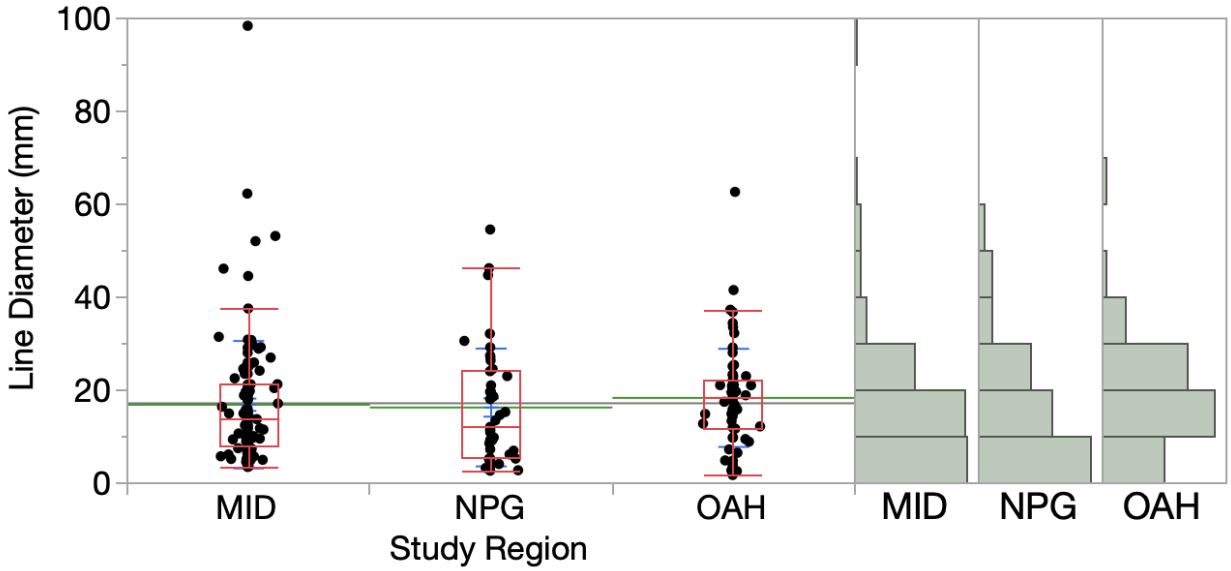

Figure 3.10. Line diameter in mm (y axis) for each line sample (black dot) from each region, listed along the x-axis. Regional means are indicated by the green horizontal line. The narrower blue bars overlapping the mean line are standard errors. The wider blue lines above and below the mean represent the standard deviation. The grey line across all three regions indicates the grand mean. Red box plots show the interquartile range, and the whiskers indicate the maximum and minimum values excluding outliers. Histograms summarizing each region are provided on the right. (Chi-squared test = 3.51, p = 0.1727)

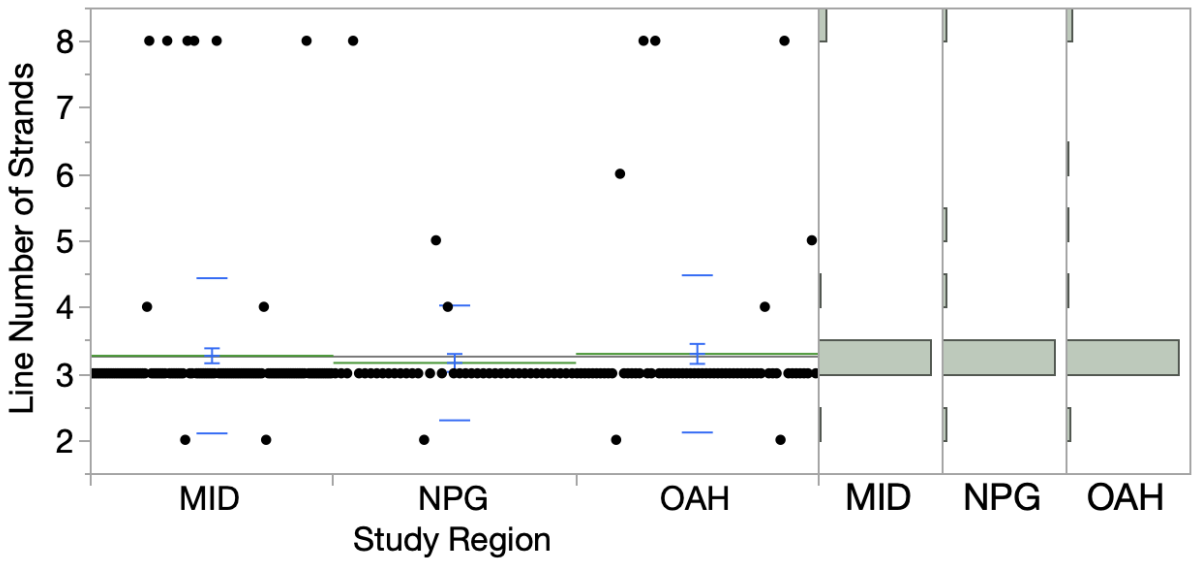

Figure 3.11. Number of strands (y-axis) for each line sample (black dot) from each region, listed along the x-axis. The regional means are indicated by the green horizontal lines. The narrower blue bars overlapping the mean line are standard errors. The wider blue lines above and below the mean represent the standard deviation. The grey line across all three regions indicates the grand mean. Histograms summarizing each region are provided on the right. (Chi-squared test = 0.08, p = 0.9616)

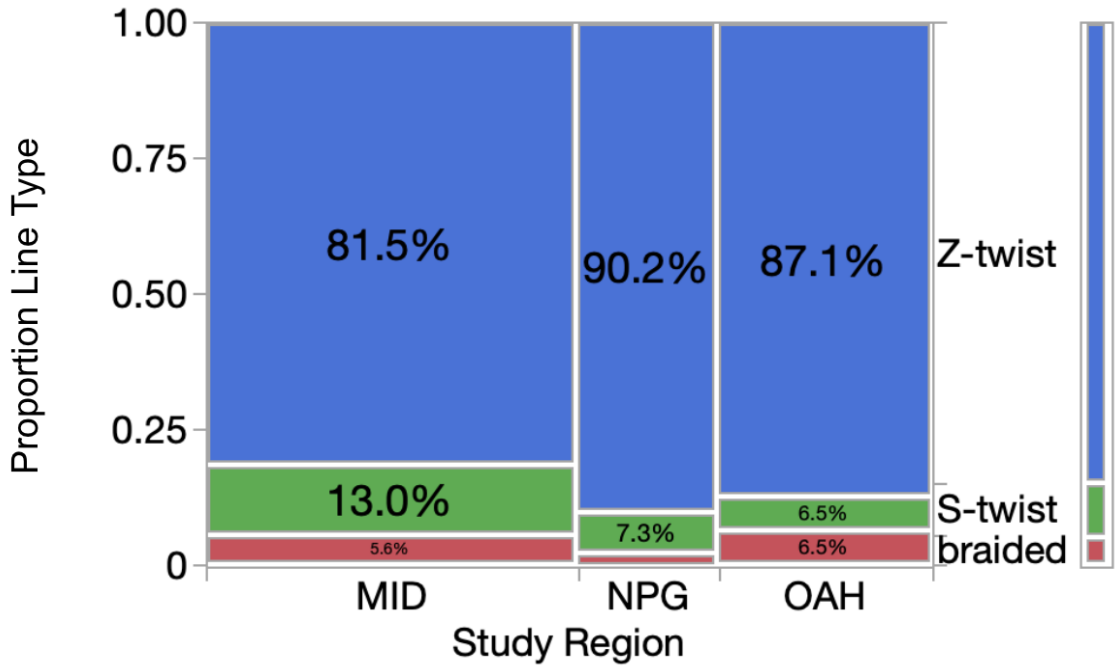

Figure 3.12. Mosaic plot of line type proportion by count. The width of the region column indicates the proportion of the total sample size. The legend on the right shows the color of each group and the average proportions across all regions. (Fisher's Exact test p = 0.6004)

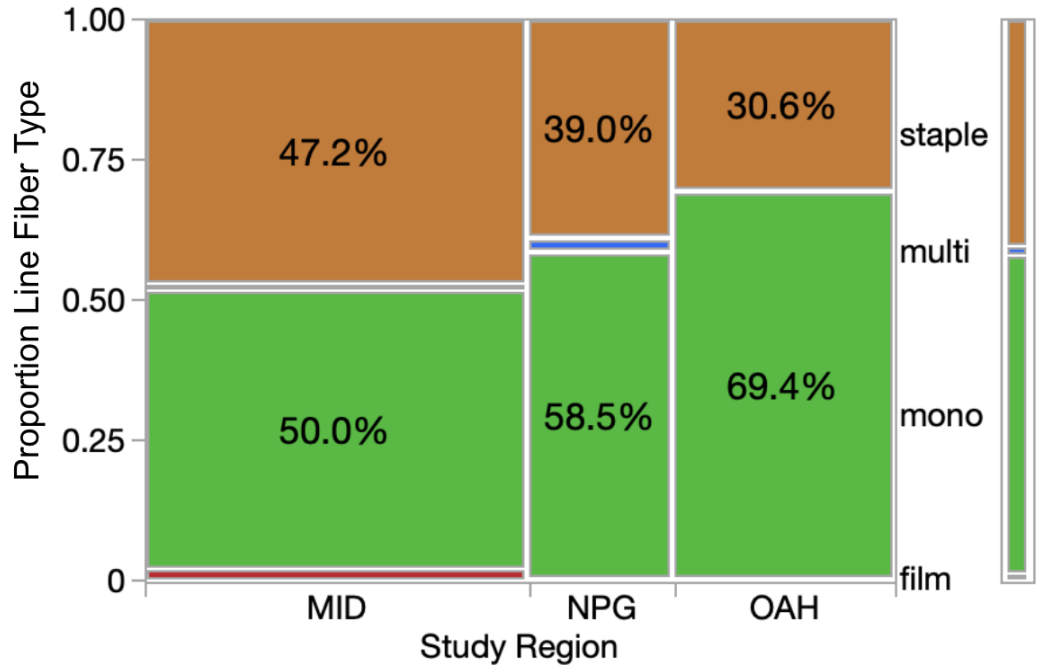

Figure 3.13. Mosaic plot of line fiber type proportion by count. The width of the region column indicates the proportion of the total sample size. The legend on the right shows the color of each group and the average proportions across all regions. (Fisher's Exact test p = 0.1340)

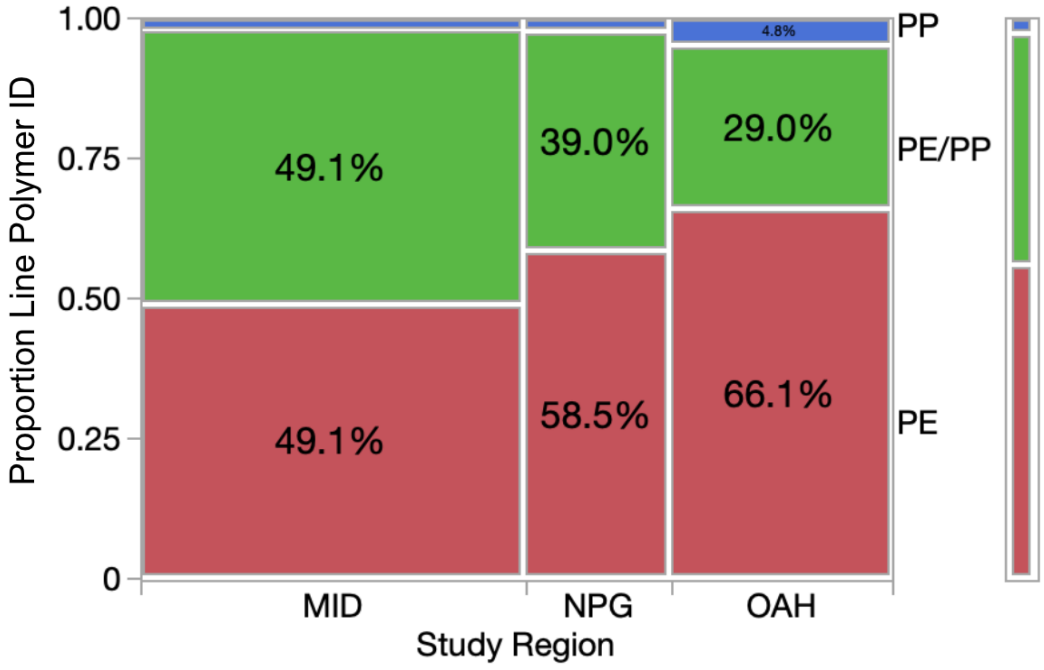

Figure 3.14. Mosaic plot of line polymer composition proportion by count. The width of the region column indicates the proportion of the total sample size. The legend on the right shows the color of each group and the average proportions across all regions. PP = polypropylene; PE = polyethylene; PE/PP = blend of PE and PP. (Fisher's Exact test p = 0.0903)

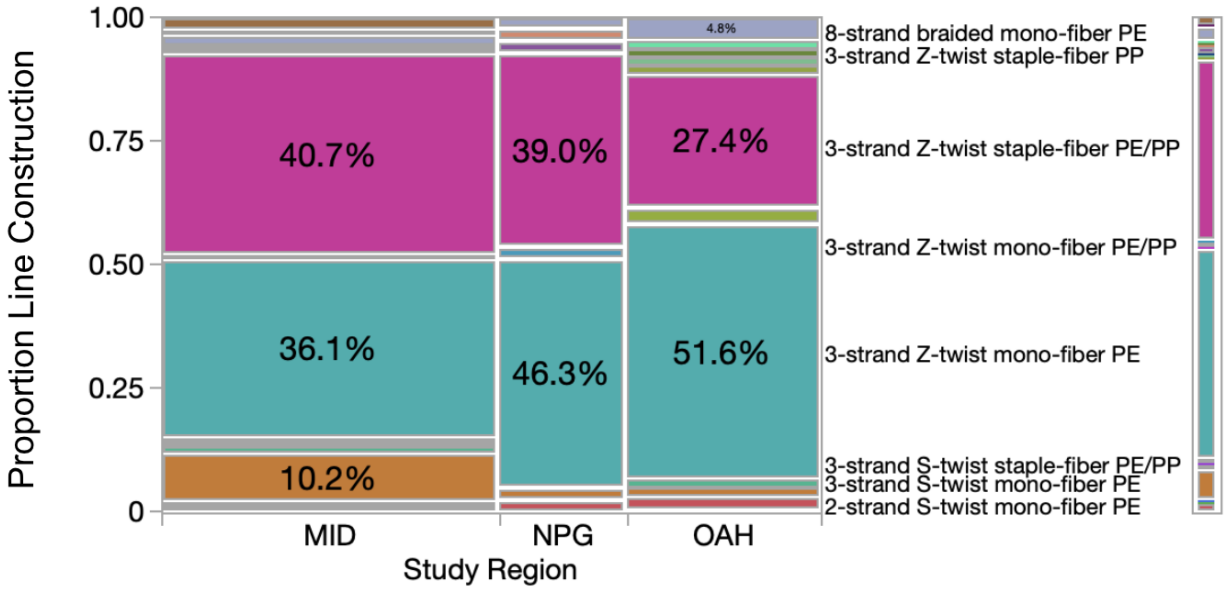

Figure 3.15. Mosaic plot of line construction proportion by count. The width of the region column indicates the proportion of the total sample size. The legend on the right shows the color of each group and the average proportions across all regions. PP = polypropylene; PE = polyethylene; PE/PP = blend of PE and PP. (Fisher's Exact test p = 0.0495)

Lines: spatial differences by mass

Contrary to the line composition by count results, composition weighted by extrapolated line sample mass showed significant differences across the regions for all variables tested, including line color, line type, line fiber type, polymer ID, and line construction. Line color weighted by mass was dominated by white (47.5%), grey (19.8%), black (10.8%), green (8.9%), and blue (8.7%) (Figure 3.16; Fisher's Exact test p = 0.0005). MID had the greatest proportion of white lines by mass of 56.7%. NPG had the greatest proportion of grey lines by mass of 37.0%. Line type was predominantly Z-twisted by mass (81.7%), and made up 98.9% of NPG lines (Figure 3.17; Chi-squared = 101.009, p = <0.0001). Line fiber type weighted by mass composed of 66.4% staple fiber, and 30.7% monofilament fiber types, and NPG had the greatest proportion of staple fiber lines at 83.3% (Figure 3.18; Fisher's Exact test p = 3.996e-16). Polymer ID weighted by mass was dominated by polyethylene-polypropylene (PE/PP) blend

(66.6%) and PE (30.3%), and NPG had the greatest proportion of PE/PE blend lines by mass at 83.3% (Figure 3.19; Chi-square = 68.3, p = <0.0001). Line construction weighted by mass was primarily 3-stranded, Z-twisted, staple fiber, PE/PP blend (54.5%), followed by 3-stranded, Z-twisted, monofilament fiber, PE (24.1%), and NPG had the greatest concentration by mass of the 3-stranded, Z-twisted, staple fiber, PE/PP blend line construction (83.3%) (Figure 3.20; Fisher's Exact Test p = 0.0005).

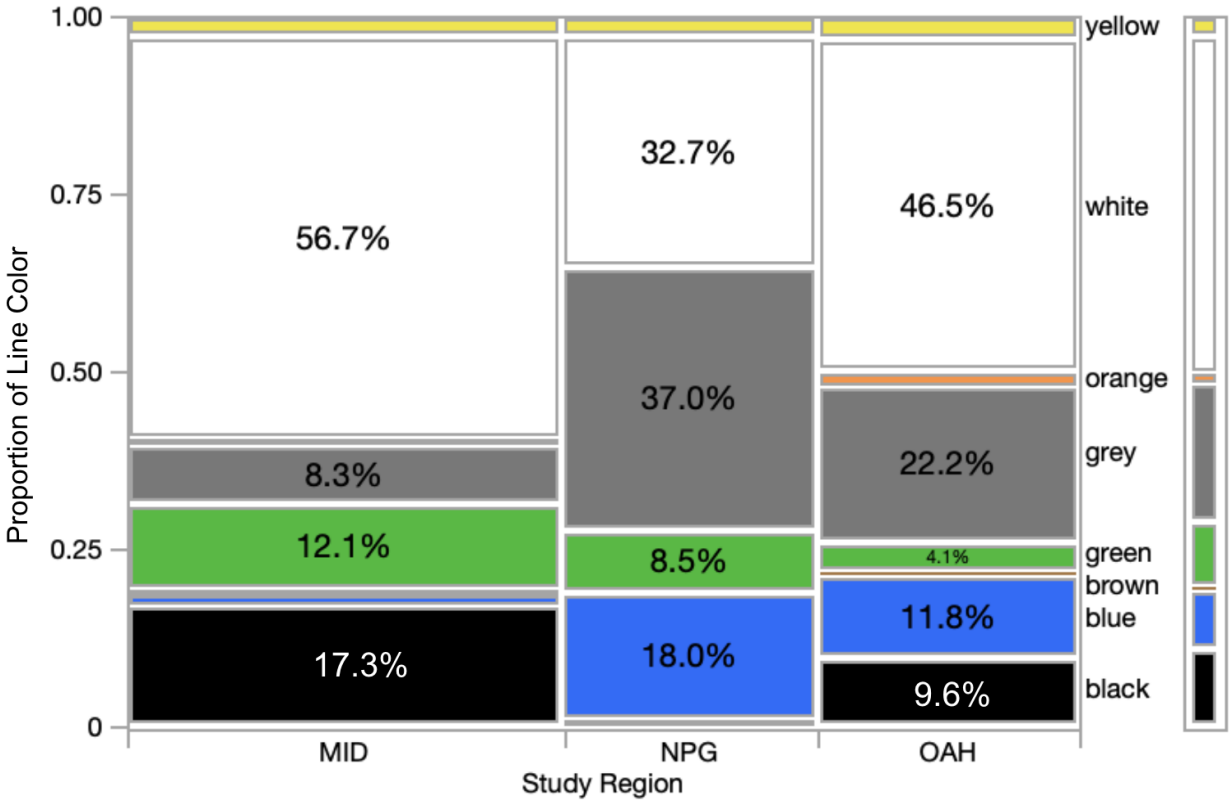

Figure 3.16. Mosaic plot of line color proportion by mass. The width of the region column indicates the proportion of the total sample size. The legend on the right shows the color of each group and the average proportions across all regions. (Fisher's Exact test p = 0.0005)

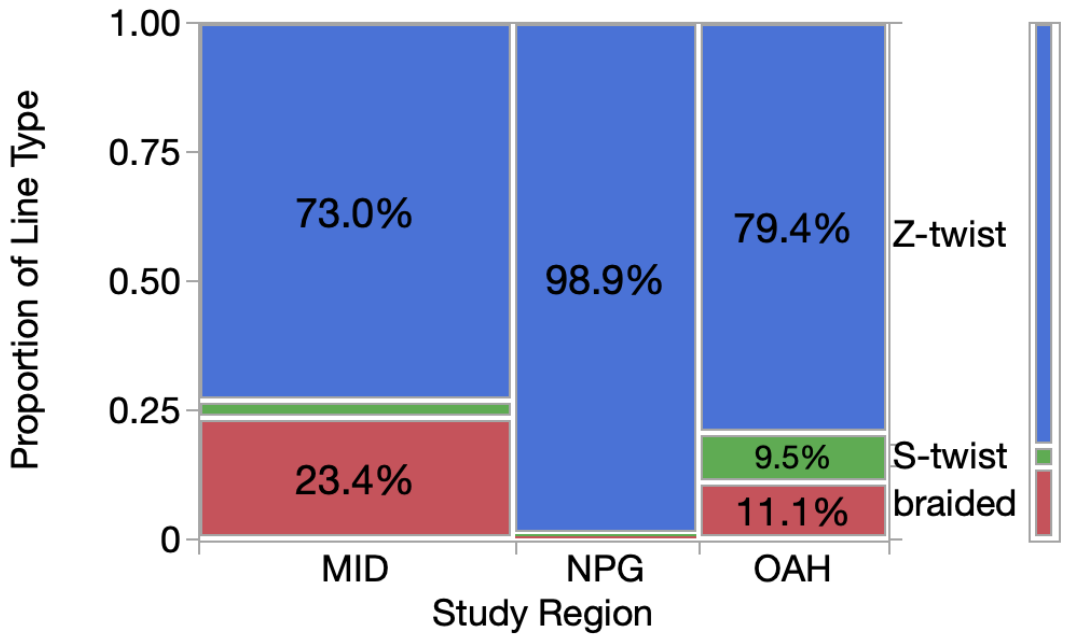

Figure 3.17. Mosaic plot of line type proportion by mass. The width of the region column indicates the proportion of the total sample size. The legend on the right shows the color of each group and the average proportions across all regions. (Chi-squared test = 101.009, p = <0.0001)

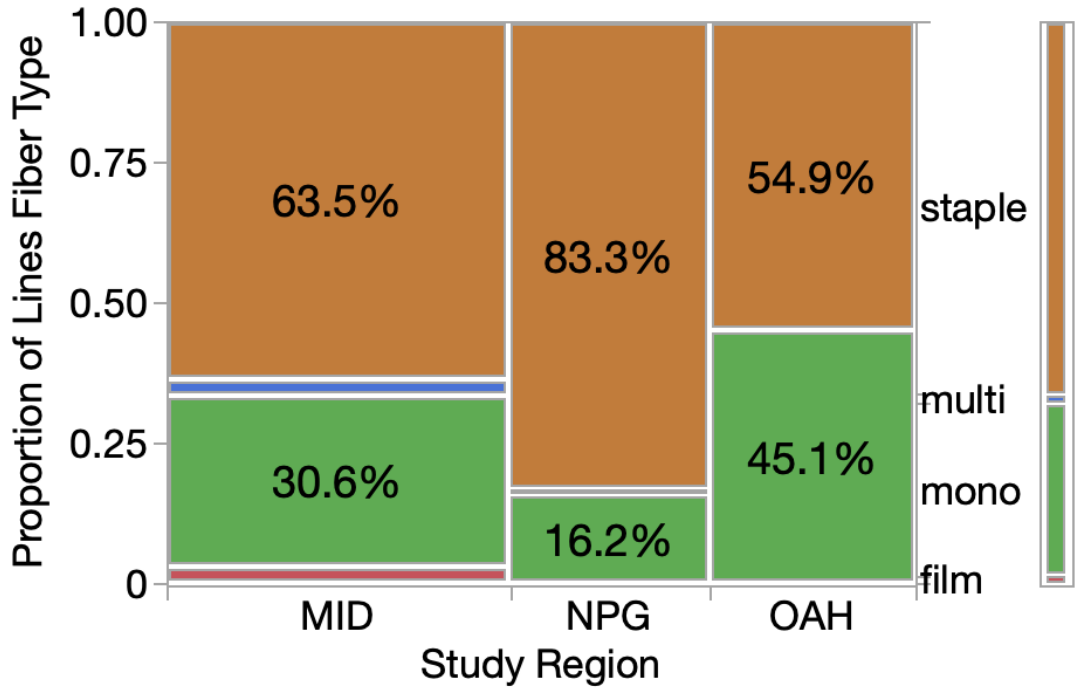

Figure 3.18. Mosaic plot of line fiber type proportion by mass. The width of the region column indicates the proportion of the total sample size. The legend on the right shows the color of each group and the average proportions across all regions. (Fisher's Exact test p = 3.996e-16)

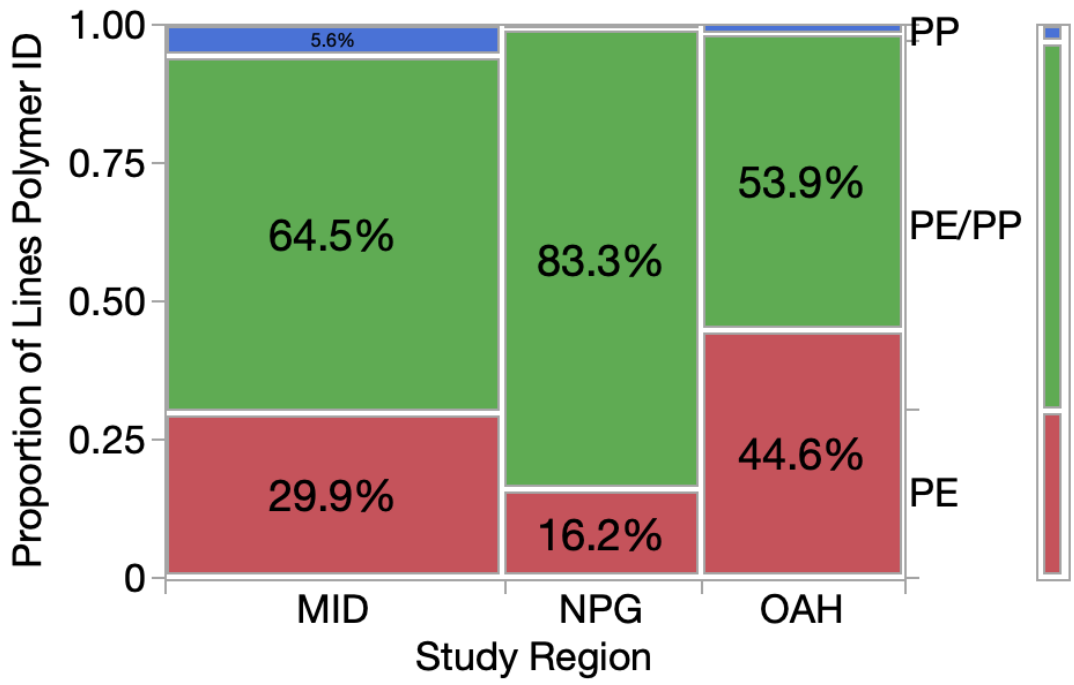

Figure 3.19. Mosaic plot of line polymer composition proportion by mass. The width of the region column indicates the proportion of the total sample size. The legend on the right shows the color of each group and the average proportions across all regions. PP = polypropylene; PE = polyethylene; PE/PP = blend of PE and PP. (Chi-squared test = 68.3, p = <0.0001)

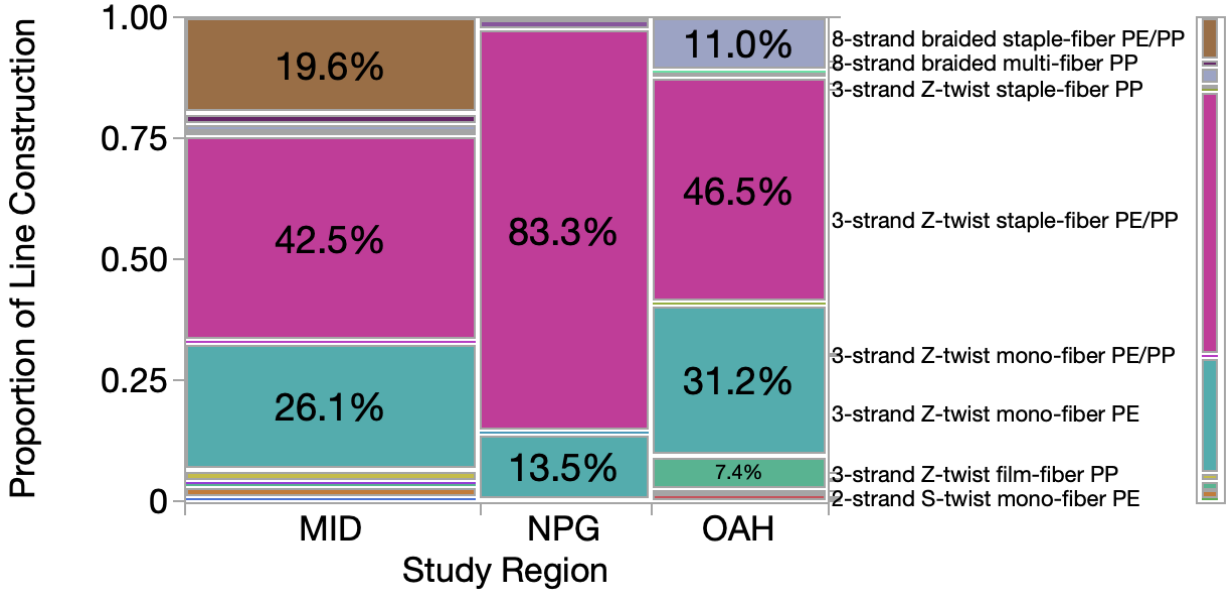

Figure 3.20. Mosaic plot of line construction proportion by mass. The width of the region column indicates the proportion of the total sample size. The legend on the right shows the color of each group and the average proportions across all regions. PP = polypropylene; PE = polyethylene; PE/PP = blend of PE and PP. (Fisher's Exact Test p = 0.0005)

Lines: multivariate tests

Multivariate analysis yielded no significant difference in line composition among the regions (MRPP p = 0.0750). NMDS for lines yielded a 2-dimensional ordination space that explained 81.9% of the variance, with a minimum stress value of 8.813 (p = 0.0010), and orthogonality of 76.1% (Figure 3.21). Axis 1 explained 34.2% of the variance, and was not significantly correlated to any variables. Axis 2 explained 47.7% of the variance, and was negatively correlated to staple fiber and PE/PP polymer ID, and positively correlated to monofilament fiber and PE polymer ID.

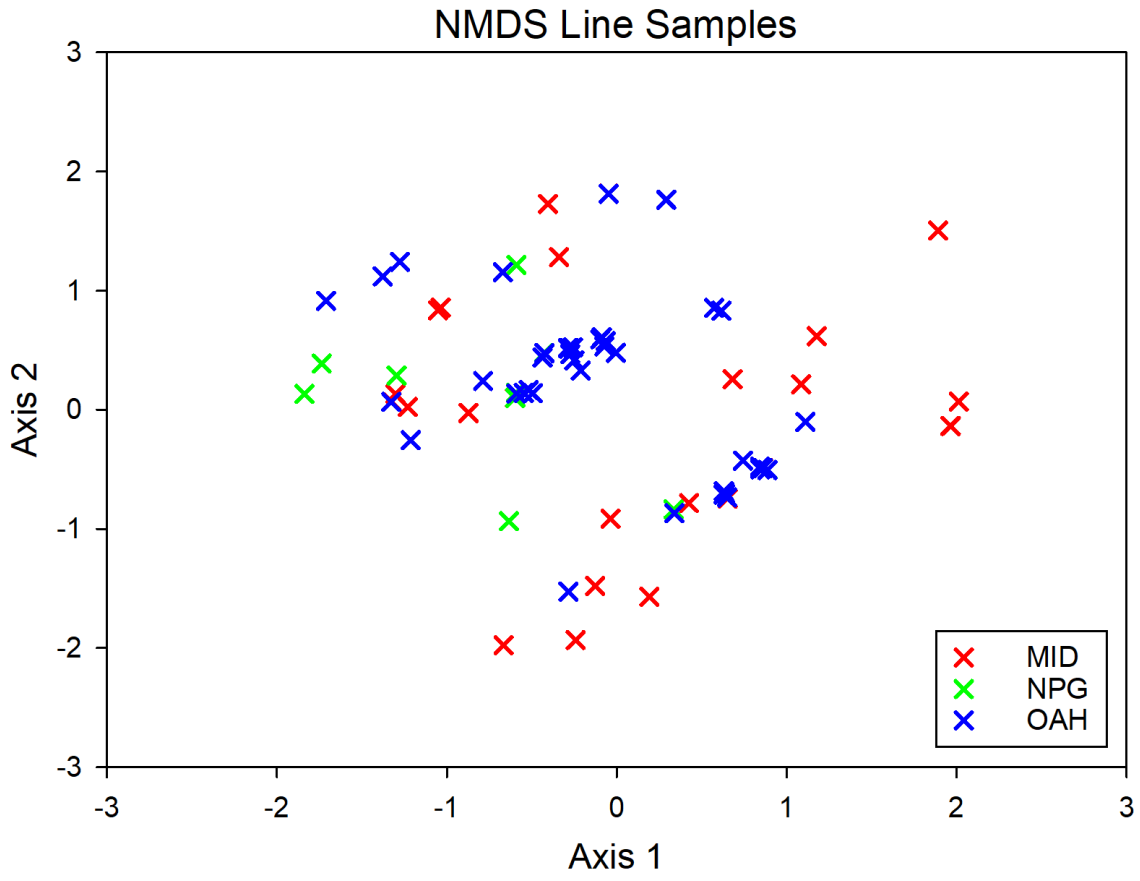

Figure 3.21. NMDS ordination plot of line samples from the three regions. Each symbol represents a line sample. (MRPP p = 0.07504)

Nets: spatial differences by count

For univariate results, average net mass was not significantly different across the regions (Figure 3.22; Chi-squared test = 5.53, p = 0.0630). Net color was primarily green (48.0%), grey (25.5%), and blue (10.0%), and there was significant regional variation with MID having a large proportion of green net and less grey net (Figure 3.23; Fisher's Exact test p = 0.0288). Biofouling of nets also showed significant regional differences (Figure 3.24; Chi-squared test = 39.78, p = <0.0001). All Wilcoxon pairwise comparisons were significantly different, with MID being the least biofouled and NPG being the most biofouled. Majority of the nets were moderately weathered (weathering code 2), and there were no regional differences (Figure 3.25; Chi-squared test = 1.34, p = 0.51). Twine diameter showed significant regional differences (Figure 3.26; Chi-squared test = 14.54, p = 0.0007), where MID nets had smaller twine diameter on average compared to both NPG and OAH (1.95 ± 0.22 mm, 2.56 ± 0.21 mm, 2.33 ± 0.22 mm, respectively). Most nets sampled were constructed with 3-stranded twine, but the number of twine strands was significantly different across all regions (Figure 3.27; Chi-squared test = 14.76, p = 0.0006). Compared to the other regions, MID had more nets with fewer strands, and OAH had more nets with a greater number of strands. Majority of net twines were Z-twisted (75.3%), followed by S-twisted (16.2%), then monofilament construction (6.6%), then braided (1.1%), and least rachel-braided (0.7%). There were significant differences across regions (Figure 3.28; Fisher's Exact test p-value = 0.0010). MID showed a greater proportion of monofilament construction nets (e.g., gillnets) and less Z-twisted twine than the other two regions. Net twine fiber type was primarily monofilament fiber (92.6%), and was significantly different across regions (Figure 3.29; Fisher's Exact test p = 0.0007). MID showed a greater proportion of single monofilament fiber nets compared to the other two regions (15.3%). Net

mesh size showed no significant regional variation, and the average mesh size was 9.71 cm ± 8.5 cm (median = 7.9 cm, IQR = 12.3 cm) (Figure 3.30; Chi-squared test = 3.84, p = 0.1470). Majority of nets were single-twine stranded (97.4%) opposed to double-twine stranded (2.6%), and there was no significant difference between regions (Figure 3.31; Fisher's Exact test p = 0.3058). Majority of nets were knotted (87.1%) opposed to knotless (12.9%), and there were no regional differences (Figure 3.32; Chi-squared test = 4.04, p = 0.1328). Polymer composition was dominated by PE across all regions (92.6%) and the remaining nets were made of nylon (7.4%), and polymer composition was significantly different across the regions, with MID showing greater proportion of nylon nets (Figure 3.33; Fisher's Exact test p = 0.0044). When concatenating the number of twines, number of twine strands, twine construction, fiber type, and polymer ID to assess net categories, regions are significantly different from one another (Figure 3.34; Fisher's Exact test p = 0.0010).

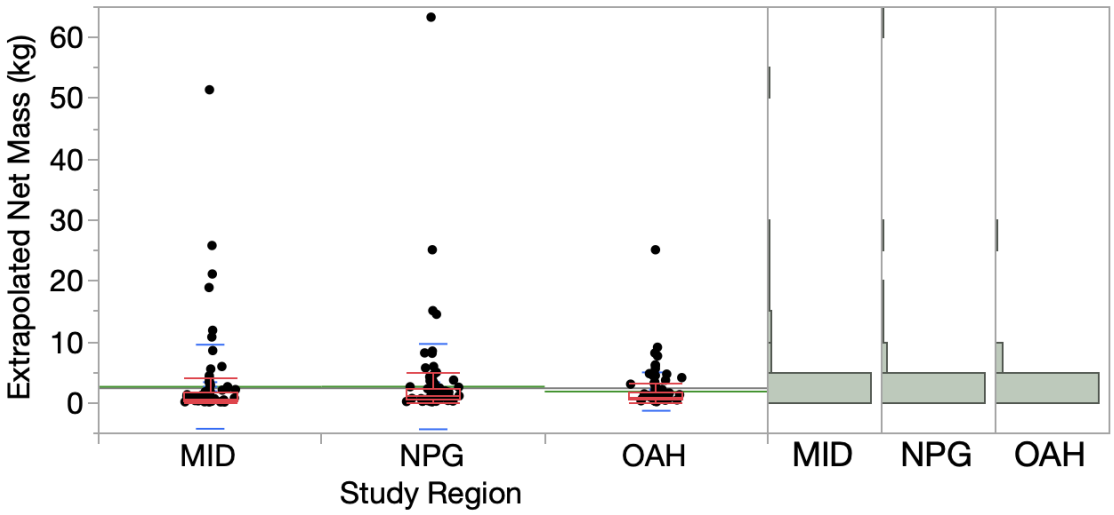

Figure 3.22. Extrapolated sample mass (y axis) for each net sample (black dot) from each region, listed along the x-axis. Regional means are indicated by the green horizontal line. The narrower blue bars overlapping the mean line are standard errors. The wider blue lines above and below the mean represent the standard deviation. The grey line across all three regions indicates the grand mean. Red box plots show the interquartile range, and the whiskers indicate the maximum and minimum values excluding outliers. Histograms summarizing each region are provided on the right. (Chi-squared test = 5.53, p = 0.0630)

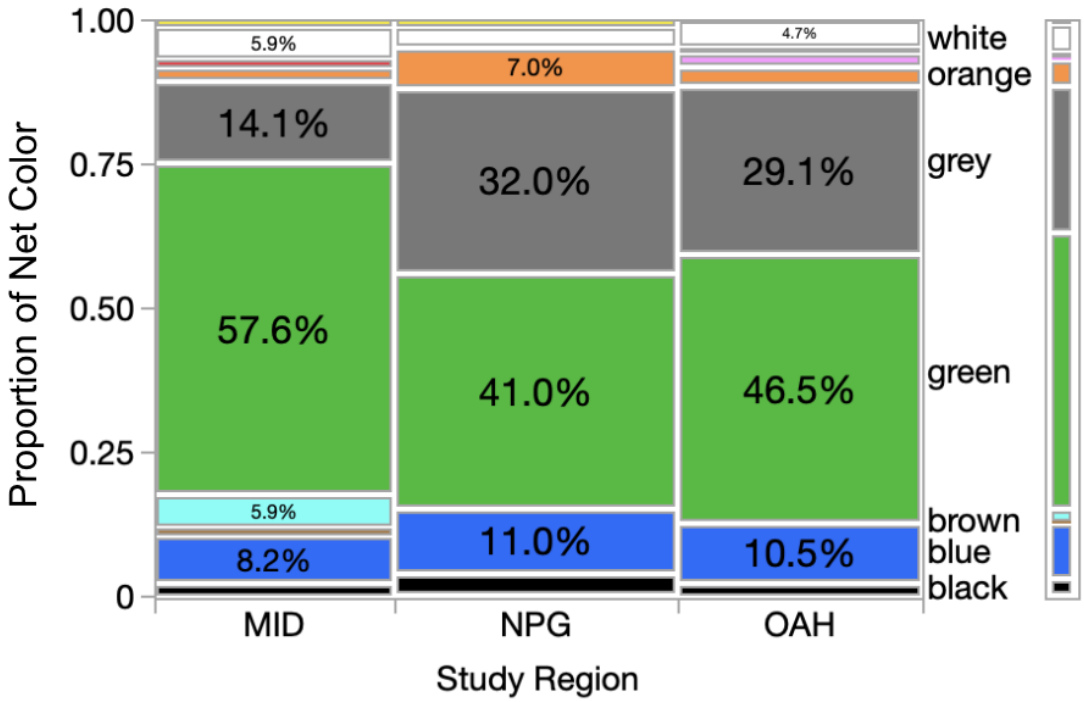

Figure 3.23. Mosaic plot of net color proportion by count. The width of the region column indicates the proportion of the total sample size. The legend on the right shows the color of each group and the average proportions across all regions. (Fisher's Exact test p = 0.0288)

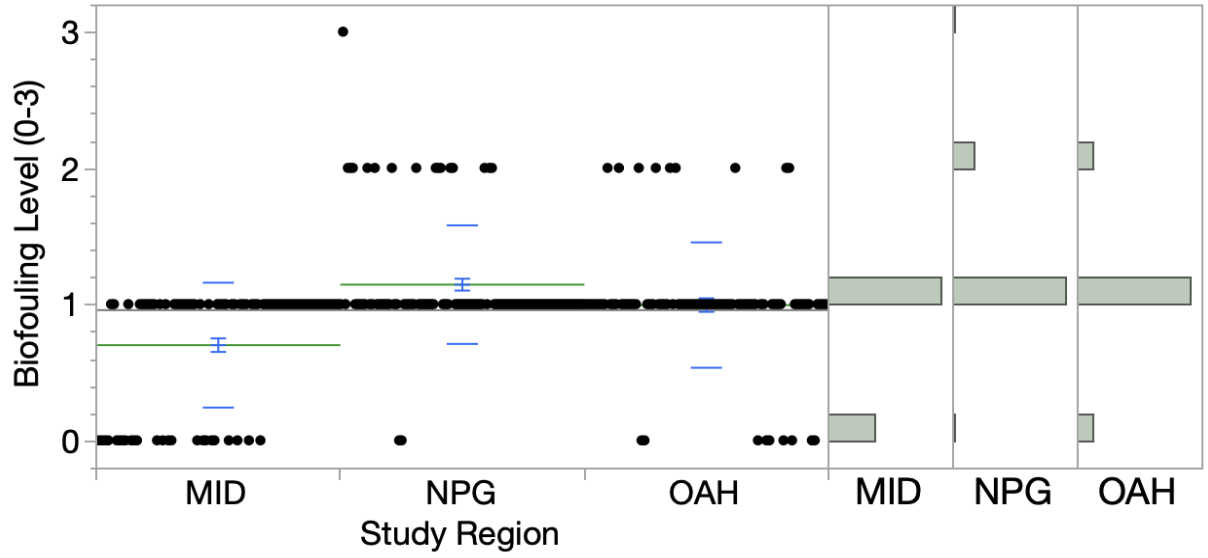

Figure 3.24. Biofouling (y-axis) for each net sample (black dot) from each region, listed along the x-axis. The regional means are indicated by the green horizontal lines. The narrower blue bars overlapping the mean line are standard errors. The wider blue lines above and below the mean represent the standard deviation. The grey line across all three regions indicates the grand mean. Histograms summarizing each region are provided on the right. (Chi-squared test = 39.78, $p < 0.0001$)

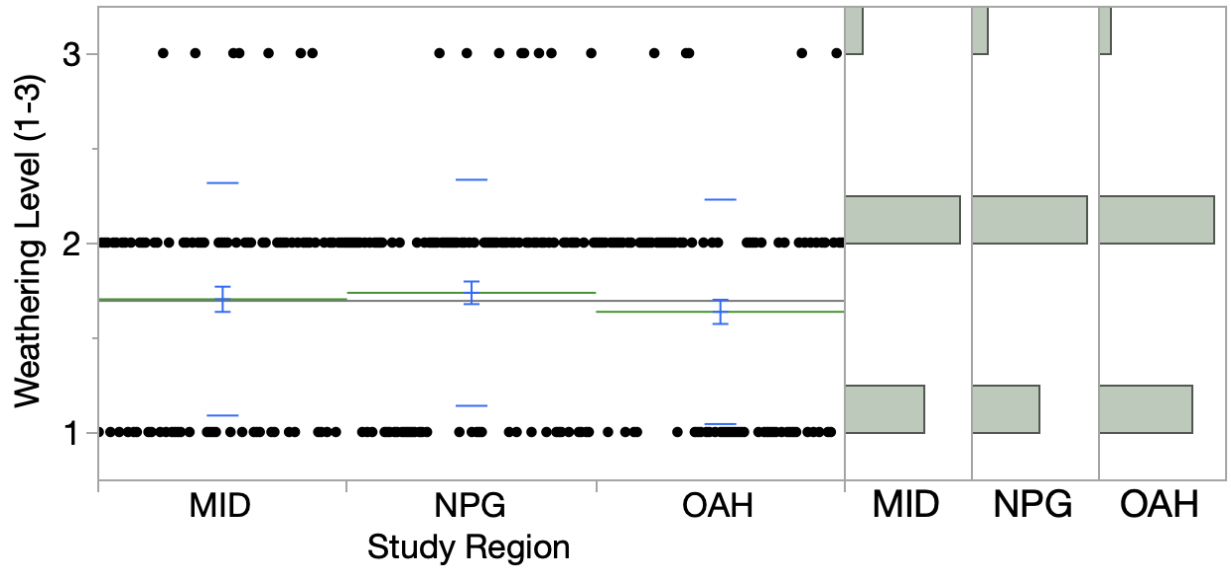

Figure 3.25. Weathering (y-axis) for each net sample (black dot) from each region, listed along the x-axis. The regional means are indicated by the green horizontal lines. The narrower blue bars overlapping the mean line are standard errors. The wider blue lines above and below the mean represent the standard deviation. The grey line across all three regions indicates the grand mean. Histograms summarizing each region are provided on the right. (Chi-squared test = 1.34, p = 0.5126)

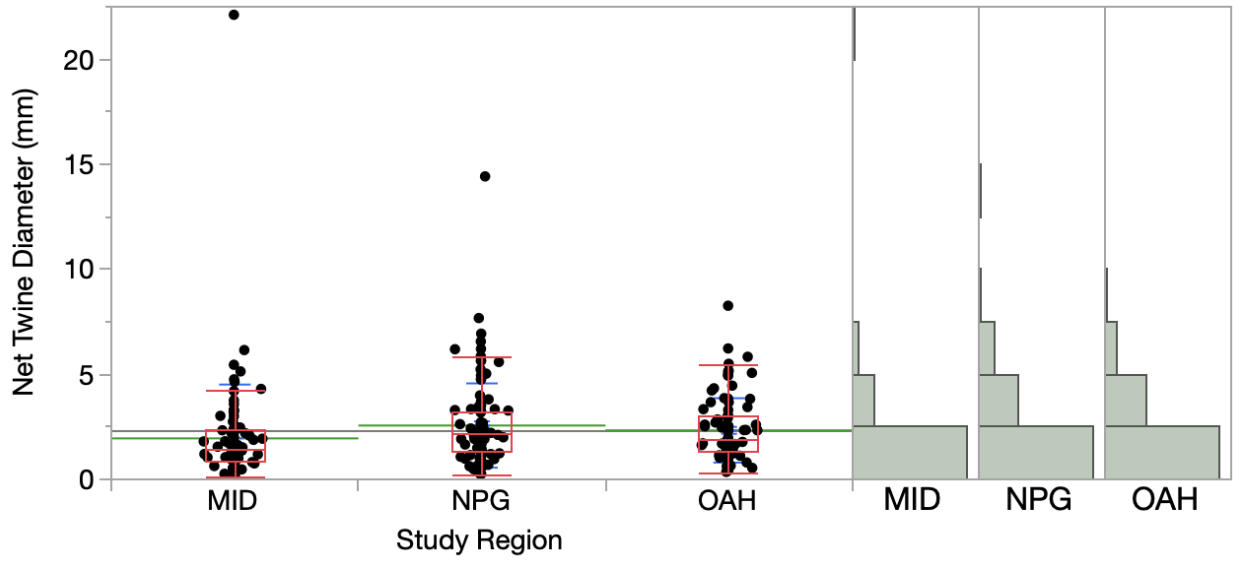

Figure 3.26. Net twine diameter in mm (y axis) for each net sample (black dot) from each region, listed along the x-axis. Regional means are indicated by the green horizontal line. The narrower blue bars overlapping the mean line are standard errors. The wider blue lines above and below the mean represent the standard deviation. The grey line across all three regions indicates the grand mean. Red box plots show the interquartile range, and the whiskers indicate the maximum and minimum values excluding outliers. Histograms summarizing each region are provided on the right. (Chi-squared test = 14.54, p = 0.0007)

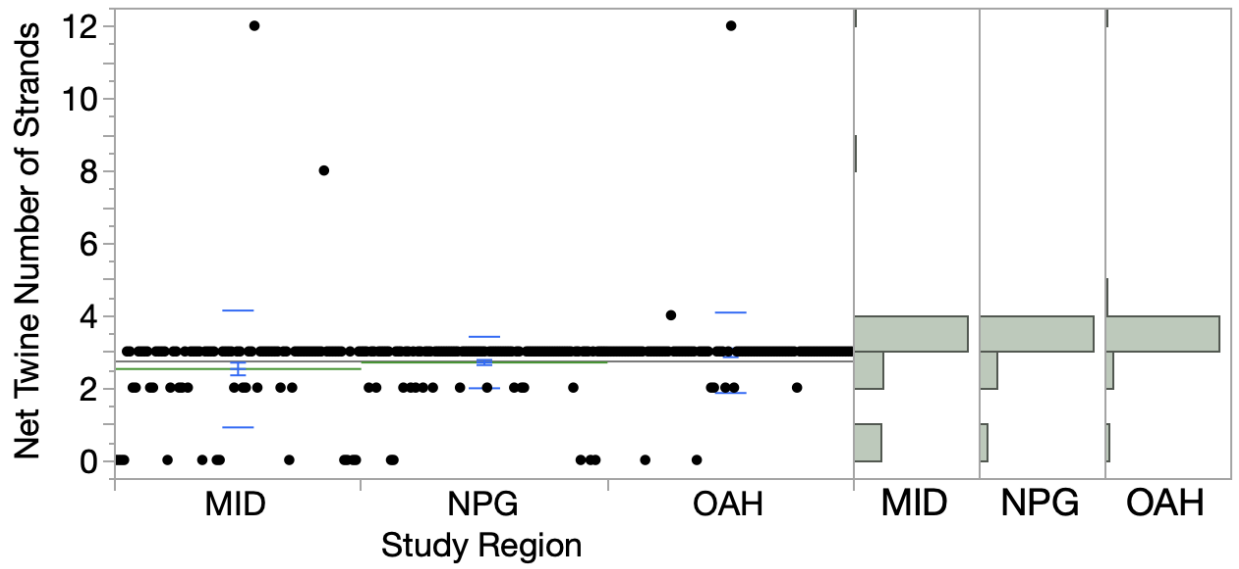

Figure 3.27. Net twine number of strands (y-axis) for each net sample (black dot) from each region, listed along the x-axis. The regional means are indicated by the green horizontal lines. The narrower blue bars overlapping the mean line are standard errors. The wider blue lines above and below the mean represent the standard deviation. The grey line across all three regions indicates the grand mean. Histograms summarizing each region are provided on the right. (Chi-squared test = 14.76, p = 0.0006)

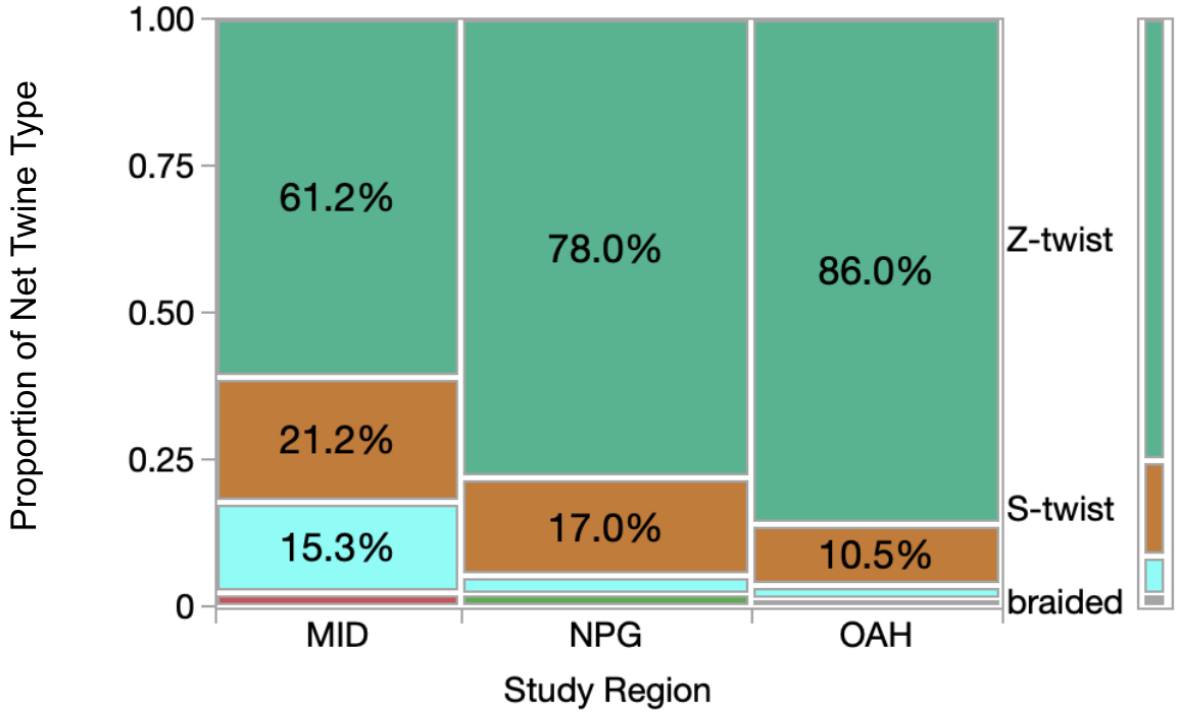

Figure 3.28. Mosaic plot of net twine type proportion by count. The width of the region column indicates the proportion of the total sample size. The legend on the right shows the color of each group and the average proportions across all regions. (Fisher's Exact test p = 0.0005)

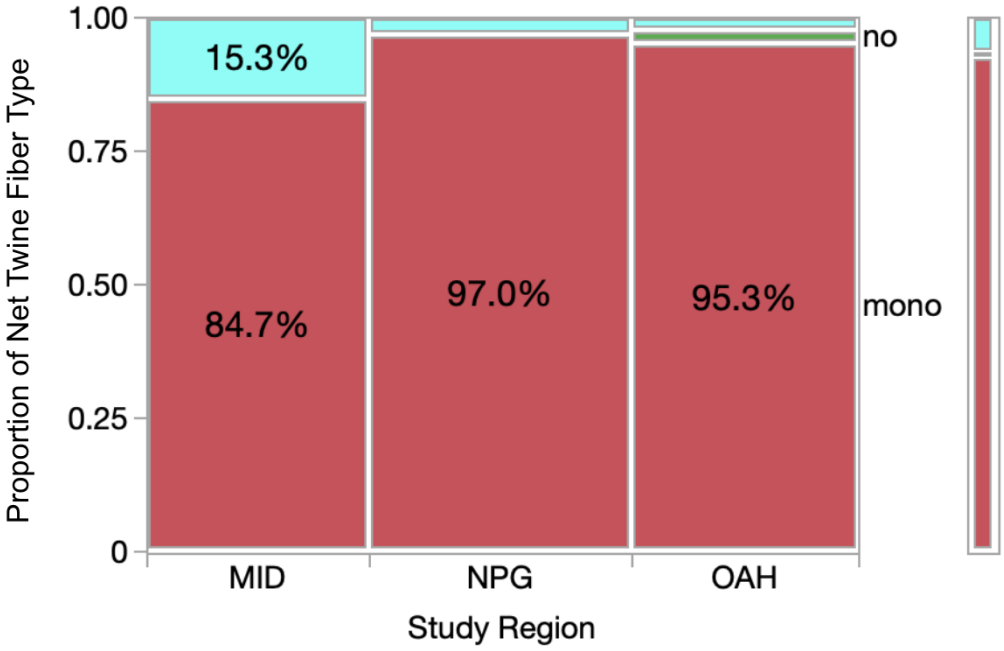

Figure 3.29. Mosaic plot of net twine fiber type proportion by count. The width of the region column indicates the proportion of the total sample size. The legend on the right shows the color of each group and the average proportions across all regions. (Fisher's Exact test p = 0.0007)

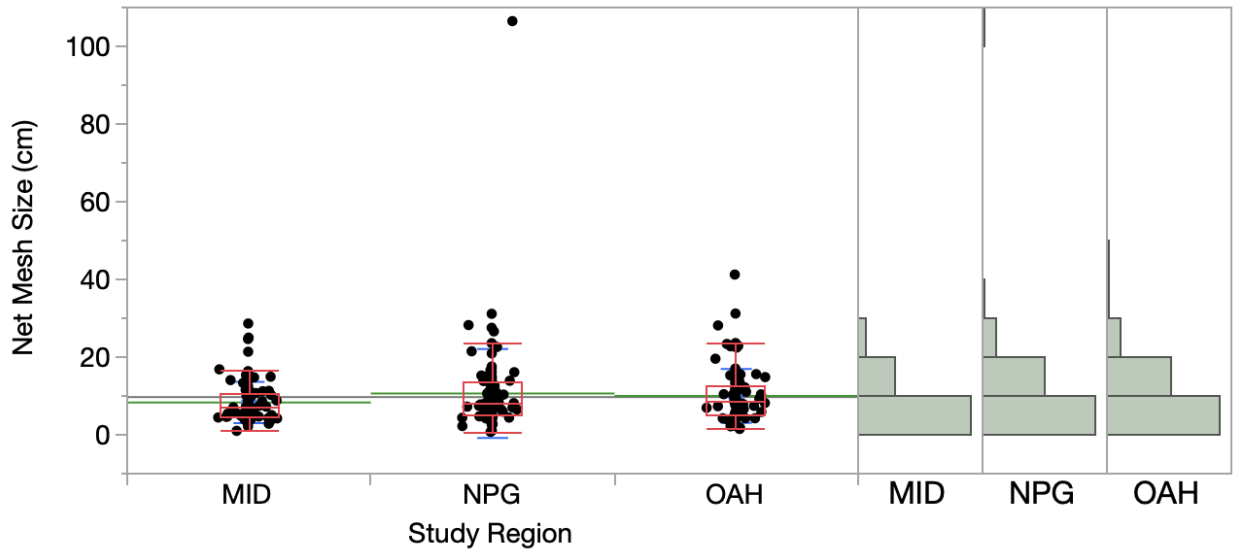

Figure 3.30. Net mesh size (y axis) for each net sample (black dot) from each region, listed along the x-axis. Regional means are indicated by the green horizontal line. The narrower blue bars overlapping the mean line are standard errors. The wider blue lines above and below the mean represent the standard deviation. The grey line across all three regions indicates the grand mean. Red box plots show the interquartile range, and the whiskers indicate the maximum and minimum values excluding outliers. Histograms summarizing each region are provided on the right. (Chi-squared test = 3.84, p = 0.1470)

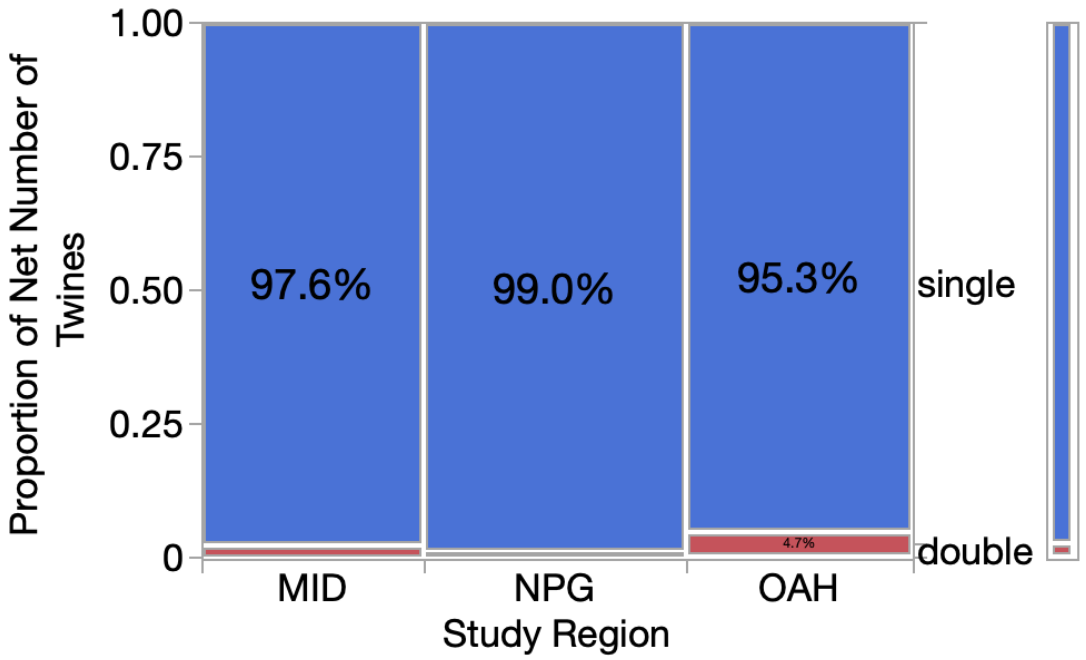

Figure 3.31. Mosaic plot of single or double net twines proportion by count. The width of the region column indicates the proportion of the total sample size. The legend on the right shows the color of each group and the average proportions across all regions. (Fisher's Exact test p = 0.3058)

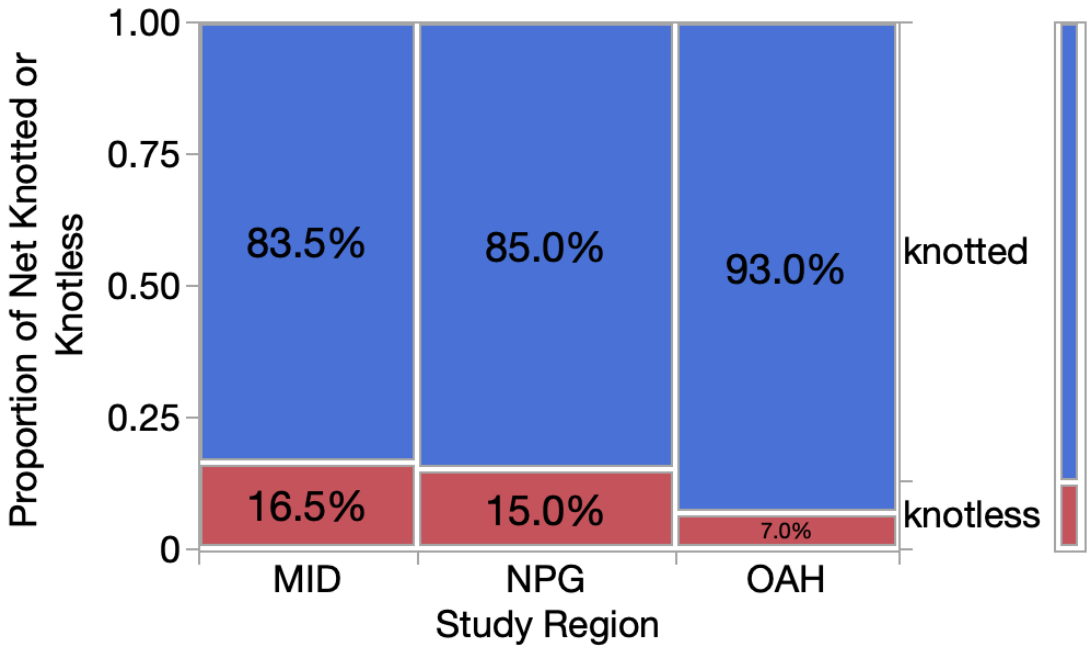

Figure 3.32. Mosaic plot of knotted or knotless net proportion by count. The width of the region column indicates the proportion of the total sample size. The legend on the right shows the color of each group and the average proportions across all regions. (Chi-squared test = 4.04, p = 0.1328)

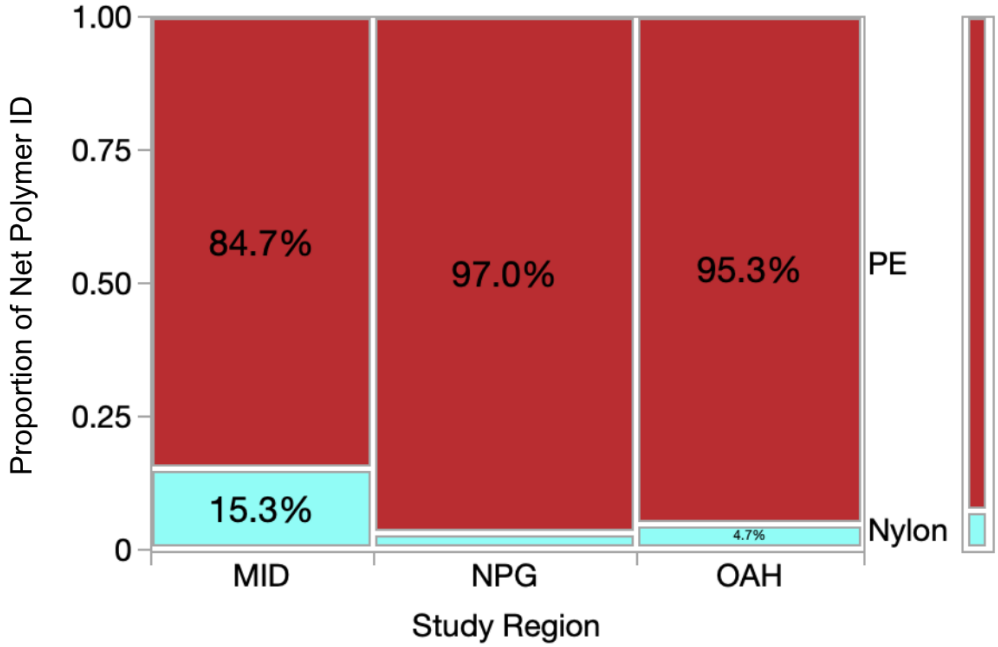

Figure 3.33. Mosaic plot of net polymer composition proportion by count. The width of the region column indicates the proportion of the total sample size. The legend on the right shows the color of each group and the average proportions across all regions. PP = polypropylene; PE = polyethylene; PE/PP = blend of PE and PP. (Fisher's Exact test p = 0.0044)

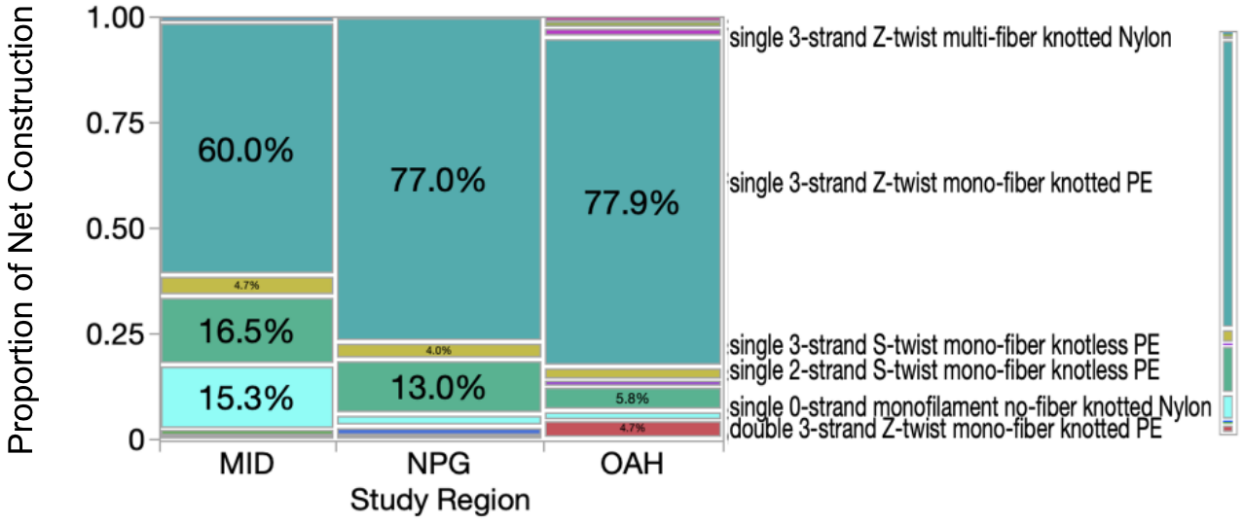

Figure 3.34. Mosaic plot of net construction proportion by count. The width of the region column indicates the proportion of the total sample size. The legend on the right shows the color of each group and the average proportions across all regions. PP = polypropylene; PE = polyethylene; PE/PP = blend of PE and PP. (Fisher's Exact test p = 0.0010)

Nets: spatial differences by mass

Seven out of eight variables tested for proportion of nets weighted by extrapolated mass were significantly different across the three regions, including net color, twine type, fiber type, polymer ID, net construction, net monofilament or not, and single or double net twine (Table 3.2). The results of these variables were consistent with the results of net proportion by count. Net color was primarily green and grey (55.8% and 22.4%, respectively). MID had 9.9% of the net mass clear, whereas the other two regions had no clear nets. NPG and OAH had a greater proportion of grey nets than MID (33.4%, 24.4%, and 7.9%, respectively) (Figure 3.35; Fisher's Exact test $p = 0.0005$). Majority of net twines weighted by mass were Z-twisted (68.3%), but 51.2% of net mass from MID was monofilament net (Figure 3.36; Fisher's Exact test $p \leq 2.2e\text{-}16$). For net twine fiber type weighted by mass, 80.5% was monofilament fiber. However, only 48.8% of MID nets are made of monofilament twine fibers (Figure 3.37; Fisher's Exact test $p \leq 2.2e\text{-}16$). 98.8% of nets were single (vs. double) twine-stranded by mass (Figure 3.38; Fisher's Exact test $p = 0.0459$). Nets were 92.9% knotted opposed to knotless by mass (Figure 3.39; Chi-squared test = 0.23, $p = 0.8924$). Net polymer ID weighted by mass was primarily PE (80.5%), but 51.2% of MID nets were composed of Nylon (Figure 3.40; Chi-squared test = 222.207, $p \leq 0.0001$). Net construction weighted by mass was dominated by single twine, 3-strand, Z-twisted, monofilament fiber, knotted, PE (67.1%) (Figure 3.41; Fisher's Exact test $p = 0.0005$).

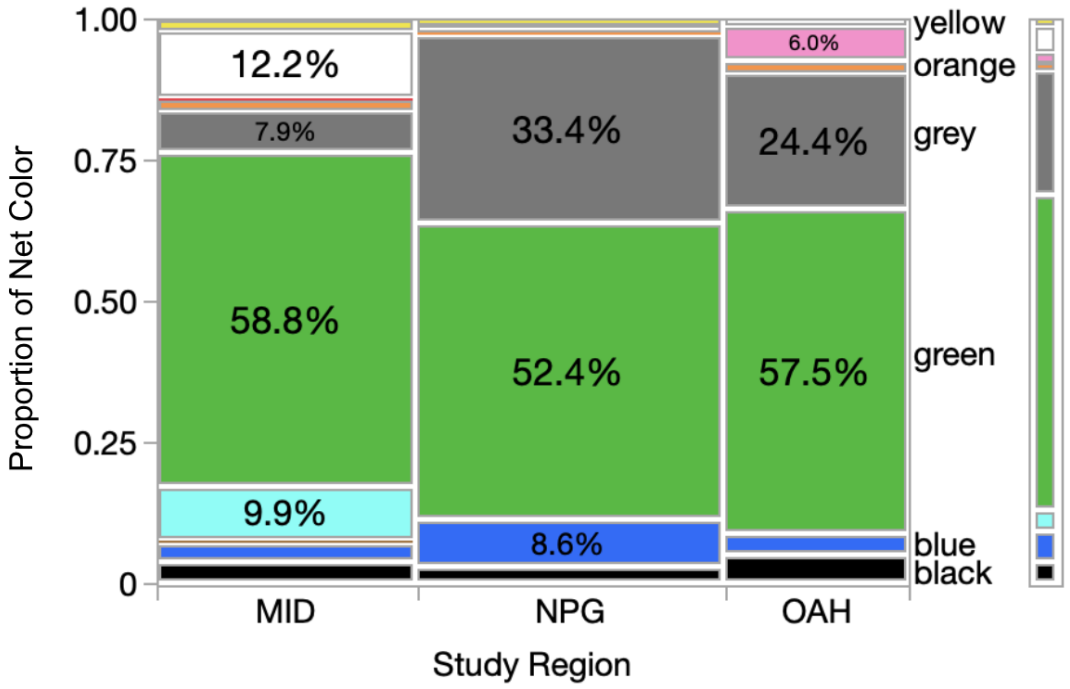

Figure 3.35. Mosaic plot of net color proportion by mass. The width of the region column indicates the proportion of the total sample size. The legend on the right shows the color of each group and the average proportions across all regions. (Fisher's Exact test p = 0.0005)

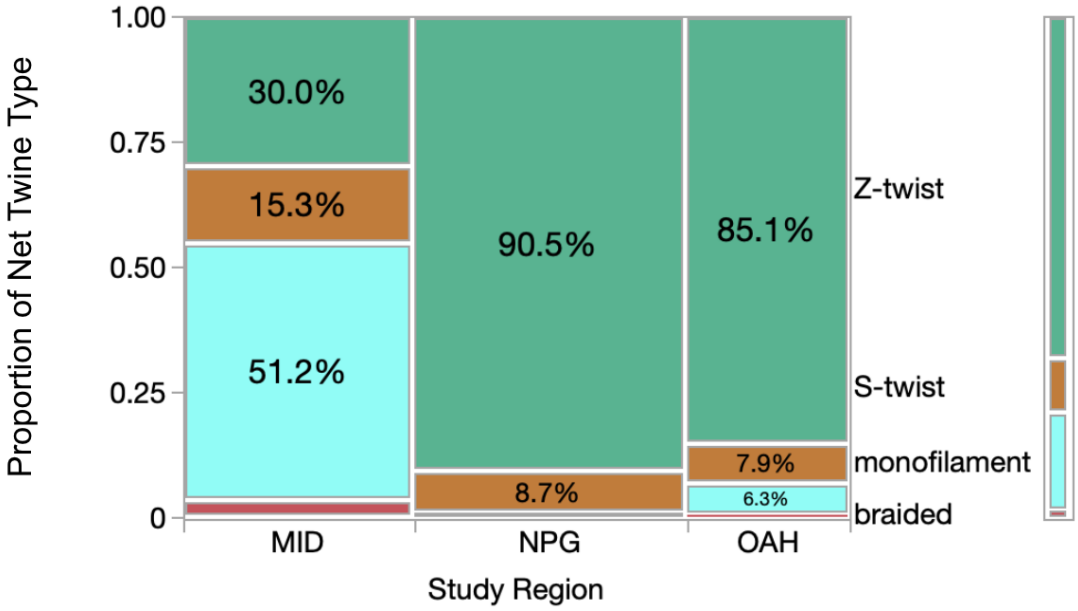

Figure 3.36. Mosaic plot of net twine type proportion by mass. The width of the region column indicates the proportion of the total sample size. The legend on the right shows the color of each group and the average proportions across all regions. (Fisher's Exact test p < 2.2e-16)

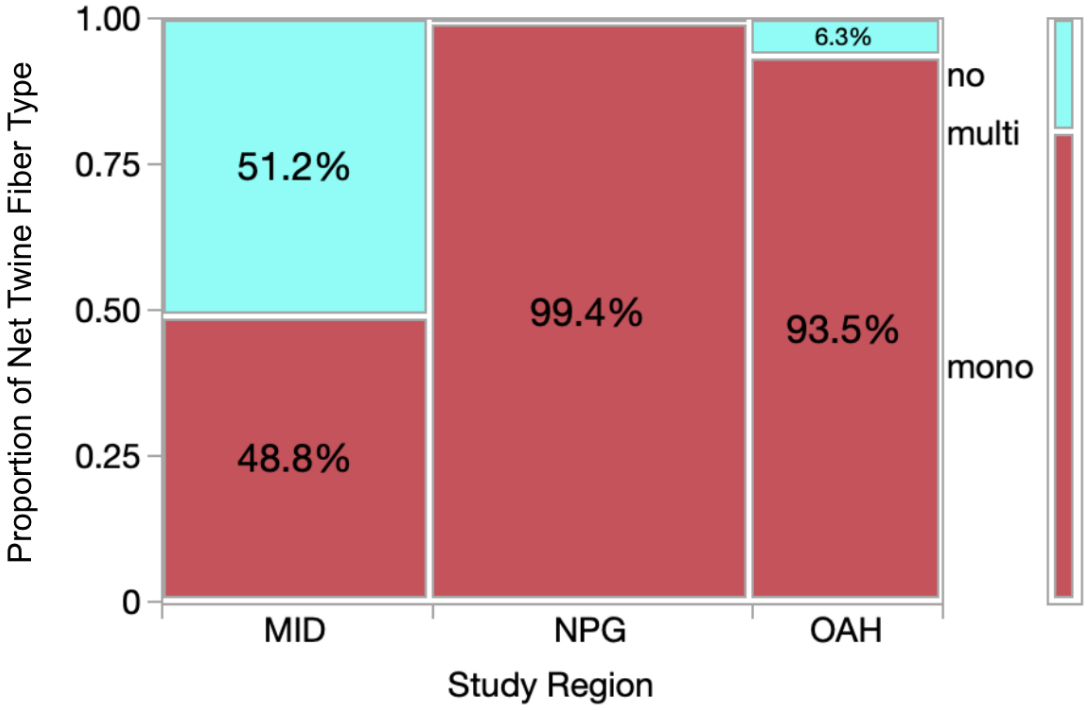

Figure 3.37. Mosaic plot of net twine fiber type proportion by mass. The width of the region column indicates the proportion of the total sample size. The legend on the right shows the color of each group and the average proportions across all regions. (Fisher's Exact test p = 2.2e-16)

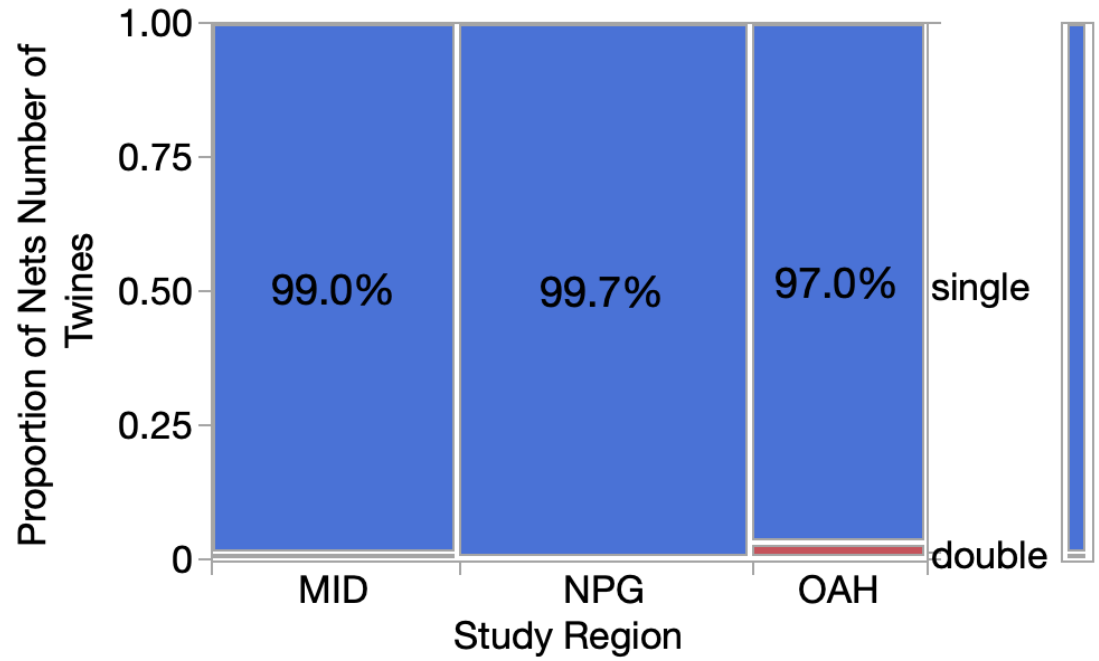

Figure 3.38. Mosaic plot of single or double net twines proportion by mass. The width of the region column indicates the proportion of the total sample size. The legend on the right shows the color of each group and the average proportions across all regions. (Fisher's Exact test p = 0.0459)

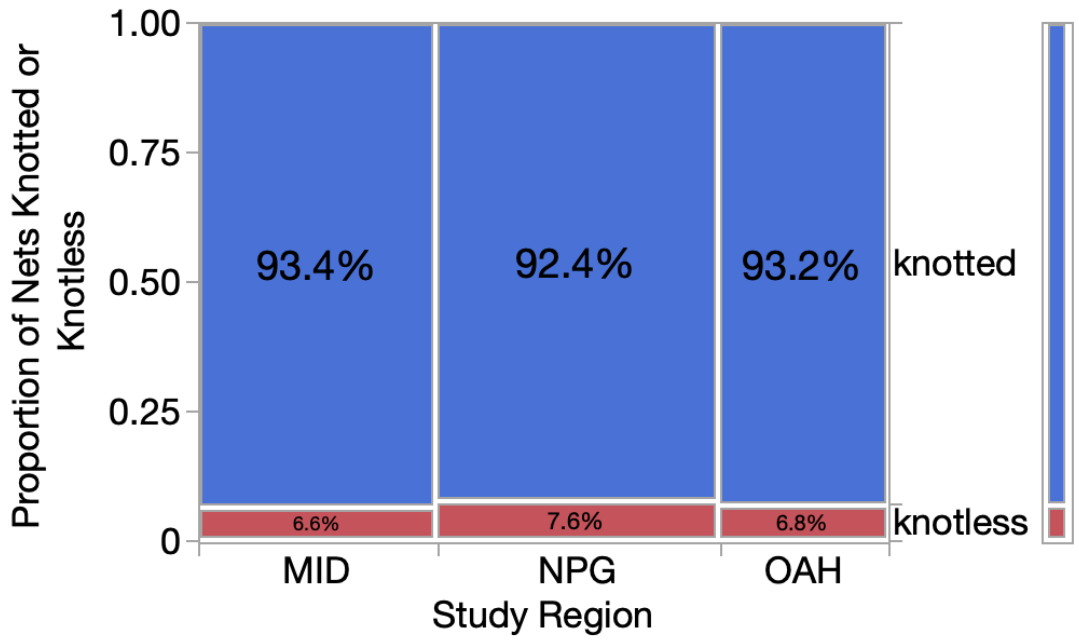

Figure 3.39. Mosaic plot of knotted or knotless net proportion by mass. The width of the region column indicates the proportion of the total sample size. The legend on the right shows the color of each group and the average proportions across all regions. (Chi-squared test = 0.23, p =0.8924)

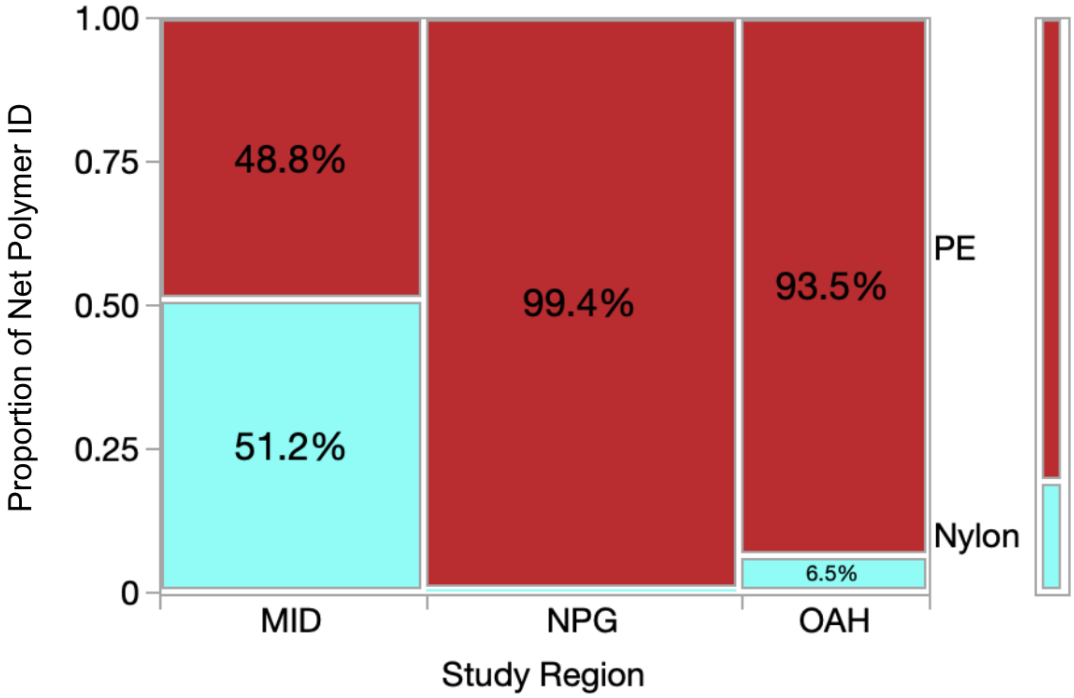

Figure 3.40. Mosaic plot of net polymer composition proportion by mass. The width of the region column indicates the proportion of the total sample size. The legend on the right shows the color of each group and the average proportions across all regions. PP = polypropylene; PE = polyethylene; PE/PP = blend of PE and PP. (Chi-squared test = 222.207, p = <0.0001)

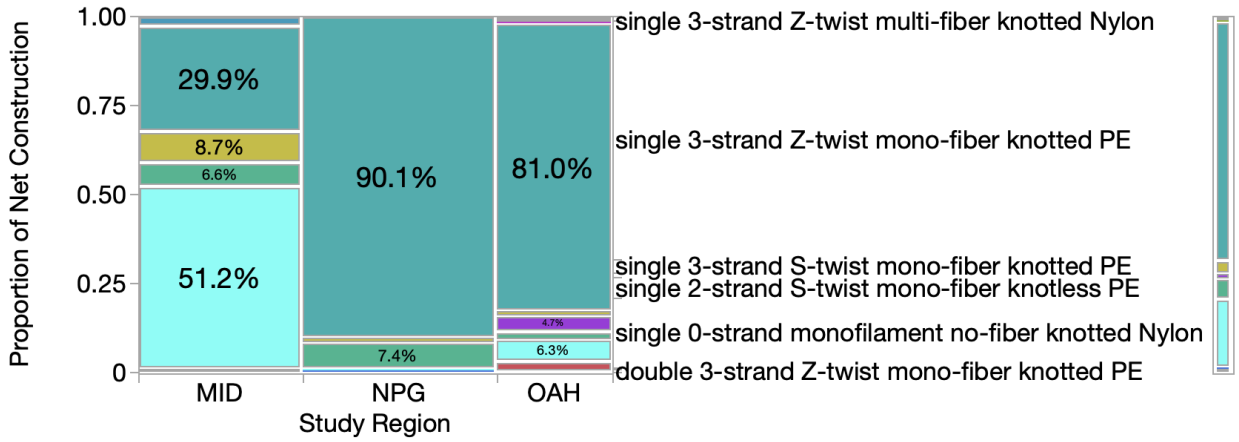

Figure 3.41. Mosaic plot of net construction proportion by mass. The width of the region column indicates the proportion of the total sample size. The legend on the right shows the color of each group and the average proportions across all regions. PP = polypropylene; PE = polyethylene; PE/PP = blend of PE and PP. (Fisher's Exact test p = 0.0005)

Nets: multivariate tests

Multivariate analyses yielded significant differences across the regions (MRPP p = >0.0001). Pairwise comparison revealed that MID nets are different from both NPG (p = 0.0004) and OAH (p = >0.0001). The MID group had significantly more green nets, clear nets, thin twine diameter, monofilament twine construction, monofilament knotted net construction, and more nylon nets than the other two regions, according to the ISA. The NMDS for nets yielded a 2-dimensional ordination space that explained 87.9% of the variance with a minimum stress of 8.789 (p = 0.001), and orthogonality of 100 (Figure 3.42). Axis 1 explained 35.5% of the variance. Axis 2 explained 52.5% of the variance. Neither axis had significant correlations to any variables in the matrices.

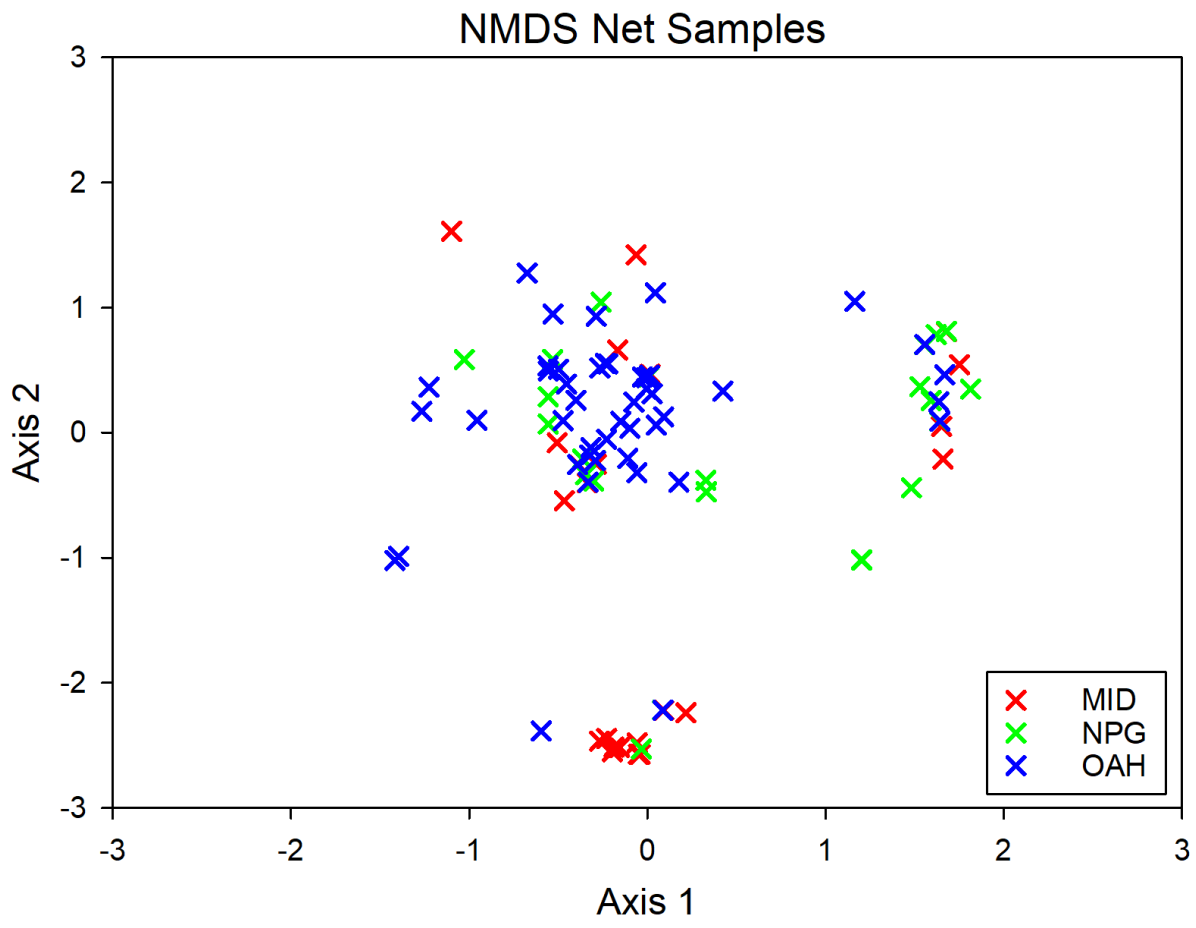

Figure 3.42. NMDS ordination plot of net samples from the three regions. Each symbol represents a net sample. (MRPP p = 0.00007)

DISCUSSION

1. Level 1: DFG event composition

The composition of DFG conglomerates by proportion of gear categories revealed that DFG conglomerates are primarily composed of nets and lines, with a consistent proportion of gear categories across the three regions. One hypothesis to explain this outcome is that, regardless of the fishery sources, the DFG lost or discarded is made up of relatively the same proportions of nets and lines and other gear types. Another hypothesis is that the DFG with very different compositions and sources mixes at sea, such that the overall proportions of the different gear types we observed represent the overall proportions of each gear type floating in oceanic convergence zones, where they are tangling together to form aggregated conglomerates of relatively equal proportions. These two hypotheses represent two extremes along a continuum of explanations, and the degree to which an event remains distinct versus mixes with other events likely depends on the amount of time it remains at sea before it is sampled.

Furthermore, average DFG conglomerates were composed of more lines than nets, by both count and mass. One possible reason for this is that there could be more sources of lines to the marine environment than just commercial fishing, including other maritime industries. However, based on our protocol comparison analysis from Chapter 2 on MID_04, the Hybrid protocol used in the current study may underestimate line proportion by count and overestimate line proportion by mass. The optimal approach in the future would be to evaluate DFG event composition by proportions of gear types using the mass of disentangled gear piles (Figures 2.24 and 2.25). Analyzing DFG composition by proportion of gear types alone fails to characterize the complexity of the conglomerates, and could lead to misconceptions that DFG composition is in fact the same across regions. The results from the event Level 1 analysis underscores the

importance of assessing DFG composition of the two most abundant gear categories, nets and lines.

2. Level 2: Line and net composition

When comparing line and net composition among regions, significant differences were revealed. Biofouling was the only variable that was significantly different across regions for both lines and nets. Midway lines and nets were significantly less biofouled compared to the other two regions. However, this variation is likely the result of different DFG collection methods across the three regions. Midway is an extremely isolated atoll with minimal human presence and only one organization doing biannual debris removals from the area. Therefore, the debris sampled from this region could have been stranded on the shoreline for months to years. Thus, no new biofouling occurred while stranded onshore, and if there were previous biofouling it likely dried and fell off. Furthermore, biofouling of nets was significantly different across all regions with nets being more biofouled in NPG than in OAH. While the reason for this result is unclear, it may indicate regional differences, and perhaps NPG events have been in the ocean longer and therefore have more biofouling. A detailed analysis of biofouling in DFG sampled at sea could help answer this question and indicate if there are different biofouling communities in the three different sampling regions, which could be used as biological indicators.

There was little variability in line composition observed from our analysis. There was a discrepancy between the univariate concatenated line construction results and the multivariate MRPP results for line composition. However, the univariate concatenation did not include color or twine diameter in the line construction comparison, and the MRPP did. Therefore, the MRPP includes all attributes of line types, beyond just construction as for the univariate results, and is more telling that there is no significant difference in the line construction across the regions.

Furthermore, the insignificance of line composition across regions could be due to our line categorization methods and the metrics we used to assess line composition. There are many subtleties in line construction that were not analyzed in this study on the "component" level. Specifically, most lines contain colored "tracer" yarns that differentiate them from other lines of similar construction types. These tracers may be the key element to aid in sourcing lines back to the source applications and manufacturers and will not be ignored in our future analysis. It is possible that by incorporating component level metrics in our line data, we would have observed significant differences among regions.

When looking at net composition across the regions, only five of the 14 variables assessed were not significantly different across the regions. Firstly, net mass and net mesh size were similar among regions, which indicates that these two traits are not good indicators of net composition and construction on their own, and perhaps similar mesh size is used for different target species and nets with different functions. Net and line samples from all three regions appear to be exposed to the same level of weathering ($p > 0.05$). Weathering may not be valuable to assess the time exposed to the environment from different regions, but may still aid in assessing the overall duration in the marine environment. All regions showed that single-stranded twisted-twine netting that is knotted is the most common construction, and that double-stranded and knotless netting are equally negligible.

Comparing results of line and net samples weighted by extrapolated mass to the unweighted results for all categorical variables revealed greater variability among regions. For nets, weighted results yielded the same significant variables as the unweighted tests. For lines, three more variables were found to be significantly different, including line color, line type, fiber type, and polymer ID (Table 3.2). For example, line color was predominantly white by mass, and

was more evenly distributed by count. Line type was only 14% braided by mass opposed to 5% by count. Line fiber type was 66% staple fiber by mass and only 41% by count. Line polymer composition was 67% PE/PP blend by mass, and only 41% by count. The most abundant line construction by mass was three stranded Z-twisted staple fiber PE/PP blend (54%), but that line type was only 36% of lines by count when the most abundant construction was three stranded Z-twisted monofilament fiber PE (43%). For nets, the most striking differences were seen in net twine type, net twine fiber type, net monofilament, and concatenated net construction results. All of which indicate that 51% of the net mass from MID is monofilament gillnet compared to just 15% by count.

The key takeaway from the net composition analysis is that MID nets were significantly different from the other two regions. This is largely driven by the greater abundance of single monofilament knotted gillnet found at MID compared to the other two regions. This type of net is clear in color, has a very small twine diameter, is made of nylon, has no twine strands because it is not a twine construction but rather a single monofilament, and it is a monofilament knotted construction. In the results section, all of the groups in the categorical mosaic plots that pertain to monofilament gillnet are shown with a cyan color in the plots. Figure 3.52 shows an example of a monofilament gillnet from MID. This regional deviation in net composition suggests different fishery sources of DFG to MID compared to the other two regions, and that gillnet fisheries may have a more direct transport pathway from their use to the northwestern atolls of the Hawaiian archipelago. If the gillnets are being deployed and lost or discarded in the western Pacific, then the dynamics of the Kuroshio current recirculation eddy could play a key role in gillnet dispersal and interaction with the Northwestern Hawaiian Islands. The strength of the recirculation eddy and its ability to retain floating debris is greater when easterly equatorial wind forcing is greater

and sea surface height anomaly is positive in the eastern North Pacific, which correlates to Pacific decadal oscillation (PDO) (Qiu & Chen, 2005). Therefore, gillnet deposition in the northwestern atolls of the archipelago may be greatest at the start of the negative phase of the PDO, when the recirculation eddy weakens from its stable convergent state, more meandering is observed in the Kuroshio Extension, and the TZCF is further south (Pichel et al., 2007, Qiu & Chen, 2005).

Figure 3.52. An example of a monofilament gillnet from event MID_04.

When comparing our results with Boland & Donohue (2003), considerable differences can be observed. It should be noted that the methods used in this study and those used by Boland & Donohue (2003) were different. Their study categorized DFG at the event level only, which we did in another publication (Royer et al. in prep.). Here, we assessed DFG events that were only conglomerates and the proportion of gear within them. They found trawl nets to be 84% of the total DFG gear types by count and 47% by mass (see Figures 5 and 6 in Boland & Donohue, 2003). Their study found lines to account for 19% of debris by mass, where our assessment found lines to account for 52% by mass. Looking at their results for monofilament gillnet, this category was only 6.6% of observed nets by count, and 12.0% by mass. Our results showed

gillnets to be 15.3% by count and 51.2% by mass at MID. This may indicate that DFG in the Northwestern Hawaiian Islands is composed of a greater proportion of monofilament gillnet than it was 20 years ago, which contradicts the global moratorium on all high seas drift-net fishing by December 31, 1992 imposed by the United Nations (Large-Scale Pelagic Drift-Net Fishing and Its Impact on the Living Marine Resources of the World's Oceans and Seas : Report of the Secretary-General., 1992).

3. Recommendations

Expanding on this DFG composition study with a temporal time series would greatly enhance our understanding of DFG composition, sources, and remediation successes over the coming years. Midway Atoll is an excellent location for a temporal time series on DFG composition because it is isolated, fishing is prohibited within Papahānaumokuākea Marine National Monument, US Department of Fish and Wildlife Service manages the atoll, and debris removal efforts can be routinely coordinated without external interference. The National Oceanic and Atmospheric Administration's (NOAA) Pacific Islands Fisheries Science Center conducted annual marine debris removal missions for most years from 1996 to 2021. A technical report on DFG composition was published by Timmers, Kistner, and Donohue in 2005, and includes valuable information on net metrics including construction, mesh size, twine diameter, and color, and they worked with a panel of experts to source many of these samples to suspected fisheries and countries of manufacture. However, this report is now outdated, and it is lacking technical innovations such as polymer identification. Furthermore, samples were not distinguished by location, and other gear categories were not considered. Much of the early efforts by NOAA aimed to determine the annual debris accumulation rate for the entire region of Papahānaumokuākea. Analysis by Dameron et al. (2005) concluded that PMNM accumulates 52

metric tons of DFG in lagoon and back reef habitat annually. Needless to say, this study is now two decades old, and does not factor in debris accumulation on shorelines throughout the monument. Furthermore, DFG composition resolution was limited to trawl, seine, gillnet, line and other categories, which are too broad to source back to fisheries of origin. A clearer picture of DFG composition from other islands and atolls within PMNM will help to reveal potential DFG sources and transport pathways and circulation dynamics of the region, and confirm our results from Midway in this study.

Conversely to Midway Atoll, time series data could begin on the Main Hawaiian Islands as well, including O‘ahu. The benefits of this region is that it is inhabited and accessible year round, which allows for continuous monitoring and is more cost effective. However, the challenges of studying DFG accumulation and composition for the Main Hawaiian Islands are due to the many players involved, inadequate synchronization of data and resources, lack of financial and staff support from state agencies, and good samaritan efforts that go unreported. DLNR has a marine debris reporting web application that has improved marine debris tracking and removal response over recent years (DLNR 2022). However, this tool is still not well known by the public and could be improved when it comes to ease-of-use, engagement, response, and data transparency. Additionally there is not currently state mobility to respond to marine debris, and the responsibility for detection, response, and removal activities are taken up by non-profit organizations. There was a debris reporting hotline (833-4DA-NETS) that was managed by DLNR but was recently taken over by Sustainable Coastlines Hawai‘i. Continued outreach efforts are underway to improve the use of this service and engage more residents in this effort. Furthermore, there is no facility in the Hawaiian Islands that processes DFG for analysis, recycling, upcycling, or repurposing. The best disposal means currently are incineration at

H-Power through the Nets to Energy Program, a multi-agency effort facilitated by the NOAA Marine Debris Program, or dumpster to landfill. This is a niche that needs to be filled, as Hawai‘i experiences some of the highest marine debris accumulation rates in the world, which likely totals over 100 metric tons annually, when factoring in the entire archipelago shoreline and nearshore habitat.

Whether DFG conglomerates are intentional or form together in convergent features at the ocean surface is up for debate. The exact mechanisms for how these large conglomerated masses of DFG form are unknown. It is unclear how many conglomerates may be intentionally constructed before being discarded into the ocean. We did identify a few conglomerates during our study that were intentionally tied together, and may have been makeshift fish aggregating devices. If this were the case, it is unknown if these makeshift FAD’s are being made locally in Hawai‘i, or coming from other Pacific fisheries. It may be possible that DFG interaction with shorelines, reefs, and low-lying atolls, particularly within Papahānaumokuākea, plays a role in forming conglomerates. Entanglement of new material could be occurring in the surf zone and then the conglomerate could be resuspended back to sea larger than it was before upon a storm surge. However, shoreline and reef interaction can also remove mass from a DFG conglomerate, and resuspension of DFG has not been thoroughly investigated. Both possibilities should be investigated. Future research and collaboration is necessary to understand the formation of DFG conglomerates, as these masses are detrimental to marine life and coral reef ecosystems.

4. Conclusion

This study utilized robust metadata to categorize different types of derelict fishing gear. Future efforts should use this gear metadata and categorization to source the different gear back to the fisheries of origin and countries of manufacture. Interdisciplinary collaboration between

scientists, fishing gear technologists, wholesalers, and fishermen is essential to achieve accurate sourcing confirmation. Understanding the point-source of DFG pollution is a massive step forward in mitigating the effects of DFG in the Hawaiian archipelago.

REFERENCES

Beaumont, N. J., Aanesen, M., Austen, M. C., Börger, T., Clark, J. R., Cole, M., Hooper, T., Lindeque, P. K., Pascoe, C., & Wyles, K. J. (2019). Global ecological, social and economic impacts of marine plastic. Marine Pollution Bulletin, 142, 189–195.

Brignac, K. C., Jung, M. R., King, C., Royer, S.-J., Blickley, L., Lamson, M. R., Potemra, J. T., & Lynch, J. M. (2019). Marine Debris Polymers on Main Hawaiian Island Beaches, Sea Surface, and Seafloor. Environmental Science & Technology, 53(21), 12218–12226.

Boland, R. C., & Donohue, M. J. (2003). Marine debris accumulation in the nearshore marine habitat of the endangered Hawaiian monk seal, Monachus schauinslandi 1999–2001. Marine Pollution Bulletin, 46(11), 1385–1394.

Bowley, J., Baker-Austin, C., Porter, A., Hartnell, R., & Lewis, C. (2021). Oceanic Hitchhikers – Assessing Pathogen Risks from Marine Microplastic. *Trends in Microbiology*, *29*(2), 107–116.

Carney Almroth, B., & Eggert, H. (2019). Marine Plastic Pollution: Sources, Impacts, and Policy Issues. Review of Environmental Economics and Policy, 13(2), 317–326.

Donohue, M. J., Boland, R. C., Sramek, C. M., & Antonelis, G. A. (2001). Derelict fishing gear in the Northwestern Hawaiian Islands: Diving surveys and debris removal in 1999 confirm threat to coral reef ecosystems. Marine Pollution Bulletin, 42(12), 1301–1312.

Gall, S. C., & Thompson, R. C. (2015). The impact of debris on marine life. Marine Pollution Bulletin, 92(1–2), 170–179.

Geyer, R., Jambeck, J. R., & Law, K. L. (2017). Production, use, and fate of all plastics ever made. Science Advances, 3(7), e1700782.

Gilman, E., Musyl, M., Suuronen, P., Chaloupka, M., Gorgin, S., Wilson, J., & Kuczenski, B. (2021). Highest risk abandoned, lost and discarded fishing gear. Scientific Reports, 11(1), 7195.

Gilman, E., Chopin, F., Suuronen, P., & Kuemlangan, B. (2016). Abandoned, lost and discarded gillnets and trammel nets: Methods to estimate ghost fishing mortality, and the status of regional monitoring and management. FAO Fisheries and Aquaculture Technical Paper, 600, I.

Jambeck, J. R., Geyer, R., Wilcox, C., Siegler, T. R., Perryman, M., Andrady, A., Narayan, R., & Law, K. L. (2015). Plastic waste inputs from land into the ocean. Science, 347(6223), 768–771.

JMP®, Version 16.2.0. SAS Institute Inc., Cary, NC, 1989–2021.

Jung, M. R., Horgen, F. D., Orski, S. V., Rodriguez, V., Beers, K. L., Balazs, G. H., ... & Lynch, J. M. (2018). Validation of ATR FT-IR to identify polymers of plastic marine debris, including those ingested by marine organisms. Marine Pollution Bulletin, 127, 704-716.

Kenkel, N.C., Orloci, L., 1986. Applying metric and nonmetric multidimensional scaling to ecological studies: some new results. Ecology 67, 919–923.

Laist, D. W. (1987). Overview of the biological effects of lost and discarded plastic debris in the marine environment. Marine Pollution Bulletin, 18(6), 319–326.

Lebreton, L., Slat, B., Ferrari, F., Sainte-Rose, B., Aitken, J., Marthouse, R., Hajbane, S., Cunsolo, S., Schwarz, A., & Levivier, A. (2018). Evidence that the Great Pacific Garbage Patch is rapidly accumulating plastic. Scientific Reports, 8(1), 1–15.

Macfadyen, G., Huntington, T., & Cappell, R. (2009). Abandoned, lost or otherwise discarded fishing gear. United Nations Environment Programme : Food and Agriculture Organization of the United Nations.

Marine Debris Response and Removal Reporting Form. (n.d.). Department of Land and Natural Resources, Division of Boating and Ocean Recreation. Retrieved May 5, 2022, from https://dlnr.hawaii.gov/dobor/reportmarinedebrishawaii/

McCune B, Grace JB, (2002) Analysis of ecological communities. MjM Software Design, Gleneden Beach, OR

Shomura, R. S., & Yoshida, H. O. (1985). Proceedings of the Workshop on the Fate and Impact of Marine Debris, 27-29 November 1984, Honolulu, Hawai‘i.

Teuten, E. L., Saquing, J. M., Knappe, D. R. U., Barlaz, M. A., Jonsson, S., Björn, A., Rowland, S. J., Thompson, R. C., Galloway, T. S., Yamashita, R., Ochi, D., Watanuki, Y., Moore, C., Viet, P. H., Tana, T. S., Prudente, M., Boonyatumanond, R., Zakaria, M. P., Akkhavong, K., … Takada, H. (2009). Transport and release of chemicals from plastics to the environment and to wildlife. Philosophical Transactions of the Royal Society B: Biological Sciences, 364(1526), 2027–2045.

Therriault, T. W., Nelson, J. C., Carlton, J. T., Liggan, L., Otani, M., Kawai, H., Scriven, D., Ruiz, G. M., & Clarke Murray, C. (2018). The invasion risk of species associated with Japanese Tsunami Marine Debris in Pacific North America and Hawaii. Marine Pollution Bulletin, 132, 82–89.

Uhrin, A. V., Walsh, W. A., & Brodziak, J. (2020). Relative abundance of derelict fishing gear in the Hawaii-based pelagic longline fishery grounds as estimated from fishery observer data. Scientific Reports, 10(1), 7767.

Walker, D. A. (2003). JMASM9: Converting Kendall's Tau For Correlational Or Meta-Analytic Analyses. Journal of Modern Applied Statistical Methods, 2(2), 525–530.

CHAPTER 4

Concluding thoughts and lessons learned

In this chapter, I will be reflecting on the strides we made over the course of this project, the lessons we learned, the outcomes, and the next steps. It is important to understand this thesis represents only a portion of the work coming out of a two+ year deep dive on DFG from the central subtropical Pacific Ocean that has been affecting Hawai‘i’s sensitive marine ecosystem for decades. Floating plastic marine debris takes on many forms, and I believe that specifically DFG poses the greatest threat to the oceans, and particularly Hawai‘i. This is evident from the magnitude of DFG that accumulates here on a continual basis. DFG in Hawai‘i has become an environmental and socio-economic issue, and it is small grass-roots organizations, including Hawai‘i Pacific University Center for Marine Debris Research, that have taken it upon themselves to address this threat in a big way.

Our project started in April of 2020, with one year of funding granted by the Norwegian Retailers Environment Fund. At that time, our team had already collected and sampled five DFG events removed from Kane‘ohe Bay. Our sampling methods at this time were developed in a way to speedily sample massive net conglomerates in as little as one hour in the field. We were limited by space and time constraints, and without a space to dissect DFG we were unable to dry and weigh DFG, and we were planning to build a database solely on the metrics we could record from the samples in the lab. We realized these limitations greatly reduced our data comprehensiveness, as we did not know how much each DFG event weighed, were not able to track our total DFG mass processed, as well and how different DFG were configured, what our sample looked like when they were disentangled, and we were unsure how this would affect our primary goal of sourcing DFG back to the source fisheries.

We were quickly granted access to a warehouse on HPU property that we converted into a “Net Shed” that became our DFG processing plant. We were able to set up a

crane scale, and had roughly 275 square meters of indoor space to stockpile DFG. In our first four months of operation, we were concerned that we would have a very small sample size to work with, as we only obtained 12 nets over the summer, and we were quickly able to process these in the field. Then, on September 19th a >1600 kg conglomerate (OAH_17) drifted into Kailua Bay, and was secured by local residents. We chased this net down through social media posts and found where the net was located and being disposed of by the residents. We launched an emergency removal effort that took an entire day and ten truck loads to transport to the net shed. This event took up most of the floor space in the net shed. It was composed of hundreds of different nets and lines and we realized that we needed to disentangle this event as a case study. After this point, the DFG started flooding in and we have collected and processed 160 DFG events totalling over 14.5 metric tons. It took our team and an army of over 100 volunteers over a year to complete the disentanglement and sampling of OAH_17, and we still have around 800 samples to process in the lab.

A key takeaway from the experience of OAH_17 and other large conglomerates that we disentangled is that this processing method deserves a larger operation that expands beyond the current capacity of CMDR, and specifically our small team of five part-time members. However, disentanglement of DFG is key for two major reasons, sourcing DFG back to the source fisheries, and effectively recycling DFG. We conducted a small in-person workshop with two experts, one who has a substantial fishing career in a diversity of fisheries from bottom and midwater trawl, to seine, and longline, and the other expert was a commercial net wholesaler who had worked on the sales and manufacturing business of the commercial fishing industry for three decades. Over this 72-hour workshop we obtained invaluable information for gear sourcing that broadened our understanding of gear construction and technology. Our feedback from the

experts was that without seeing the gear in full size and in person, being able to feel the material and observe its construction, it is incredibly challenging to source the gear back to the source fishery. This workshop also highlighted the necessity for interdisciplinary collaboration when it comes to protecting our shared ocean resources and the impacts of DFG. DFG pollution serves no party beneficially, and even the fishermen themselves are aware of the state of our overfished and plastic polluted oceans. Another example of this awareness came from one of the Hawai‘i Longline Association vessels that collaborated with our net bounty program to obtain nets from the pelagic North Pacific Gyre. This vessel ran over a large DFG conglomerate in transit to their fishing grounds and it blew out both of their engines and left them dead in the high seas. They had to be towed over 100 nautical miles back to Honolulu and incurred an expense exceeding $40,000. It is apparent that reducing DFG in the ocean will require more engagement with fishermen around the world.

Disentangling DFG also allows for material to be sorted by polymer, which provides economic incentives to collect DFG. Over 80% of DFG by mass, analyzed in the regional comparison, was composed of polyethylene. This can be upcycled into a variety of new products, including asphalt roadways, building bricks, insulation material, plastic lumber, and other moldable material. I hope we see a commercial DFG processing operation develop in Hawai‘i in the next few years, resulting in Hawai‘i becoming a central hub for upcycled marine debris for the North Pacific.

There were several aspects of our methods where we bit off more than we could chew, one already mentioned was the Disentanglement sampling protocol, and another was lab categorization and processing of samples. This effort was at first split between research technician Raquel Corniuk and myself, but after about a year into the project we divided our

efforts and I focused in the net shed while she led the lab effort. Raquel did much of the lab categorization single handedly, but she would utilize help in the form of students, volunteers and other lab staff when available. The lab processing was certainly the bottleneck of our sampling efforts. Less than half of all the samples collected in the field have been processed in the lab, to date. We could have used two full time lab staff on this project to keep pace with the inflow of DFG. Furthermore, as we analyzed samples in the lab, we discovered the levels of complexity of gear, especially lines, and collecting data down to the component level was far too time consuming for our research needs. However, it should be noted that a detailed investigation on line components from a smaller subset of our samples has the potential to uncover key distinctions for sourcing lines back to the manufacturers based on the subtle variations of colored tracer yarns in line twine strands. In summary, we were understaffed on many accounts.

The future of the work is to create a virtual and physical DFG survey to be broadcasted and shared with fisheries experts around the Pacific Rim nations to help identify the fishery and manufacturer sources of the DFG we are finding in Hawai‘i and surrounding waters. Additionally, there are many more stories and findings to be extracted from our database and all of the physical samples we have archived, and our Google Drive database needs to be converted into an open source web app or relational database of some sort to encourage accessibility and collaboration. Chapter 3 of my thesis serves as the third publication in progress of a four (possibly more) paper series spurring from our robust efforts. The first paper will give an overview of DFG event types found in Hawai‘i (Royer et al., in prep.). The second will focus on the polymer ID methods for DFG developed for this project (Corniuk et al., in prep.) . And the fourth will summarize the results of the sourcing efforts, working with fisheries experts around the Pacific. It is clear that we need boots on the ground to validate the sources of DFG we are

finding here in Hawai‘i by visiting fishing ports in foreign nations around Southeast and West Asia, as well as Central and South America. This is where I intend to serve my duty for this cause in the coming years.

APPENDIX

Appendix 1: (Chapter 2) DFG event measurements datasheet

https://docs.google.com/document/d/1Dz6dHwWmGdR0MS7K4RuJg1AHKNljtZDUA6NSlJfIzn0/edit?usp=sharing

Appendix 2: (Chapter 2) DFG sampling datasheet

https://docs.google.com/document/d/1EKzuja0qtM8vvqtPE3Ml9kC4s_UQMl8qhRQo5lQYPTk/edit?usp=sharing

Appendix 3: (Chapter 2) Data Dictionary

https://docs.google.com/spreadsheets/d/e/2PACX-1vTMVAQlJ1hQmIVByZtonQwGKIKdER8sGz52LJCDQLIYXBF4p67IF--37fdWJfkZs0d16Go1St-zjdf9/pubhtml

Appendix 4: (Chapter 3) DFG event data and sample data, multivariate workbook

https://docs.google.com/spreadsheets/d/1t5CStr89Eb3hmVmVbg1BO3Vd3nE8uXGC/edit?usp=sharing&ouid=102579944794120852196&rtpof=true&sd=true